5. Results and Discussion

This chapter describes the characterization of solution properties of four protein–DNA complexes and their components, namely Omega, Arc, KorB, and Sac7d. Accordingly, the chapter is divided into seven subchapters that describe the results obtained for the four proteins, followed by separate discussions for each protein. Subchapters One and Two are devoted to the main project, namely Raman difference spectroscopic studies on protein Omega and its complexes with DNA. Omega–operator DNA complexes were studied extensively as far as it can be accomplished by means of Raman difference spectroscopy. Part of this work has been recently published (*36*).

Subchapters Three and Four represent results on Arc repressor and Arc operator DNA complexes. Although emphasis was primarily oriented on the identification of new Raman markers of protein DNA interaction in the ribbon-helix-helix (RHH) family that are important for the characterization of Omega–operator DNA complexes, the system provides more. It is not only an interesting system for Raman spectroscopists but also of interest for structural biologists and biochemists because it provides some new insights into the binding specificity.

The KorB-operator DNA complex is characterized in the fifth subchapter. A Raman study of this complex was published before the crystal structure was available (*91*). The crystal structure of the DNA binding domain of KorB and its operator DNA has recently appeared (*57*) and the already published Raman data are reinterpreted according to the published structure. Fortunately, few reinterpretations of the Raman date were necessary. The fifth subchapter also represents the characterization of the complex of wild type KorB and operator DNA. The crystal structure of this complex is still not available.

Subchapters Six and Seven are devoted to Sac7d, a minor groove binding protein. Supported by the knowledge of crystal structures of several Sac7d-DNA complexes, the interpretation of the Sac7d Raman spectra enabled an extended characterization of the binding site on the decamer d(GAGGCGCCTC)$_2$. Three possible binding sites could not be discriminated. Moreover, Raman data indicate Sac7d driven partial B- to A-form DNA transition. The results of this study were recently published (*92*).

5.1. Results and Interpretation: Omega Protein

5.1.1. Raman Signature of Oligonucleotides

Choice of Oligonucleotides. The ω_2 protein recognizes and binds specifically to at least two consecutive copies of the 7-bp repeat units (top strand 5'–$^{A}/_{T}$ATCAC$^{A}/_{T}$–3') symbolized by arrows with heads at the 3' end (⟶), or inverse 7-bp repeat units (top strand 5'-$^{A}/_{T}$GTGAT$^{A}/_{T}$-3') symbolized by arrows with heads at the 5' end (⟵). In the promoter region, the heptads are arranged in different modes with direct and inverted repeats (Figure 1.3). To characterize the ω_2–operator DNA complex in the solution state, diheptads were studied with all heptad orientations which exist in the promoter region of *copS*, δ and ω genes (Figure 5.1). Moreover, oligonucleotides with the four heptad repeat units in different orientation ($\longrightarrow_2\longleftarrow$ $\longrightarrow$ and $\longrightarrow_4$) as well as a monoheptad (⟶) were chosen (Figure 5.1). For a more detailed analysis of the conformation of the ω_2–operator DNA complex, several modifications in the heptad sequences were made. First, two sequences REF1 and REF2 with the same base pair content as diheptads were selected as non-operator DNA models. These oligonucleotides (Figure 5.1) contain no heptad sequence and ω_2 should not or only unspecifically bind to them. Second, the central GC base pair of the first heptad was exchanged in the diheptad $\longrightarrow_2$ by CG (MUT). It is expected that ω_2 binds to the unmodified site, whereas weaker binding might occur to the modified heptad via unspecific interactions. The heptad sequences were extended by flanking GC base pairs (e.g. 5'–GCG $\longrightarrow\longleftarrow$ GG–3') to protect the ends of oligonucleotides from fraying.

Raman Spectra of Diheptad $\longrightarrow\longleftarrow$. The Raman spectrum of the oligonucleotide with a diheptad sequence in head to head orientation is shown in Figure 5.2. Traces 1 and 2 show the spectra of $\longrightarrow\longleftarrow$ in D_2O and H_2O buffer, respectively. Wavenumber positions of the major peaks are labelled in Figure 5.2 and summarized in Table 5.1. The peak positions are in general accordance with those of DNA given previously in the literature (*88-89, 93-94* and references therein).

The backbone conformation markers at 837 and 1092 cm^{-1} in H_2O and at 833 and 1091 cm^{-1} in D_2O are diagnostic of B-DNA (*89*). The nucleoside conformation markers identify C2'-*endo*/*anti* conformers. The spectra shown in Figure 5.2 are the signature of $\longrightarrow\longleftarrow$, and provide the basis for the interpretation of the difference spectra shown in the following Figures.

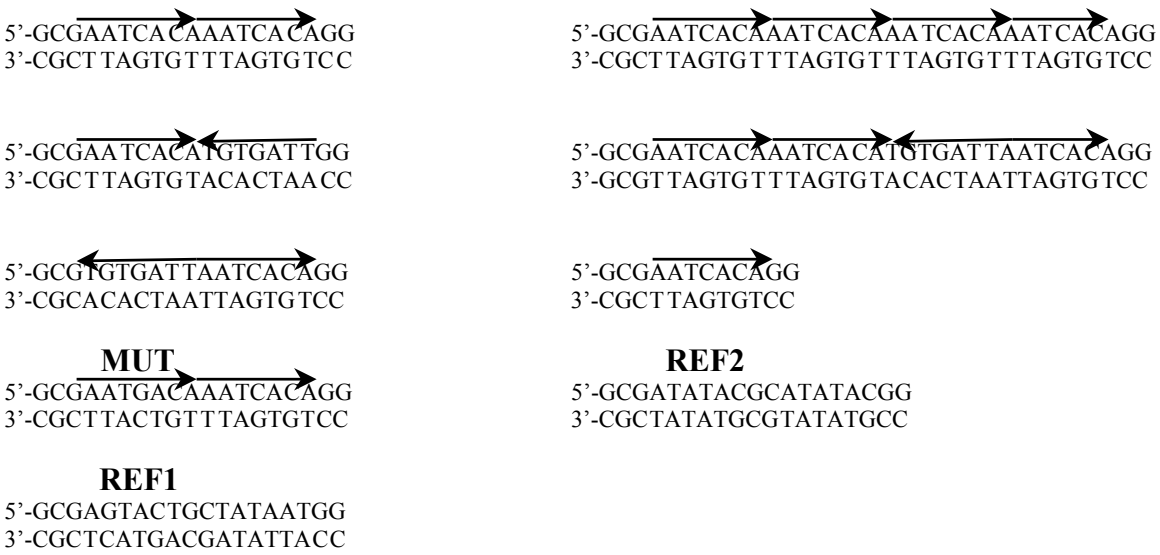

Figure 5.1: Nucleotide sequences of the oligonucleotides containing mono-, di- and tetraheptad-sequences used in this study. The oligonucleotides were designed as operator DNA models with heptads in direct (⟶) and inverted (⟵) orientations as indicated by arrows. The MUT oligonucleotide is a modified diheptad ($⟶_2$), where the central CG base-pair is exchanged for GC. The REF1 and REF2 sequences served as non-operator DNA models. The flanking basepairs were used to prevent fraying.

Table 5.1: Vibrational Assignments for Raman Markers of ω_2 operator DNA in H_2O and D_2O solutions[a]

H_2O	D_2O	Assignment[b]	H_2O	D_2O	Assignment[b]
667	661	T	1291	1291	C
682	682	G	1303	1304	A
728	721	A	1317	1318	G
750	738	T	1344	1332	A, G
771	785	C, T	1344	1346	A
790	785	bk	1364	1359	G
807	813	A	1376	1378	T, A, C
837	833	νOPO	1421	1420	2′-$CH_2\delta$, A
894	894	bk	1444	1443	$CH_2\delta$
921	922	bk	1462	1462	5′-$CH_2\delta$
968	968	bk	1489	1483	G, A
1014	1017	T, G, C	1511	1501	A
1052	1050	νCO	1530	1522	C
1092	1091	νPO_2^-	1577	1577	G, A
1144	1158	T	1603	1623	C, G, A
1178	1189	G	1649	1659	C, T
1217	1213	C, T	1668	1677	T
1239	1239	T, C	1695	1677	G
1255	1263	A, C	1716	1677	G
1267	1263	C			

[a] Raman data are from the spectra of diheptad ⟶⟵ shown in Figure 5.2. Frequencies are in wavenumber units (cm^{-1}).

[b] Abbreviations: ν and δ indicate stretching and deformation vibrations, respectively, of atoms listed; bk indicates vibration of DNA backbone; A, T, G, and C indicate vibrations of the deoxynucleosides including modes localized in the purine or pyrimidine base or delocalized modes (base plus furanose moieties). For other details of vibrational assignment, see text.

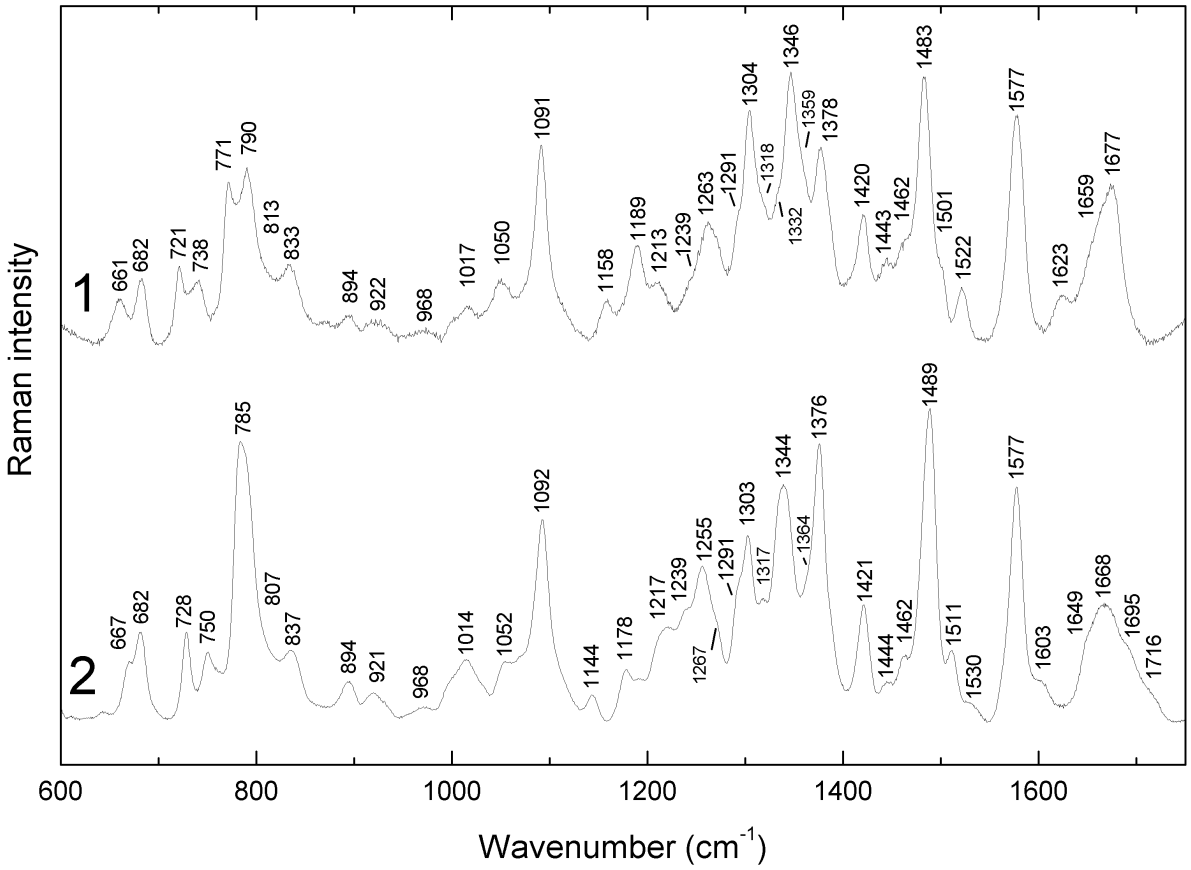

Figure 5.2: Raman spectra of 19-bp oligonucleotide ⟶⟵ in H_2O (2) and D_2O (1) solution. Sample buffer is 50 mM Tris-HCl pH 7.5 for spectrum (2) or pD 7.5 for spectrum (1) and 50 mM NaCl; data were collected at 22 °C in the spectral region 600-1750 cm^{-1}. Concentrations are 23 mg/mL (H_2O) and 14 mg/mL (D_2O). Spectra were normalized with respect to the integrated intensity of the phosphate band near 1092 cm^{-1} and the adenine-guanine band near 1580 cm^{-1} (*94-95*). Peak positions of prominent Raman bands are labelled, the given wavenumbers are accurate to within ± 0.5 cm^{-1}.

Raman signatures of oligonucleotides composed of diheptads and of reference oligonucleotides with the same base pairs content but arbitrary sequences. Figure 5.3 compares the Raman spectrum of ⟶⟵ (trace 1) with the spectra of $⟶_2$ (trace 2), ⟵⟶ (trace 3), MUT (trace 4), REF1 (trace 5), and REF2 (trace 6), respectively. Three times enlarged difference spectra shown in Figure 5.3 were calculated by the subtraction of $⟶_2$ (trace 2), ⟵⟶ (trace 3), MUT (trace 4), REF1 (trace 5), and REF2 (trace 6) spectrum from the ⟶⟵ spectrum. The data indicate primarily C2'-endo/anti deoxynucleoside conformers with gauche$^-$ (g^-) conformations for the phosphodiester torsion angles α and ζ (*88-89*). Figure 5.3 also demonstrates that although all the oligonucleotides adopt similar B-DNA structures, they differ in conformational details. The nature of structural differences of all Raman difference spectra of Figure 5.3 can be inferred from the interpretation of the difference spectrum (spectrum of ⟶⟵ minus spectrum of REF2) that exhibits the most pronounced differences.

The difference peak at 840 cm^{-1} and trough at 828 cm^{-1} indicate parent bands centered at 837 cm^{-1} in ⟶⟵ and 832 cm^{-1} in REF2 (not shown), respectively, and reflect different average backbone conformations of the two oligonucleotides. Similar differences have been observed between the spectra of oligonucleotides with AT- and GC-rich sequences and attributed to different minor-groove and major groove dimensions (*88, 96-97*). For AT rich sequences, the B-form marker occurs near 838-840 cm^{-1}. However, for sequences which are GC rich the phosphodiester Raman marker is located near 828-830 cm^{-1}. The X-ray crystal structures of oligonucleotides indicate relatively wide minor groove for GC-rich domains and relatively narrow minor groove for AT-rich domains (*98*). The data suggest that the major groove of ⟶⟵ is broader than that of REF2. The results clearly demonstrate that conformational details of both oligonucleotides are strongly influenced by the base pairs composition.

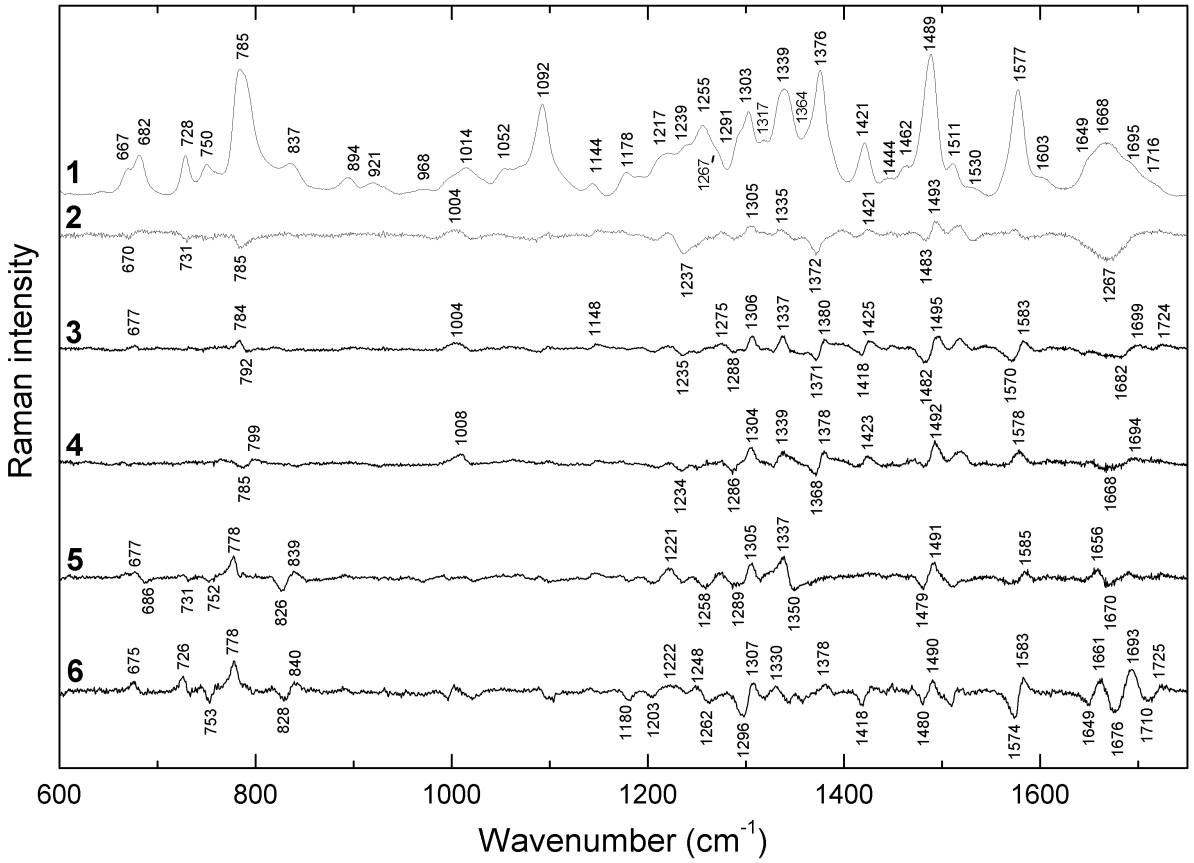

Figure 5.3: Trace 1 represents the H2O spectrum of ⟶⟵ given previously in Figure 5.2. Traces 2-6 indicate Raman difference spectra calculated by subtraction of $⟶_2$ (trace 2), ⟵⟶ (trace 3), MUT (trace 4), REF1 (trace 5), and REF2 (trace 6) from the spectrum of ⟶⟵. Experimental conditions are as given in the legend of Figure 5.2. Spectra were normalized with respect to the integrated intensity of the phosphate band near 1092 cm^{-1}.

The band at 1418 cm^{-1} is assigned to the CH_2 scissoring modes of C5'H_2 and C2'H_2 groups (*99*), the difference trough at 1418 cm^{-1} shows that this furanose Raman band changes its intensity without an apparent change in wavenumber. The perturbation reflects an altered residue environment rather than altered helix geometry (*100*). A change in deoxyribose ring vibrations is consistent with the interpretation given above for the 840/828 cm^{-1} difference feature.

Difference peaks near 675, 726, and 778 cm^{-1}, as well as difference features between 1200 and 1700 cm^{-1} reflect distinct sequence-directed base stacking. Adenine and thymine residues contribute to difference features at 675, 726, 1248/1262, 1307/1296, 1490/1480, 1583/1574, and 1661/1676 cm^{-1}. Because all dT and dA residues are centrally located and therefore expected to be stably paired in both oligonucleotides, these differences do not indicate fraying of AT pairs. The differences at 778, 1490/1480, 1493 and 1725/1710 cm^{-1} can be assigned to dC and dG residues. The relatively large contributions at 1490/1480 (primarily dG) and 1583/1574 cm^{-1} (both dA and dG) reflect more effective stacking of the purines in ⟶⟵. These minor wavenumber shifts together with features at 1725/1710 (dG) and 1307/1296 cm^{-1} (dA) might also indicate changed hydrogen bonding states of specific groups of adenine and guanine in the major and minor grooves. Subtle deoxynucleoside conformational differences and sequence-specific base stacking geometries may also contribute to the features at 675 (dT), 726 (dA), 753 (dT) and 778 cm^{-1} (dC), such contributions are also consistent with changed major-groove dimensions.

All the sequences have significantly different stacking properties and deoxynucleoside conformations. However, two groups with different major-groove dimensions could be defined. First, REF1 and REF2 indicate similar peak/trough feature at 839/826 and 840/828 cm^{-1}, respectively, reflecting very similar dimensions of the major groove. Second, ⟶⟵, $⟶_2$, ⟵⟶, and MUT have broader major-grooves compared to that of REF1 and REF2 according to the position of the B-DNA conformation marker near 837 cm^{-1} (*88, 96-98*). The major groove width is probably very similar in all of these oligonucleotides, because the 837 cm^{-1} band does not indicate any difference feature. However, very minor changes in the backbone structure of MUT are indicated by peak/trough features near 790 cm^{-1} that are sensitive to torsions of the DNA backbone (angles $\alpha, \beta, \gamma, \zeta$). It is a surprising observation that the oligonucleotides with operator DNA sequences that bind ω_2 specifically have broader major-groove dimensions than those with arbitrary sequences that are expected to bind unspecifically.

One base pair exchange (GC to CG) in the 19-bp long sequence of $\longrightarrow_2$ causes surprisingly significant perturbations to the stacking (compare trace 2 and 4 of Figure 5.3). Not only the stacking of guanine at 1490 cm^{-1} and cytosine at 1234 cm^{-1} is altered by the exchange, but also stacking of neighbouring adenines and thymines indicated at 1304, 1339, 1578, and 1376 cm^{-1} is influenced. Peaks in the difference spectrum (trace 4) indicate that bases in MUT DNA are more effectively stacked than those in $\longrightarrow\!\!\leftarrow\!\!\longrightarrow$ and $\longrightarrow_2$.

5.1.2. Raman Signature of Omega Protein

Figure 5.4 shows the Raman spectrum of the homodimeric omega protein, ω_2, in fully protonated (non-exchanged) form measured in H_2O buffer (trace 2), and the Raman spectrum of the partially deuterated ω_2 obtained in D_2O (trace 1). Trace 3 shows the computed Raman difference spectrum (trace 1 minus trace 2) and represents the native exchange, i.e. the exchange of hydrogen atoms that are exchangeable in the folded state of ω_2. Assignment of all the Raman bands of trace 2 and their corresponding H→D exchange wavenumbers of trace 1 are given in Table 5.2.

Information about the secondary structure of natively exchanged and protected sites of ω_2 can be deduced from the large difference features at the positions of the amide I and amide III bands (in H_2O) and the positions of the amide I' and amide III' bands (in D_2O). The Raman intensity at the positions of the amide III and amide I bands is reduced and causes troughs in the difference spectrum. Concomitantly, the Raman intensity at the positions of the amide III' and amide I' bands is increased and gives rise to difference peaks. Several trough/peak features are caused by the native state-deuteration induced frequency shift of amide III to amide III´. The contribution to the trough at 1237 and a peak 978 cm^{-1} is caused by β-strands, the trough/peak feature at 1274/966 cm^{-1} indicates α-helix, and feature at 1237 and 1249/926 cm^{-1} is caused by irregular structures. A weak band at 1260 cm^{-1} remains in the amide III region of ω_2 because of incomplete deuteration of α-helixes under the applied conditions of native exchange. The features of the amide I and amide I´ bands with troughs and peak, respectively, near 1681 and 1655 or 1638 cm^{-1} provide additional Raman signatures for native (incomplete) deuterium exchange of secondary structure elements.

A very weak amide II band at 1550 to 1560 cm^{-1} (Figure 5.4-2) represents N-H in-plane bending and C-N stretching of trans peptide groups. Deuteration of those groups

causes an intense amide II' band at 1465 cm^{-1} (Figure 5.4-1), and results in the most prominent feature of the difference spectrum with a peak at 1468 cm^{-1} (Figure 5.4-3). This band can be assigned to non-α-helical (unprotected) sites of ω_2 (*101*).

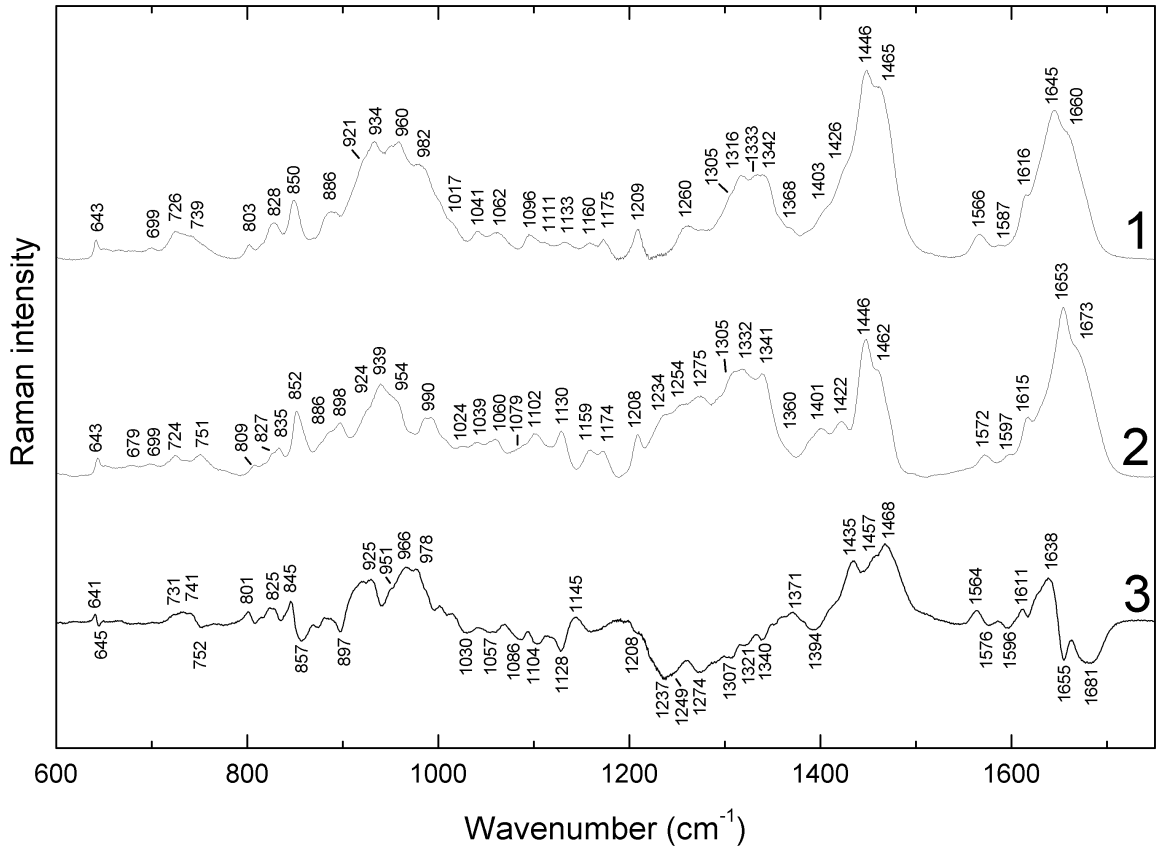

Figure 5.4: Raman spectra of ω_2. (1) Natively H→D exchanged ω_2. (2) Native ω_2. (3) Difference spectrum (spectrum 2 minus spectrum 1). Experimental conditions are as given in the legend of Figure 5.2. Peaks in the difference spectrum 3 appear when natively unprotected protons are exchanged against deuterons and the Raman bands are shifted. Peak positions of prominent Raman bands are labelled by the respective wavenumbers that are accurate to within ± 0.5 cm^{-1}.

Environment of Tyrosine Side Chains. The intensity ratio I_{850}/I_{830} of the tyrosine Fermi doublet at ~850 and ~830 cm^{-1} is an indicator of the tyrosine environment as it is sensitive to hydrogen bonding of phenolic OH groups (*82*). The crystal structure of ω_2 shows that the omega dimer is stabilized by monomer-monomer interactions between helices B and B' (*21*). Tyr66 makes a hydrogen bond with Glu61' and a salt-bridge is formed between Lys65 and Glu61'. The Tyr62 OH group is located on the surface of ω_2 and possibly makes a hydrogen bond with surrounding water molecules. The Fermi doublet of the four tyrosines of ω_2, Tyr 62, Tyr 66, Tyr 62', Tyr 66', has peaks at 852 cm^{-1}, 834, and 827 cm^{-1}. The intensity ratio of 2.3 indicates that tyrosine hydroxyls of ω_2 are acceptors of very strong hydrogen bonds formed with very acidic hydrogens of proton

donors (*82*). The result demonstrates that the hydrogen bonds of tyrosines formed to stabilize the omega dimer (ω_2) are reasonably strong. After H→D exchange (Figure 5.4-1) these bands marginally shift to 828 and 850 cm^{-1}, respectively, and change the intensity profiles, with the band at 828 cm^{-1} becoming sharper and more intense than the band at 850 cm^{-1}.

Several other tyrosine and aliphatic amino acid side-chains bands contribute to the ω_2 Raman spectra shown in Figure 5.4-1 and 5.4-2. The assignment of Raman bands and corresponding H→D exchange wavenumbers are listed in Table 5.2.

Table 5.2: Vibrational Assignments for Raman Markers of ω_2 in H_2O and D_2O solutions[a]

H_2O	D_2O	Assignment[b]	H_2O	D_2O	Assignment[b]
643	643	Y	1159	1160	V, I, [C-C stretch]
699	699	M	1174	1175	Y, [CH_3]
724	726	Y, M	1208	1209	Y
751	739	I, L, K, [CH_2], [CH_3]	1234		AmIII (strand)
809	803	?	1254		AmIII (coil, turns)
827	828	Y		1260	AmIII (helix)
835	828	Y	1275		AmIII (helix)
852	850	Y	1305	1305	[CH_2], AmIII (helix)
898	886	A, [C-C stretch]	1332	1333	[CH_2]
	921	AmIII (coil, turns)	1341	1342	[CH_2]
939	934	K, V, L, [C-C stretch]	1401	1403	[COO^-]
954	960	[CH_3]	1422	1426	[CH_2], [CH_3]
	960	AmIII (helix)	1446	1446	K, I, L, [CH_2]
	982	AmIII (strand)	1462	1465	A, I, V, L, Y [CH_2]
990		I, [C-C stretch]		1468	AmII
1024	1017	Y	1572	1566	?
1039	1041	[C-O, C-N stretch]	1597	1587	?
1060	1062	K, A, [C-C stretch]	1615	1616	Y
1102	1096	[C-C, C-N stretch]	1653	1645	AmI (helix)
1130	1133	V, I, L, [C-C stretch]	1673	1660	AmI (strand, coil)

[a] Raman data are from ω_2 spectra shown in Figure 5.4.
[b] Assignments to specific amino acid side chains (one letter abbreviations) are based upon literature data (*101-103*). Square brackets indicate chemical group frequencies common to more than one type of side chain. Amide (Am) modes are diagnostic of the indicated secondary structure.

Omega Variants. Two ω_2 variants were used to further characterize the ω_2–DNA complex. First, the β-sheet of ω_2 recognizes the major groove of the operator DNA and most probably some of the amino acids of the β-sheet make direct contacts with bases of operator DNA. The mutation of amino acids from the β-sheet that are able to make hydrogen bonds could provide information about key Raman features and identify direct

contacts with the operator DNA. As an attempt in this direction, ω_2-T29A, a mutant of ω_2, in which the Thr29 from the β-sheet was substituted by alanine, was introduced to reveal direct contacts with DNA. Second, the N-terminal arms of ω_2 might organize themselves along the DNA backbone as it is observed in the crystal structures of Arc repressor and Met repressor–operator DNA complexes (*29-30*). Arc and MetJ repressors and ω_2 belong to the same protein family and therefore similarities in the structures are expected. The ω_2-ΔN18 is a variant where the first 18 N-terminal residues were deleted. Some Raman markers would disappear in the spectrum of the ω_2-ΔN18–operator DNA complex compared to the spectrum of the ω_2–DNA operator complex, if the eighteen N-terminal amino acids of ω_2 participated in the interaction.

ω_2-T29A. The spectrum of ω_2-T29A is shown in panel A of Figure 5.5 (red trace) and compared with that of ω_2-wild type (blue trace). The difference spectrum (black trace) calculated by subtraction of ω_2-T29A spectrum from ω_2 spectrum shows only minor differences pointing to very similar structures of both variants. The Raman bands of ω_2-T29A are located at the same positions as ω_2 wild type. Wavenumber positions are the same as given in Table 5.2.

ω_2-ΔN18. Panel B of Figure 5.5 shows the spectrum of ω_2-ΔN18 (top trace) and a difference spectrum (bottom trace) that was computed from the spectra of ω_2 and ω_2-ΔN18 and smoothed for clarity. The bands of tyrosine were used to normalize the Raman spectrum of ω_2-ΔN18. The Raman spectrum of ω_2-ΔN18 differs significantly from that of ω_2. The most prominent differences are indicated by the shape of amide I and amide III bands. The deletion of N-terminal part of ω_2 may cause conformational changes in the protein structure. Those changes would lead to the perturbations of particular Raman vibrations in the ω_2-ΔN18. Thus, the Raman difference spectrum is a sum of contributions of the 18 deleted amino acids and the Raman signals coming from conformational changes between the common regions of ω_2-ΔN18 and wild type ω_2. A very intense broad peak at 1670 cm^{-1} of amide I and a band near 1250 cm^{-1} of amide III represent the secondary structure of the eighteen N-terminal amino acids. The positions of the bands indicate that the N-terminal amino acids are mostly unordered.

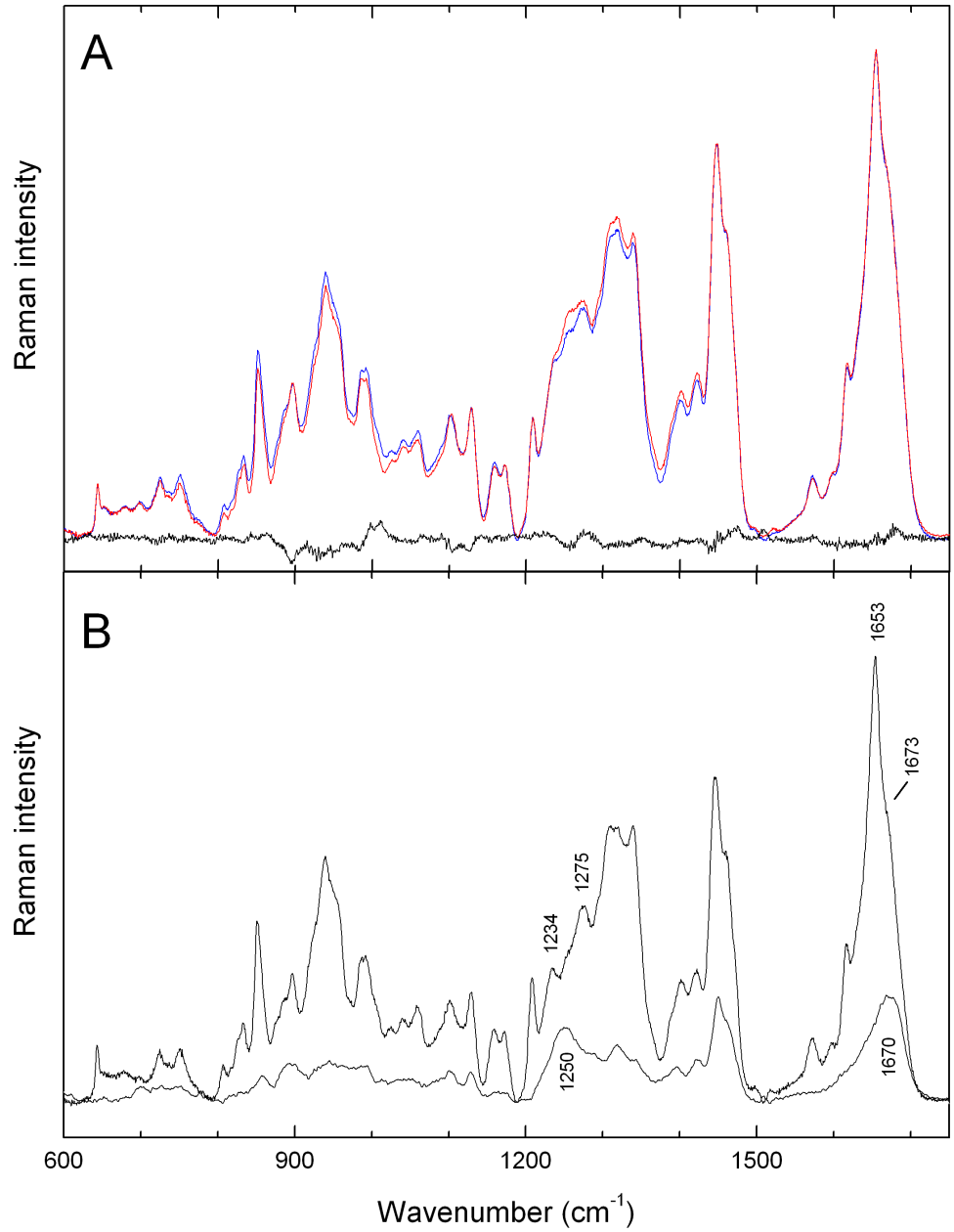

Figure 5.5: Raman spectra of ω_2 variants. (A) Raman spectra of ω_2 wild type (blue trace), ω_2-T29A (red trace) and their difference spectrum (black trace = blue trace – red trace). (B) Raman spectrum of ω_2-ΔN18 (top trace) and difference spectrum (bottom trace) calculated by subtraction of ω_2-ΔN18 spectrum from ω_2 wild type spectrum. Secondary structure elements are labelled with respective wavenumbers. Experimental conditions are as given in the legend of Figure 5.2.

5.1.3. Raman Signatures of the ω_2-DNA Complexes

Raman Analysis of the ω_2-⟶⟵ Complex. The Raman spectra of the ω_2-⟶⟵ complex and its components are given in panels A and B of Figure 5.6. Panel A shows the Raman spectrum of fully protonated ω_2, and panel B shows the spectrum of partially deuterated ω_2. The blue, green, and red traces represent the spectra of ω_2, ⟶⟵, and complex, respectively, as given before in Figures 5.4 and 5.2. The black

trace is the computed difference spectrum that was obtained by subtraction of the component spectra (green and blue traces) from the spectrum of the complex (red trace). When necessary, peak positions of deuterated samples will be given in parentheses.

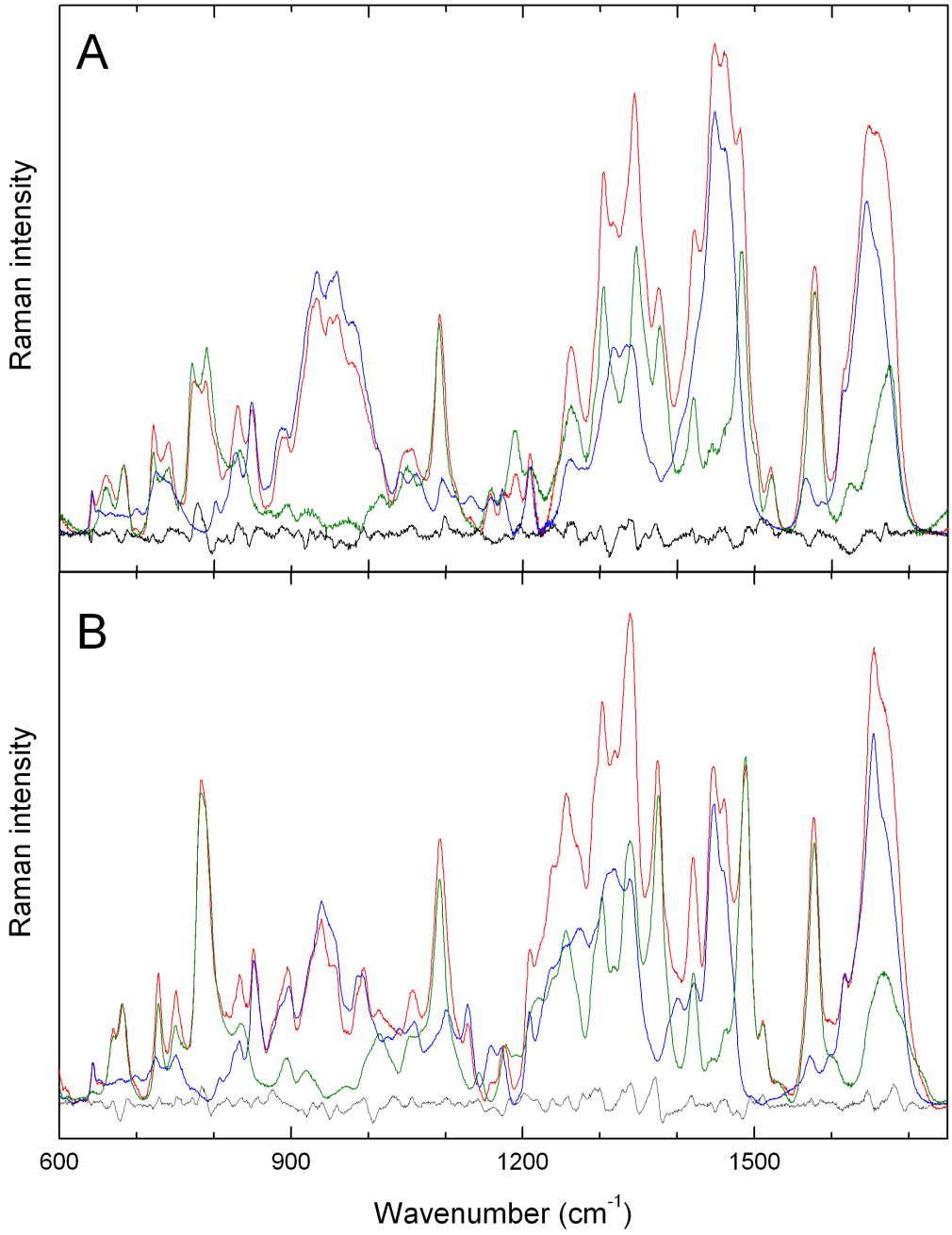

Figure 5.6: Raman spectra of ω_2, ⟶⟵ and ω_2⟶⟵ complex. (A) Protein in D_2O buffer; (B) protein in H_2O buffer (50 mM Tris-D_2O, pH or pD 7.5 and 50 mM NaCl). Protein concentrations are 63 mg/mL (H_2O) and 42 mg/mL (D_2O); spectra were excited at 488 nm, and data were collected at 22 °C in the region 600-1750 cm^{-1}. The blue traces show the Raman spectra of the isolated native and natively exchanged ω_2 from Figure 5.4. The green traces show the Raman spectra of ⟶⟵ from Figure 5.2. The red traces show the spectra of the ω_2⟶⟵ complex. The black bottom traces show the computed difference spectra obtained by subtraction of the isolated component spectra from the experimental spectrum of the complex. The spectra are normalized to represent the same amounts of protein and DNA in the complex and in free form.

Figure 5.7 shows the two amplified and, for clarity, smoothed difference spectra from Figure 5.6 (black traces) that are used for the further analysis. For smoothing the 11-point Savitsky-Golay algorithm was used. The features of the difference spectra provide information about conformational changes, structural rearrangements and interactions between the components of the complex.

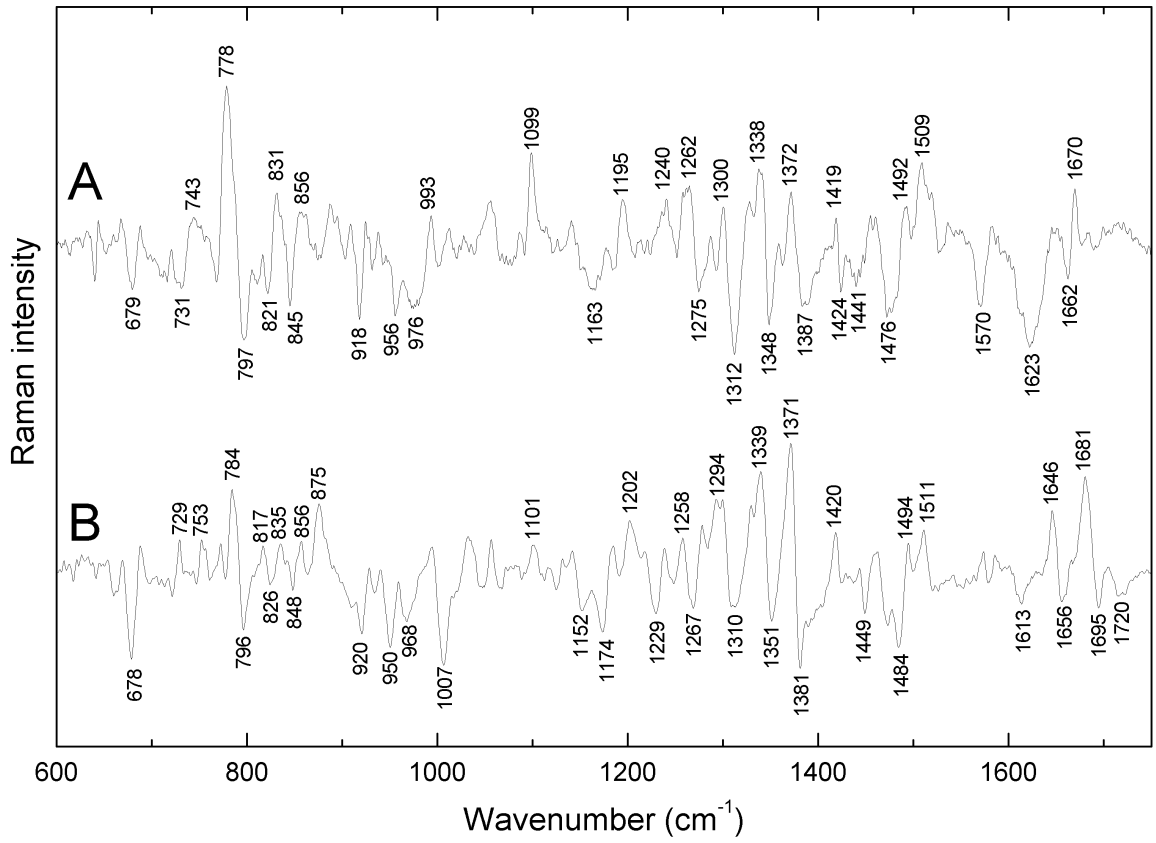

Figure 5.7: Enlarged Raman difference spectra (black bottom traces from Figure 5.6) of the ω_2⟶⟵ complex in D_2O buffer (A) and in H_2O buffer (B). Spectra were smoothed using the 11-point Savitsky-Golay algorithm.

The comparison of Raman difference spectra (Figure 5.8) of the ω_2⟶⟵ complex (green trace) and ω_2-REF2 mixture (red trace) reveals specific interactions between ω_2 and operator DNA. The red trace of Figure 5.8 clearly indicates spectral differences caused by interaction of ω_2 and REF2 oligonucleotide. Such alterations of the vibrations reflect unspecific binding of ω_2 to REF2 oligonucleotide at ~1 mM concentration. The difference features of ω_2⟶⟵ complex clearly exceed those of ω_2-REF2 mixture. We define that the difference features of ω_2-DNA complex reflect specific interaction only when they are stronger than that of ω_2-REF2 complex. Corresponding differences will be described below.

Backbone Conformation and Deoxynucleoside Conformation of ⟶⟵. The region between 700 and 900 cm^{-1} is characteristic for Raman markers of DNA backbone geometry (*89*). The 781 (771) cm^{-1} peak in the Raman spectra of DNA is assigned to cytosine. The 791 (790) cm^{-1} peak is assigned to a stretching vibration of backbone phosphodiester groups and diagnostic of B-form DNA backbone geometry, specifically of torsion angles α and ζ in *gauche*$^{-}$ range (*100, 104-105*). The 782 cm^{-1} cytosine and 791 cm^{-1} backbone bands overlap in DNA spectrum (measured in H_2O) to form a large 785 cm^{-1} peak. In D_2O, the frequency of the cytosine peak changes to 771 cm^{-1}, and the bands are clearly separated. The difference spectra show a prominent peak/trough feature at 796/784 (797/778) cm^{-1} that is probably caused by contributions only from the DNA backbone because of the position of the feature in higher wavenumber region. The H_2O and D_2O difference features indicate small conformational perturbations of the C5′-O5′-P-O3′-C3′ backbone network of DNA upon ω_2 binding (*96, 100*). Consistent with this observation are peak/trough features exhibited near 826/835 (821/831) and 848/856 (845/856) cm^{-1} (*90, 96*).

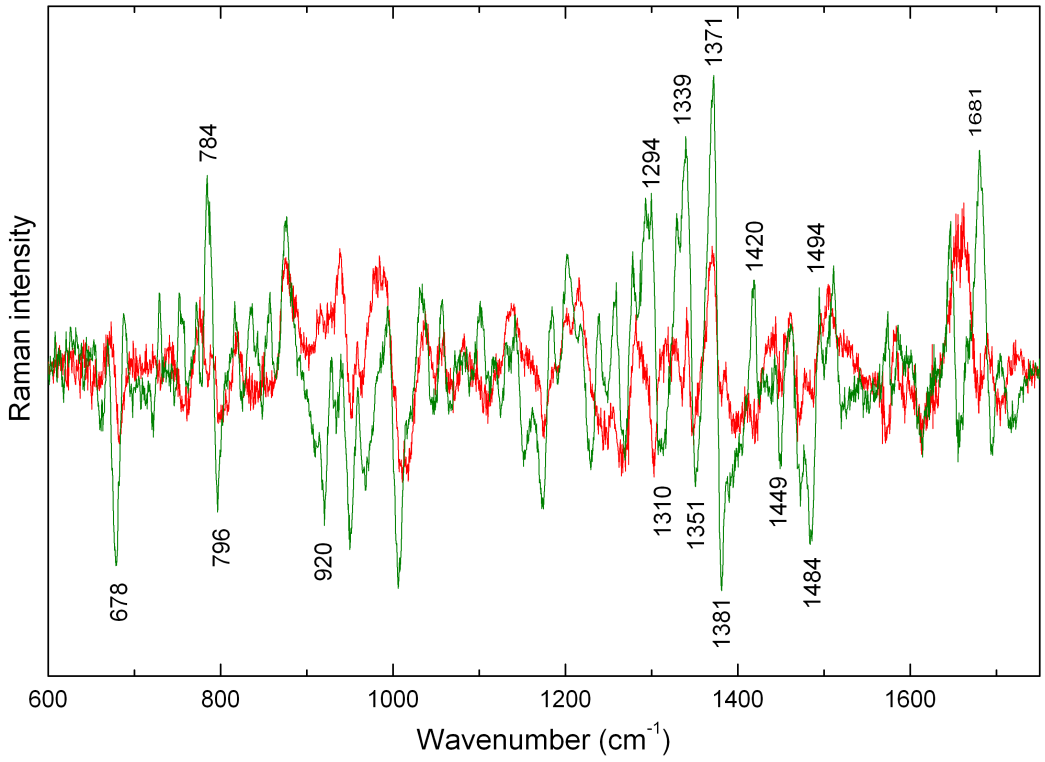

Figure 5.8: Enlarged Raman difference spectra. The green trace shows the difference spectrum of the ω_2-⟶⟵ complex from Figure 5.6-B and the red trace shows the difference spectrum of the ω_2-REF2 mixture from Figure 5.13. The most prominent differences are labelled by respective wavenumbers.

The double stranded oligonucleotide ⟶⟵ is composed of 47% GC and 53% AT base pairs. The difference spectra (Figure 5.7) indicate perturbations of the deoxynucleoside conformation of G, C and T residues. A very small thymine band at 750 (738) cm^{-1} is distorted under the influence of ω_2 binding. The troughs at 678 (679) cm^{-1} indicate small changes at dG. Perturbations in the cytosine nucleoside conformation marker is reflected in the difference spectra A (H_2O) and B (D_2O) by the peak at 1258 (1262) cm^{-1}.

Deoxyribose Ring and Protein CH_2/CH_3 Vibrations. Furanose vibrations were identified in Raman spectra of DNA near 930, 1420 and 1460 cm^{-1} and assigned to backbone vibrations (*95, 99-100*). In the spectrum of the ω_2 operator DNA the peak positions of those bands are at 921 (922), 1421 (1420) and 1462 cm^{-1} (Figure 5.2). Protein bands overlap with DNA in these spectral regions. An intense band at 939 cm^{-1} is due to a C-C stretch of α-helix, a COO^- symmetric stretch vibration causes the 1401 cm^{-1} peak, a band at 1422 cm^{-1} reflects CH_2 and CH_3 deformations; at 1446 cm^{-1} CH_2 scissoring modes are found (Figure 5.4). In Figure 5.7 a trough at 920 (918) cm^{-1} and at 1449 (1441) cm^{-1} as well as a peak at 1420 (1419/1424) cm^{-1} may be assigned to backbone vibrations of the DNA and/or changes in the protein. The furanose Raman bands change their intensity, the perturbations probably reflect an altered furanose environment, e.g. hydrophobic contacts with protein and maybe slight bending of DNA (*96*).

Protein changes at 1420 and 1449 cm^{-1} indicate altered CH_2 vibrations caused by rearrangement of protein side chains upon binding. The protein band at 1341 (1342) cm^{-1} is assigned to twist/wag vibrations of CH_2 groups. This band may contribute to the peak/trough feature at 1339/1351 (1338/1348) cm^{-1} is quite possible and could reflect rearrangement of protein side chains because of ω_2-ω_2 interaction upon cooperative binding of at least two ω_2 to its operator DNA. Similar effect was described in Arc-repressor-operator DNA complex (*29*).

Raman Markers of Base Environment and Interaction. Raman bands in the interval 1200-1750 cm^{-1} are sensitive to specific interactions between DNA bases and major groove-binding proteins (*93-94, 106-107*). The very intense Raman marker of the N7 guanine ring at 1490 cm^{-1} serves as an indicator of the protein-DNA interaction in the major groove. This band shifts upon hydrogen bond donation to an acceptor either to lower wavenumber (*90, 94, 106*) causing a peak/trough feature at ~1470/1490 or to higher wavenumber (*91*) resulting in a derivative band profile with difference peak at ~1495 cm^{-1}

and trough at ~1480 cm^{-1}. In the difference spectrum (Figure 5.7), the peak/trough feature at 1494/1484 (1492/1476)) cm^{-1} indicates hydrogen bond formation between guanine N7 and protein side chains. A further Raman marker assignable to major groove binding of proteins is a band near ~1720 cm^{-1} attributed to guanine O6 interactions (*90-91, 106*). The 1720 cm^{-1} difference trough observed in the difference spectra could be caused by guanine O6 forming a hydrogen bond with protein side chains. Altogether, the observations are consistent with the interaction of guanine with protein side chains from the β-sheet, which are able to produce two hydrogen bonds. The Arg31 could be responsible for such a contact (*21*). The x-ray diffraction data of ω_2⟶$_2$ crystal are currently available and the first model structure has been prepared, in which Arg31 contacts the guanine (Wilhelm Weinhofen personal communication).

The adenine Raman marker bands at 1339 (1346) and 1303 (1304) cm^{-1} are altered upon ω_2 binding. The peak/trough feature at 1339/1350 cm^{-1} of the adenine band near 1344 cm^{-1} was assigned to interactions of adenine $N6H_2$ and/or N7 in the Arc-operator DNA complex (see Chapter 5.3.3). Similarly, the peak/trough feature at 1339/1351 cm^{-1} could reflect the hydrogen bond formation of adenine $N6H_2$ and/or N7 groups. Another adenine derivative feature with peak at 1300 (1294) cm^{-1} and trough at 1312 (1310) cm^{-1} points to the existence of a direct contact of an adenine residue with ω_2.

The Raman peak at 1376 (1378) cm^{-1} is assigned to the thymine exocyclic $C5H_3$ group. Intensity increase of this band is correlated with increased hydrophobicity in the surrounding of thymine $C5H_3$ groups, as observed in repressor–DNA complexes where the thymine $C5H_3$ groups are shielded by hydrophobic side chains of the bound repressor (*90, 94*). The difference spectrum of ω_2⟶⟵ complex shows a peak/trough feature 1371/1381 (1372/1387) cm^{-1}. For the hSRY-HMG–DNA system, similar features were observed but so far not definitely interpreted, although protein contacts are considered as possibly responsible (*100*). In addition, the thymine C4O vibrations at ~1650 and ~1673 (1667) cm^{-1} (*105, 108*) indicate peak/trough features at 1646/1656 cm^{-1} in H_2O and 1670/1662 cm^{-1} in D_2O solution suggesting a hydrogen bond formation of ω_2 with C4O of thymine.

These Raman difference features show that possible candidates for direct contacts in the major groove of the operator DNA with ω_2 are guanine, adenine, and thymine residues. The interaction marker for cytosine contacts has not been revealed so far. It is expected to

be found in the region of most prominent cytosine Raman bands between 1200 and 1300 cm^{-1} (see Chapter 5.3.3).

Secondary Structure of ω_2. In the difference spectra, features between 1200 and 1300 cm^{-1} could be assigned to conformational changes of ω_2 upon complex formation. In the complex, amide III and amide I overlap with strong bands of DNA. Therefore in some spectral regions it is difficult to discriminate between spectroscopic signals from protein or DNA. H→D exchange helps to assign at least the amide III band because it shifts from 1230-1310 cm^{-1} in H_2O to the lower wavenumbers (900-1000 cm^{-1}) of the amide III' band where protein overlaps with weak DNA bands. However, comparison of the H_2O and D_2O difference spectra does not exhibit clear spectral changes of the amide III' and III bands between 900 and 1000 cm^{-1}, as well as between 1300 and 1220 cm^{-1}, respectively. Complex formation obviously induces only minute changes in regions of the protein spectrum where secondary structure is indicated. These changes, if any exist, are very difficult to detect by means of Raman difference spectroscopy. We conclude that the ω_2 secondary structure is conserved in the complex and very similar to that of free ω_2 in solution.

Raman Analysis of ω_2 Protein in the Complexes with Mono- Di- and Tetraheptads. The monomers of ω_2 dimer are C2-symmetry-related counterparts. The ω_2 binds specifically and with high affinity to at least two consecutive copies of a heptad sequence (Figure 5.1). Sequences of oligonucleotides composed of diheptads in ⟶⟵ and ⟵⟶ orientation have a palindromic symmetry of the two ω_2 binding sites (heptads) and will probably bind the omega dimers in a symmetry related manner. Oligonucleotides with heptads in head-to-tail orientation ⟶⟶ apparently do not have symmetry-related binding sites. Therefore the two ω_2 dimers should bind sequentially and the resulting complex should not have a two-fold symmetry axis. The promoter sequences of genes regulated by ω_2 are not only composed from symmetric diheptads, but also there are up to 10 heptads in different orientation, including sequential arrangements (Figure 1.3). To gain an understanding of the symmetry effects on ω_2 binding, complexes of ω_2 with DNA containing heptads in different orientation and number were studied. Differences in the spectra are expected to reveal different binding modes of ω_2 to the diheptads because of different orientations of the heptads that result in different symmetries of the DNA.

Figure 5.9 shows the Raman difference spectra of complexes formed between ω_2 and ⟶, $⟶_2$, ⟶⟵, ⟵⟶, $⟶_4$, $⟶_2⟵⟶$ (from top to bottom). The

description of the Raman difference spectra is similar to that given above for the ω_2-⟶⟵ complex. The most prominent Raman difference features are highlighted by dashed lines that are labelled by respective wavenumbers. Surprisingly, all the difference spectra exhibit very similar spectral perturbations. They originate from bands of the deoxy-ribosyl-phosphate backbone and of purine and pyrimidine base residues, and provide strong evidence in favor of similar molecular mechanisms of binding. As mentioned above, the protein secondary structure is conserved upon binding. However, small changes in the conformations of protein side chains are expected because of possible ω_2-ω_2 interactions during cooperative binding and contacts with DNA.

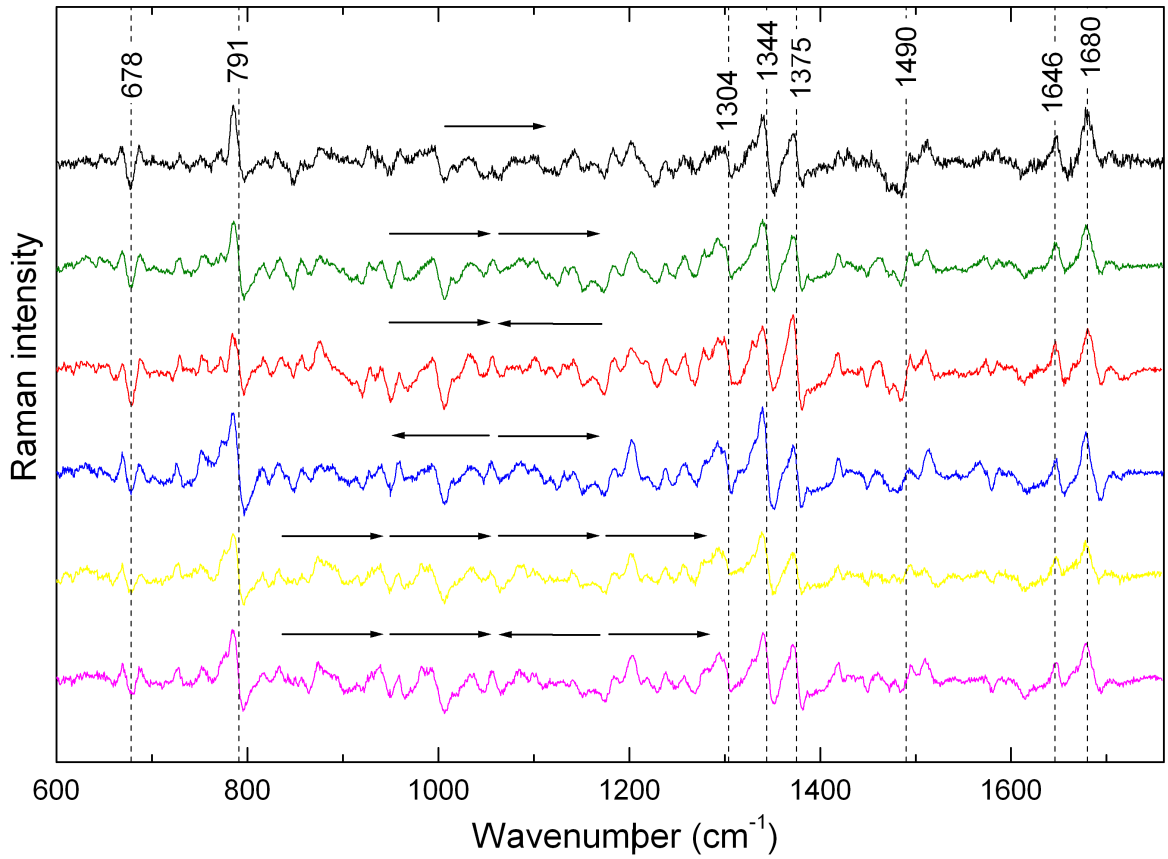

Figure 5.9: Raman difference spectra of ω_2-DNA complexes. Arrows represent the respective heptad sequences in orientations indicated by arrowheads. Experimental conditions were as given in the legend of Figure 5.6. Concentrations of ω_2 protein in the complexes are 85 mg/ml (ω_2⟶), 65 mg/ml (ω_2⟶$_2$), 63 mg/ml (ω_2⟶⟵), 68 mg/ml (ω_2-⟵⟶), 65 mg/ml (ω_2⟶$_4$), and 66 mg/ml (ω_2⟶$_2$⟵⟶). Spectra of complexes were normalized with respect to the integrated intensity of the phosphate band near 1092 cm^{-1}.

Intensity differences in the spectra of the ω_2-diheptad complexes occur at three most prominent Raman difference bands near 1375 (dT), 1344 (dA, CH_2 twist/wag), and 791 cm^{-1} (B-DNA backbone). The Raman intensities correspond to the Raman scattering

probabilities and the number of scattering molecular groups. For example, if a group X of molecule 1 interacts with a group Y of molecule 2 in the complex, the Raman difference band reflecting such interaction will occur. If there are two molecular interactions between groups X and Y of the same molecules, the Raman difference band will be located in the same position and its intensity will be higher. Differences in Raman intensities of the spectra shown in Figure 5.9 could be caused, first, by a different number of interacting residues. Such differences might reflect symmetry properties.

Second, the conformations of the diheptad oligonucleotides differ in a sequence dependent manner and are affected by the orientation of the heptads (Figure 5.3). The interaction between ω_2 and oligonucleotides may be influenced by a different geometry (symmetry) of DNA backbone and slightly different conformations of base residues (Figure 5.9) that are in close contact with protein side chains.

Third, differences in the conformation of the studied diheptads are characterized mostly by stacking interactions (Figure 5.2). Spectral changes upon complex formation could be caused by perturbations in stacking interactions.

Fourth, the backbone band at 791 cm^{-1} reflects changes in torsion angles α and ζ in *gauche*$^-$ range (*100, 104-105*). Raman marker of the DNA backbone occurs near 791 cm^{-1} and is composed from contributions of vibrations of all O-P-O groups. If the torsion angles α and ζ in *gauche*$^-$ range of one or more O-P-O groups are altered, the respective Raman difference band will appear near 791 cm^{-1}. The intensity of the feature will depend on the number of altered O-P-O groups and probably also reflect changes in the size of the torsion angles. Differences in the intensity of the Raman difference feature near 791 cm^{-1} might be attributed to different alterations in the size of the torsion angles α and ζ in the ω_2-diheptad complexes and/or to different number of O-P-O groups involved in the interaction in the ω_2-diheptad complexes. Thus, probably this feature also indicates different symmetry of the ω_2-DNA complexes.

Fifth, different symmetry of the binding sites might cause different ω_2-ω_2 interaction. Omega dimer forms four α-helices and one β-ribbon. In the Arc-, MetJ- and CopG-operator DNA complexes the helices of CopG, MetJ and Arc dimers interact and form a tetramer (*28-30*). Omega protein belongs to the same structural superfamily and therefore it is expected to make similar protein-protein contacts. If the binding site is switched from $\longrightarrow\!\!\leftarrow\!\!\longleftarrow$ to $\longleftarrow\!\!\longrightarrow$ or to $\longrightarrow_2$ and ω_2 preserves the same bases for interaction on each heptad, the orientation of ω_2 at the DNA must change. This would

affect the protein regions that are participating in intermolecular contacts. Such factors might contribute to the different intensities near 1344 cm^{-1}.

The complex formation between ω_2 and oligonucleotides composed of diheptads (tetraheptads) perturbs furanose vibrations and/or overlapping protein vibrations of CH_2 scissoring and deformation near 921, 1444, and 1420 cm^{-1}. A trough at 921 and a peak at 1421 cm^{-1}, however, do not occur in the ω_2-⟶ complex. These difference bands could be assigned to slight bending and/or ω_2-ω_2 interaction which are not expected in the complex containing only one ω_2 and one DNA heptad.

The Raman difference spectra of the two ω_2-tetraheptad complexes that are shown in Figure 5.9 do not reveal any significant differences compared to those of ω_2-⟶ and ω_2-⟶$_2$. The tetraheptad containing oligonucleotides bind four ω_2 per molecule. The signals of corresponding vibrations in the difference spectra are coming from four interaction sites on the DNA molecule. Small heptad orientation dependent differences in the perturbations of the DNA might be smoothed out by overlapping of these signals. Thus, the Raman difference spectra of ω_2-teraheptad complexes show average features similar to those of the ω_2-⟶$_2$ complex (Figure 5.9) and no symmetry differences could be revealed.

ω_2-T29A in Complex with ⟷. Interesting results were expected from the analysis of ω_2-T29A binding to an oligonucleotide composed of heptads. Thr29 is possibly engaged in direct interactions with DNA residues. Comparison of wt-ω_2 and ω_2-T29A binding to DNA could provide the identification of direct interactions of ω_2 with ⟷. The difference spectra would indicate missing Raman features in ω_2-T29A-DNA complex compared to that of ω_2-DNA, if Thr29 participated in a contact with DNA.

Figure 5.10 shows the difference spectra of the ω_2-T29A-⟷ complex (green trace) and the ω_2-REF2 mixture (red trace). The difference spectra demonstrate striking similarities between ω_2-T29A-⟷ complex and ω_2-REF2 mixture. These similarities reflect comparable unspecific interactions in both complexes. The loss of Thr29 completely changes the binding mode of ω_2-T29A and the protein binds no longer specifically to the ⟷. The substitution of an amino acid from the possible recognition region, which does not change the secondary structure of the protein, leads to complete loss of the binding specificity. The results suggest that the Thr29 directly participates in binding of ω_2 to the operator DNA and show that ω_2 uses the anti-parallel β-

ribbon to recognize the operator DNA sequence. However, the results do not provide the DNA base residue making very probably the hydrogen bond with Thr29.

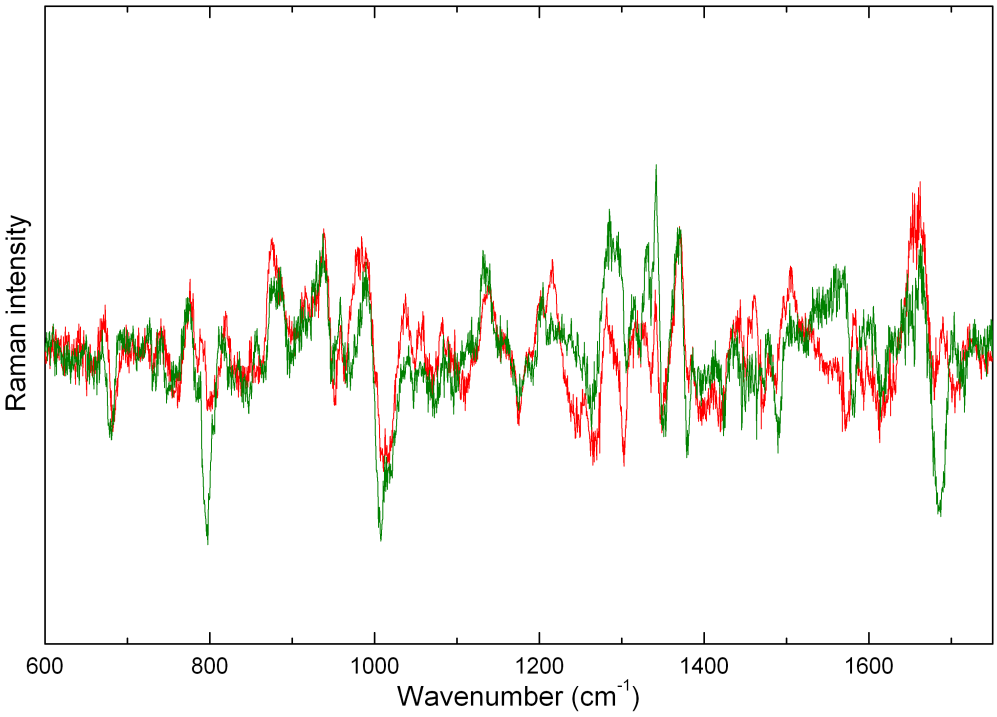

Figure 5.10: Enlarged Raman difference spectra. The red trace is identical with the black bottom trace of the ω_2-REF2 mixture shown in Figure 5.13. The green trace indicates the difference spectrum of the ω_2-T29A-←——→ complex. Experimental conditions were as given in the legend of Figure 5.6. The concentration of ω_2-T29A in the complex was 70 mg/ml. Spectra of complexes were normalized with respect to the integrated intensity of the phosphate band near 1092 cm^{-1}.

The ω_2-ΔN18-——→←—— Complex. The unstructured N-terminal parts of both Arc and MetJ repressors are involved in protein-operator DNA interaction and come into close distance with phosphate backbone (*29-30*). Similarities in the structure of ω_2-——→←—— and in the crystal structures of the Arc repressor– and MetJ repressor–operator DNA complexes (*29-30*) are expected. Out of 27 unordered N-terminal amino acids, 21 were not identified in the crystal structure of ω_2 (*21*). These amino acids could organize themselves along the phosphate backbone and the corresponding interaction would be reflected in the Raman difference spectrum. To analyse the importance of N-terminal amino acids of ω_2 for the binding to DNA, a deletion mutant missing 18 N-terminal amino acids, ω_2-ΔN18, was constructed. If N-terminal amino acids of wt-ω_2 interact with phosphates, these interactions and concomitantly the binding mode of ω_2 variants should be changed, and the difference spectrum of ω_2-ΔN18-——→←—— complex would show dissimilarities compared with that of the ω_2-——→←—— complex.

Figure 5.11 shows the Raman difference spectra of ω_2-ΔN18⟶⟵ (green trace) and ω_2⟶⟵ (red trace). Surprisingly, the spectra are nearly identical hardly indicating any differences in the structural changes that the two proteins might undergo upon DNA binding. Also, the difference spectra indicate the same conformational perturbations of the DNA. There are no extra features, and no features missing, either. Accordingly, either the 18 N-terminal amino acids do not interact with operator DNA or the interaction is not detectable by means of Raman difference spectroscopy.

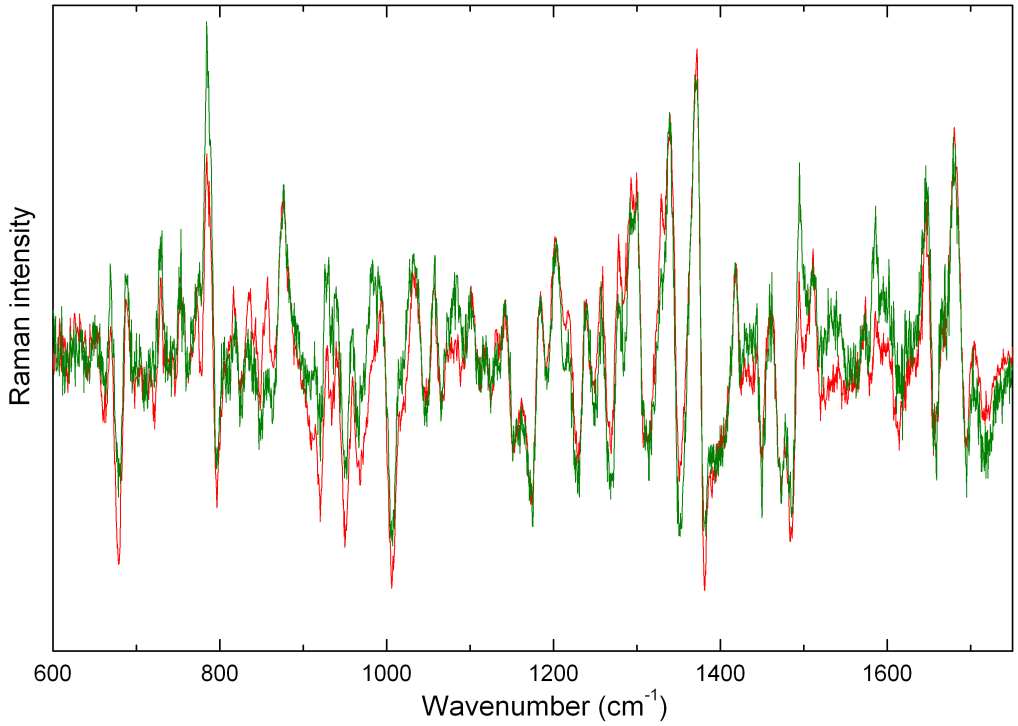

Figure 5.11: Enlarged Raman difference spectra. The red trace was shown as black bottom trace of ω_2-⟶⟵ complex in Figure 5.6. The green trace indicates the difference spectrum of the ω_2-ΔN18-⟶⟵ complex. Experimental conditions were as given in the legend of Figure 5.6. Concentration of ω_2-ΔN18 in the complex was 25 mg/ml. Spectra of complexes were normalized with respect to the integrated intensity of the phosphate band near 1092 cm^{-1}.

The ω_2-MUT Complex. The ω_2 binds with high affinity the sequences $\longrightarrow_2$, ⟶⟵, $K_{d,app}$ ~20 nm, and ⟵⟶ $K_{d,app}$ ~130 nm (*35*). Two heptads in inverted ⟶⟵ and divergent ⟵⟶ orientation have palindromic symmetry which allows the symmetry related binding of ω_2 to each of the two heptads, whereas adjacent heptads in tandem orientation $\longrightarrow_2$ are not symmetry related but provide identical binding sites for the ω_2, therefore the complex might differ in details of its conformation when compared to those of ⟶⟵ and divergent ⟵⟶. The modified sequence of $\longrightarrow_2$ called MUT,

where the central CG base pair of the first heptad was substituted by GC (Figure 5.1), has similar symmetry as the ⟷. The modification in ⟶$_2$ resulting in MUT introduces the central 5'-TGA-3' palindromic stretch in the oligonucleotide sequence.

Figure 5.12 compares the ω_2-MUT and ω_2⟶$_2$ complexes. Both difference spectra exhibit very similar profiles except of the difference band at 1679 cm^{-1} and peak/trough feature at 785/797 cm^{-1}. The features are significantly lower in the ω_2-MUT complex. The binding to just one site of the oligonucleotide would decrease intensities of all features. This decrease is probably less than 50%, as might be expected from the loss of one binding site, because of unspecific interactions with the modified half-site of the oligonucleotide. Introducing the symmetry element to the ⟶$_2$ oligonucleotide (MUT), it was expected to change the symmetry of ω_2 binding. As a consequence, the resulting difference spectrum should become similar to that of the ω_2-⟷ complex and differ from that of the ω_2-⟶$_2$ complex, if the central 5'-TGA-3' palindromic stretch was the main target of ω_2 binding.

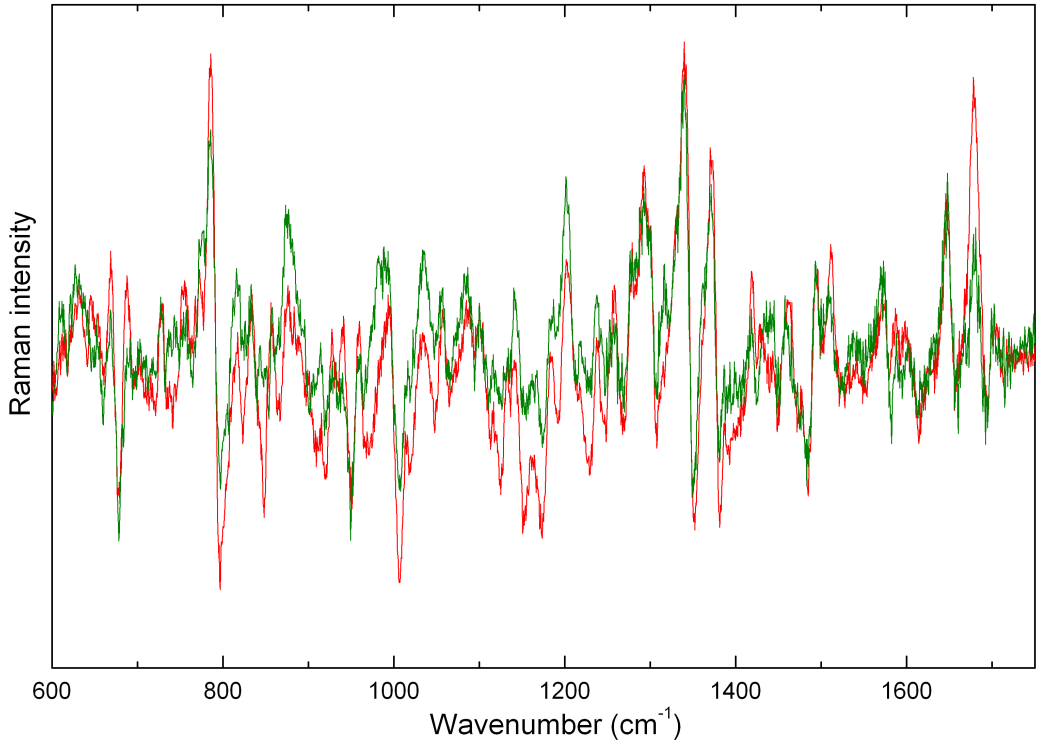

Figure 5.12: Enlarged Raman difference spectra. The red trace indicates the difference spectrum of the ω_2-⟷ complex, and the green trace indicates the difference spectrum of the ω_2-MUT complex. Experimental conditions were as given in the legend of Figure 5.6. Concentration of ω_2 in the ω_2-MUT complex was 66 mg/ml. Spectra of complexes were normalized with respect to the integrated intensity of the phosphate band near 1092 cm^{-1}.

The modification of the $\longrightarrow_2$ sequence does not apparently change the binding mode of ω_2. According to intensities of both difference spectra in Figure 5.12, it is quite likely that two ω_2 bind per MUT molecule that obviously provides two binding sites for ω_2. To reach the same binding mode as in the ω_2-$\longleftrightarrow$ complex, probably it would be necessary to substitute further base pairs within the heptad sequence. That would actually lead to the complete transformation of the central pentameric stretches of $\longrightarrow_2$ to that of $\longleftrightarrow$. The last and the first base pair can be substituted by GC without decreasing binding affinities (*35*). The Raman difference spectra suggest that not only the central stretch 5'-TGA-3', but also the base pairs at both ends of the stretch are important for symmetry-related binding of ω_2.

The Unspecific Interaction of ω_2 with REF2. The Raman spectrum of the ω_2-REF2 mixture is shown in Figure 5.13 (red trace). The green trace represents the oligonucleotide spectrum, and the red trace 3 is the ω_2 spectrum. The black trace is the Raman difference spectrum obtained by subtraction of the component spectra (green and blue traces) from the spectrum of the complex (red trace). The black bottom trace is the three times enlarged difference spectrum. Difference bands are labelled with respective wavenumbers only when they reflect an intensity change of at least 3% of its parent band.

The B-form conformation markers at 832 and 791 cm^{-1} indicate no difference features. The conformation of DNA backbone of REF2 oligonucleotide is not influenced by unspecific interactions with ω_2. The difference spectra reflect only small perturbations in the nucleoside conformation markers near 682 cm^{-1} (dG), 774/758 cm^{-1} (dC), and 1265 cm^{-1} (dC).

Increased hydrophobicity in the surrounding of thymine $C5H_3$ groups increases the intensity of the band near 1378 cm^{-1}, as observed in the Raman spectrum of wild type λ repressor–operator DNA complex (*90*), where the thymine $C5H_3$ groups are shielded by hydrophobic side chains of the repressor. Similarly, the difference spectrum of the ω_2-REF2 mixture shows a difference peak at 1370 cm^{-1} indicating shielding of thymine $C5H_3$ groups from water environment and giving evidence of close distance of both REF2 and ω_2. A trough at 1302 cm^{-1} shows that REF2 DNA is more effectively stacked in the mixture with ω_2 than free in solution.

The contacts of amino acid side chains and DNA are probably indicated by the peak/trough feature at 1460/1471 cm^{-1} as well as by troughs at 1419 and 1398 cm^{-1} assigned to protein CH_2 vibrations. Such contacts are possibly reflected also in C-C

stretching vibrations. The difference spectrum exhibits a corresponding trough at 1174 cm^{-1} and peaks at 1137, 984, 939 cm^{-1}.

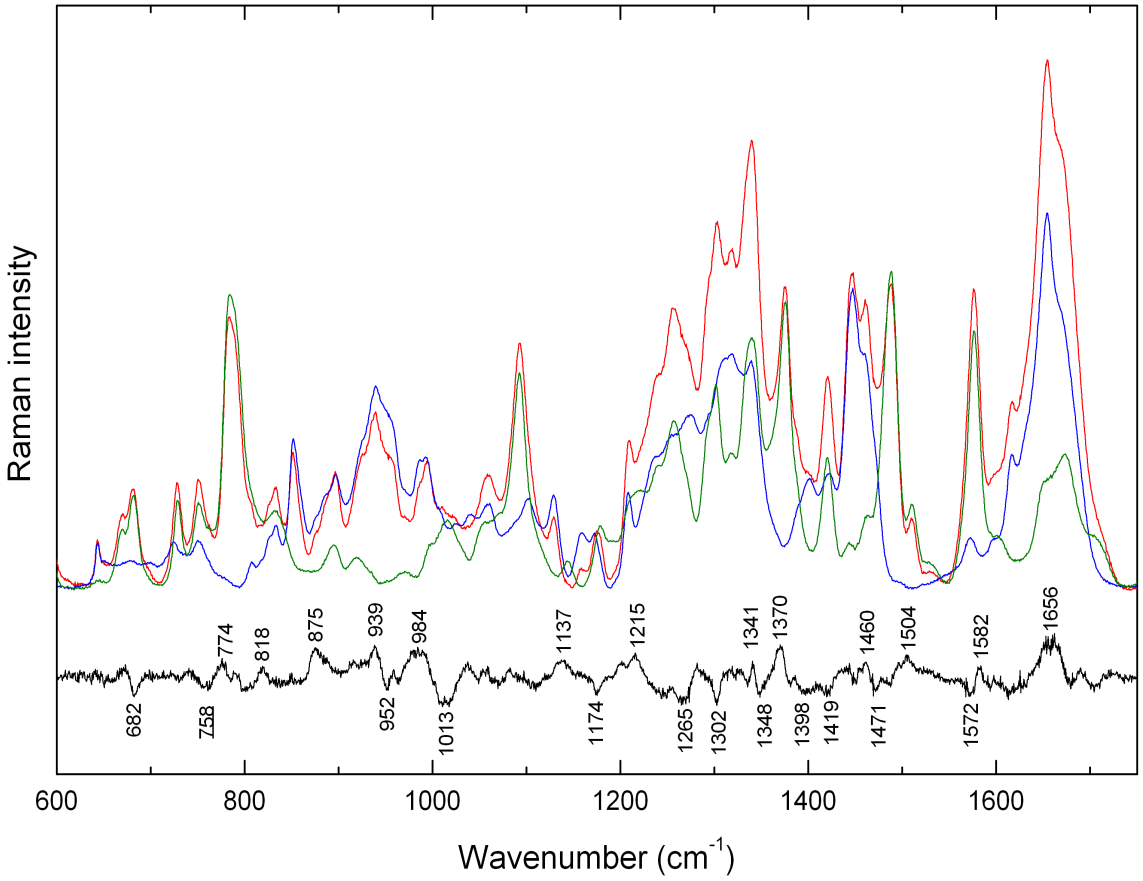

Figure 5.13: Raman spectrum in the region 600-1750 cm^{-1} of a mixture of ω_2 and REF2 oligonucleotide (black trace). The blue trace shows the Raman spectrum of the isolated ω_2 from Figure 6.2. The green trace shows the Raman spectrum of REF2 oligonucleotide. The black bottom trace shows the computed difference spectrum obtained by subtraction of the isolated component spectra from the experimental spectrum of the complex (red trace). The spectra are normalized to represent the same amounts of protein and oligonucleotide in the complex and in free form.

The very broad trough at 1013 cm^{-1} could be assigned to both DNA and protein. The bands of REF2 (dG, dT) overlap with C-C stretching bands of amino acid side chains. The same band appears in the difference spectra of ω_2-operator DNA (*36*). It is not possible to distinguish whether the band is caused by changes in the guanine and/or thymine environment or by perturbations of C-C stretching vibrations. Nevertheless, the band could be considered as an indicator of unspecific interaction of ω_2 and DNA.

5.2. Discussion: Omega Protein

The crystal structures of repressor-DNA complexes of MetJ (*30*), Arc (*29*), CopG (*28*), and NikR (*31*) have shown that in those cases two repressor dimers bind to double-stranded operator DNA. The binding centers between two dimers are separated by 8 bp, 11 bp, 9 bp, and 16 bp for MetJ, Arc, CopG, and NikR, respectively. For the ω_2 protein, the binding centers of two dimers are 7 bp apart in agreement with the heptad repeat organization of operator DNA. Raman difference spectra (Figure 5.7) exhibit the interaction with adenine, guanine, and thymine in the major groove showing that the central 5′-TCA-3′ (5′-AGT-3′) motif of the heptads might be the main target site for ω_2 binding to operator DNA. This is in agreement with hydroxyl radical footprinting experiments (*35*). Two TCA sites of the operator sequence are separated by 4 bp. The space between the directly interacting binding sites amounts to be 5 bp and is identical for both CopG and Arc operator. The size of the binding sites is different; Arc repressor covers 6 bp on each half-site and CopG 5 bp.

The comparison of DNA sequences with the same base pair composition (Figure 5.3) clearly demonstrates that even a single base pair exchange (GC to CG) in the sequence causes perturbations to the DNA conformation. Such conformational changes might be critical for protein-DNA recognition process. Difference spectra of Figure 5.3 have also shown two groups of oligonucleotides with sequence dependent differences of the major-groove dimensions. Interestingly, the major groove of oligonucleotides that bind ω_2 unspecifically is narrower than the major groove of the heptads in the operator DNA sequence. Probably ω_2 binding is sensitive to the dimensions of the major-groove.

A major difference in the heptad arrangements of the studied oligonucleotides concerns the symmetry of the binding sites. The diheptads ($\longrightarrow\!\!\longleftarrow$ and $\longleftarrow\!\!\longrightarrow$) contain symmetry elements with different sequences, and the diheptad $\longrightarrow_2$ is without palindromic sequence element (Figure 5.1). Nevertheless, ω_2 binds to these diheptads with very similar affinity and specificity (*35*). Sequence selective recognition by ω_2 was tested by substitution of every base pair of the upstream heptad (5'-$^{A}/_{T}$ATCAC$^{A}/_{T}$-3') of a diheptad, whereas the downstream heptad was not modified (35). The results revealed that replacement of a base pair from the pentameric central 5'-ATCAC-3' stretch reduces the binding affinity dramatically. However, substitution of the first or last base pair of the heptad does not affect the binding. The same study has shown that the insertion of 1 to 7

bp between two diheptads reduces the binding affinity by 5- to 6-fold. The Raman difference spectra of operator DNAs (Figure 5.3) clearly indicate differences in stacking and minor perturbations to the DNA backbone. Probably, the geometries of the DNA backbone in the central 5'-ATCAC-3' stretch are essential for the high affinity binding of ω_2 to operator DNA. Any changes in the pentameric central stretch of the heptad sequence would not only lead a loss of specific interactions but also change the DNA backbone geometry and concomitantly reduce the binding affinity to the oligonucleotide with modified sequence. A substitution of a base pair must not obligatorily change the hydrogen bonding pattern with ω_2. The Raman difference spectrum of ω_2-MUT complex (central CG of the first heptad of $\longrightarrow_2$ was changed into GC) did not exhibit any significant differences in comparison to the ω_2-$\longrightarrow_2$ complex (Figure 5.11). The binding affinity of ω_2 to the MUT sequence is obviously decreased (*35*); nevertheless, a complex is formed at the high concentration of about 1 mM used for the Raman measurement.

Modification of $\longrightarrow_2$ (change of the central CG of the first heptad into by GC) introduces a symmetry element to the sequence (Figure 5.1). The first heptad contains now a central 5'-TGA-3' triplet that forms a palindrom together with the 5'-AGT-3' triplet of the second heptad. The arrangement of the 5'-TGA-3' and 5'-AGT-3' elements is identical to that in the $\longleftarrow\longrightarrow$ diheptad. According to the Raman spectrum the ω_2-MUT complex indicates no perturbations in comparison with the ω_2-$\longrightarrow_2$ complex spectrum. Specific interactions of ω_2 with the modified $\longrightarrow_2$ either remain similar to that in the ω_2-$\longrightarrow_2$ complex or can not be identified because of limitations of the Raman spectroscopy technique. Since the binding of ω_2 is not affected by the CG to GC substitution, it is reasonable to assume that ω_2 does not make a hydrogen bond to the central GC or does not distinguish between G and C or bind to both G and C. The presence of the TGA/AGT element in the ω_2-MUT complex is not sufficient for the appearance of difference features that are similar to that of the ω_2-$\longleftarrow\longrightarrow$ complex. The data support the notion that the pentameric central 5'-GTGAT-3' stretch in $\longleftarrow\longrightarrow$ and 5'-ATCAC-3' stretch in $\longrightarrow\longleftarrow$ contains the binding sequence and probably also represents the most favorable local conformation of DNA for ω_2 binding.

Arc, CopG and ω_2 differ in the number of amino acids that compose the DNA-binding β-sheets. The NMR structure of Arc repressor (PDB 1arr) identified amino acids 6 to 16 in the β-sheet. The crystal structures of Omega (*21*) and of CopG (*28*) have shown

that β-sheets are comprised of amino acids 28 to 32 and 2 to 8, respectively. The amino acids of the β-sheet make hydrogen bonds with base residues in the major groove of the operator DNA. The antiparallel β-ribbon of ω_2 is very short and consists only of 10 amino acids. Two arginine residues (Arg31 and Arg31') and threonine residues (Thr29 and Thr29') are directed toward the solvent out of the protein β-sheet core (*21*). The interaction of Arg31 with the DNA has been suggested recently (*21*). To check whether the Thr29 is involved in the interaction with operator DNA the ω_2 variant with a Thr29 to Ala29 exchange (ω_2-T29A) was introduced. Collected Raman spectra of wt-ω_2 and ω_2-T29A (Figure 5.5A) indicate very similar structures and show only very small differences probably caused by minor local rearrangements. Raman difference spectra of the ω_2-T29A-⟵⟶ and ω_2-REF2 complexes (Figure 5.10) indicate that the ω_2 variant with a Thr29 to Ala29 exchange completely looses its specificity to the operator DNA binding sites. The spectrum of ω_2-T29A-⟵⟶ complex reflects only unspecific interactions of operator DNA and ω_2-T29A. The present data suggest that ω_2-Thr29 is essential for the ω_2-operator DNA interaction. Consequence of the Thr29 to Ala29 exchange is possibly the loss of some direct contacts (e.g. hydrogen bonds) of ω_2-T29A in the complex with operator DNA which transforms specific to unspecific interactions similar to the situation in the ω_2-REF2 complex.

To gain further information about the complexity of ω_2 binding, ω_2-ΔN18 variant with 18 deleted N-terminal amino acids was constructed to check the role of the stretch of unordered N-terminal amino acids (*21, this work*) in the interaction with operator DNA. Both Arc and Met repressor contact the phosphate backbone with their N-terminal amino acids (*29-30*). Nearly identical Raman difference spectra of ω_2-ΔN18-⟶⟵ and ω_2-⟶⟵ complexes (Figure 5.11) indicate very similar conformations of both complexes. The interaction of 18 N-terminal amino acids with phosphate backbone is either invisible to the means of Raman spectroscopy or there is no such a contact. In addition, it has been shown that plasmid-based variants of ω_2 lacking the first 20 residues, specifically repress utilization of chromosomal based $P\delta$ promoter (*35*). Therefore, the involvement of a flexible N-terminus in binding of ω_2 and operator DNA is quite unlikely. However, the N-terminal unordered stretch is 27 residues long and the data do not rule out that amino acids located close to the β-sheet might interact with the phosphate backbone. Such interactions are known in the Arc– and MetJ–operator DNA complexes (*29-30*).

DNase I and chemical footprinting showed that ω_2 protein binds with comparable high affinity to diheptads in $\longrightarrow_2$ and $\longrightarrow\longleftarrow$ orientation, $K_{d,app}$ ~ 20 nM, but binds to a diheptad in the $\longleftarrow\longrightarrow$ orientation with ~ 6-fold lower affinity, $K_{d,app}$ ~ 130 nM (*35*). The differences in dissociation constants among ω_2-diheptad complexes possibly reflect different symmetries within the complexes. The similar effect was observed for Raman difference spectra of ω_2-diheptad complexes (Figure 5.9), in which several Raman features are perturbed differently. In addition, diheptads (Figure 5.3) that specifically bind ω_2 have similar conformations but differ in their stacking properties. The most striking dissimilarities occur between the difference spectra of ω_2-$\longleftarrow\longrightarrow$ and ω_2-$\longrightarrow\longleftarrow$ complexes. Perturbations in difference features of ω_2-diheptad complexes (Figure 5.9) could be caused by a different number of contacts with adenine and thymine, and/or ω_2-ω_2 interaction, and/or different local conformational perturbation of adenosine and thymidine.

5.3. Results and Interpretation: Arc Repressor

5.3.1. Fluorescence and CD Measurements of Arc and Arc–DNA Complexes

Figure 5.14 shows tryptophan fluorescence spectra of Arc-wt (trace 2), Arc-F10H (trace 4), Arc-wt– and Arc-F10H–operator DNA complexes (trace 1 and 3). The peak positions of the Arc-wt (327 nm) and Arc-F10H (333 nm) fluorescence spectra differ by ~6 nm indicating that the mutation of phenylalanine to histidine significantly influences the surrounding of Trp14 and decreases the hydrophobicity of the Trp14 environment. In the complex with operator DNA, the fluorescence spectra of both complexes downshift for ~2 nm. Thus, the Trp14 environment becomes slightly more hydrophobic. The mixture of Arc-wt or Arc-F10H and non-operator DNA exhibits no change. This indicates, as expected, that Arc-wt and Arc-F10H do not bind to DNA with arbitrary sequence at the conditions of the experiment, and consequently the hydrophobicity of the Trp14 surrounding is not disturbed.

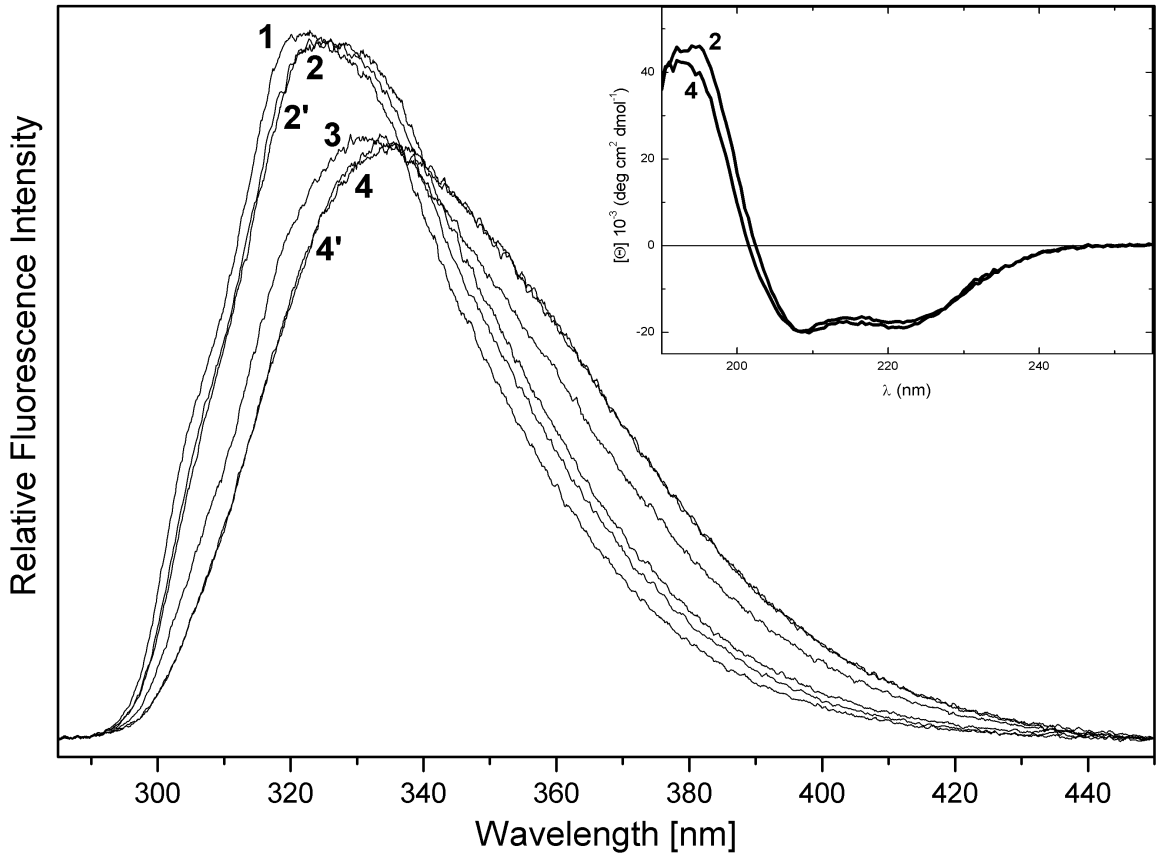

Figure 5.14: Fluorescence spectra (285-450 nm, 280 nm excitation) of Arc-wt–operator DNA complex (trace 1), Arc-wt (trace 2), Arc-wt–REF2 mixture (trace 2'), Arc-F10H–operator DNA complex (trace 3), Arc-F10H (trace 4), and Arc-F10H–REF2 mixture (trace4'). The samples were measured at concentrations ~0.09 mg/mL for proteins and ~0.13 mg/mL for complexes. Insert: CD spectra of Arc-wt (spectrum 2) and Arc-F10H (spectrum 4) at concentrations of ~0.6 mg/mL. Fluorescence and CD data were collected in 50 mM Tris/HCl, 100 mM KCl, 10 mM $MgCl_2$, at pH = 7.4 and at 23 °C.

The inset of Figure 5.14 shows CD spectra of Arc-wt (trace 2) and Arc-F10H (trace 4) that are very similar with only minor wavelength shift of the zero point transition indicating very similar secondary structures of the two proteins.

5.3.2. Raman Signature of Arc-wt and Arc-F10H Repressor Proteins

Figure 5.15 shows the Raman spectra of Arc-wt (solid trace) and Arc-F10H (dashed trace). The spectra are characterized by strong amide I bands (1640-1680 cm^{-1}) centred near 1650 cm^{-1} and by complex amide III bands (1230-1310 cm^{-1}). For a more detailed comparison of the two Raman spectra a difference spectrum was computed (Figure 5.15, bottom trace) by subtraction of the Arc-F10H spectrum from that of Arc-wt. A positive difference peak indicates higher Raman intensity in the spectrum of Arc-wt compared to the intensity at the corresponding position in the spectrum of Arc-F10H, and a negative difference trough is caused by lower intensity in the spectrum of Arc-wt and higher intensity in the spectrum of Arc-F10H.

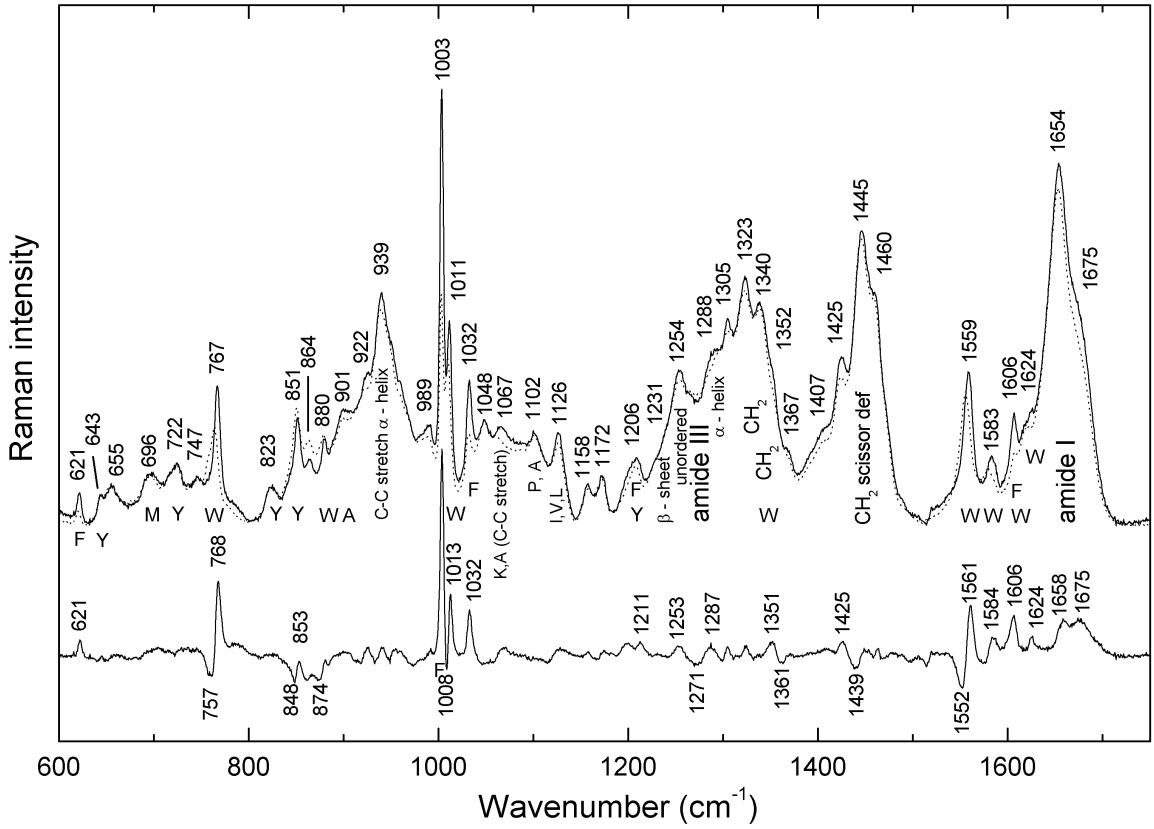

Figure 5.15: Raman spectra in the region 600-1750 cm^{-1}. The spectra at the top are that of Arc-wt (solid trace) and Arc-F10H (dashed trace). The bottom trace shows the Raman difference spectrum (solid trace minus dashed trace). Samples contained 20 and 41 mg/mL of the Arc-wt and the Arc-F10H, respectively, in 50 mM Tris/HCl, 100 mM KCl, 10 mM $MgCl_2$, at pH 7.4. The samples were excited at 488 nm and the data were collected at 22 °C. Spectra were normalized with respect to the CH_2 scissoring vibration at 1445 cm^{-1}. Raman band assignments to amino acids (one letter code) or amide vibrations are from ref 94, 102-103.

Phenylalanine. The difference peaks near 622, 1004, 1032, 1211, 1584, 1606 cm^{-1} indicate Phe vibrations and reflect the fact that Phe residues (Phe10/10') are present in Arc-wt but not in Arc-F10H.

Environment of Tyrosine Side Chains. Tyrosine forms a doublet in the Raman spectrum of Arc-wt with a very sharp, relatively intensive peak at 851 cm^{-1} and a smaller and broader band at 823 cm^{-1} (Figure 5.15, solid trace). The intensity ratio I_{851}/I_{823} has an extraordinarily high number of 2.9 and points to the formation of a very strong hydrogen bond with the phenoxyl oxygen of tyrosine as an acceptor (*82*). In Arc-F10H the higher wavenumber component of the tyrosine doublet changes its frequency as indicated by the peak/trough feature at 853/848 in the difference spectrum (Figure 5.15, bottom trace). The intensity of the band remains the same, thus, the difference feature does not reflect a change in the hydrogen bonding state of the Tyr residues in the mutant protein.

Tryptophan. Both Arc-wt and Arc-F10H contain a unique Trp14/14' that is localized in the DNA-binding β-sheet of the protein. The Trp band near 1549 cm^{-1} (called W3 mode) assumes wavenumber values between 1542 and 1557 cm^{-1} depending on the absolute value of the $C_\alpha C_\beta$-C_3C_2 torsion angle $|\chi^{2,1}|$ which usually varies between 60° and 120°. According to ref 109 the torsion angle $|\chi^{2,1}|$ can be calculated from experimentally determined wavenumber X of the W3 mode using the empirical equation: $X = 1542 + 6.7(\cos 3|\chi^{2,1}| + 1)^{1.2}$. In the Arc-F10H spectrum the band is positioned at 1555 ± 0.5 cm^{-1}. This wavenumber position corresponds to an average $|\chi^{2,1}|$ value of ~106°. In the Arc-wt spectrum the band has the extreme position of 1559 ± 0.5 cm^{-1}, and the protein difference spectrum shows a very prominent difference peak/trough feature at 1561/1552 cm^{-1} with 35 % relative intensity change compared to the parent band of Arc-wt. This observation suggests a large conformational difference for Trp14/14' in Arc-wt and Arc-F10H. Unfortunately, for extreme wavenumbers below 1542 and above 1557 cm^{-1} the empirical equation given above is not applicable because the calculation would result in senseless absolute values >1 for the cosinus function. Therefore $|\chi^{2,1}|$ cannot be calculated in the usual manner. However, the NMR structure of Arc-wt (PDB 1BAZ) shows a value $\chi^{2,1}$ of approximately –9°. From the NMR data of Arc-wt and the Raman data of Arc-F10H follows that a point mutation in the neighbourhood of Trp14/14' results in a remarkably large rotation of the Trp residue from –9° in Arc-wt to ~|106°| in Arc-F10H.

The Trp vibrations are very sensitive to the indole ring environment. In Arc-wt the position of the indole ring vibration at 880 cm^{-1} (called W17 mode) is indicative for a

buried Trp residue with an exocyclic 1NH group that is not (or only weakly) participating in hydrogen bond formation (*84*). The position and intensity of this band differs in the spectra of Arc-wt and Arc-F10H. In the Arc-F10H spectrum, a new band with lower intensity appears at 878 cm^{-1} as shown by the difference trough at 874 cm^{-1} (Figure 5.15, dashed trace). This feature indicates that Trp14/14' of Arc-F10H forms a hydrogen bond of obviously higher bond strength compared to that in Arc-wt. The observation correlates with the perturbation of the $|\chi^{2,1}|$ angle described before.

Hydrophobic interactions may influence the hydrogen bonding state of Trp14/14'. For model compounds in solution the components of the Fermi doublet of tryptophan are found at about 1360 and 1340 cm^{-1}. The intensity ratio $R=I_{1360}/I_{1340}$ serves as a hydrophobicity marker. The 1360 cm^{-1} component of the doublet is strong in hydrophobic solvents whereas in hydrophilic environment the 1340 cm^{-1} component is stronger. R is below 0.9 for hydrophilic solvents and higher than 1.1 for hydrophobic solvents (*84*). The intensity ratio cannot be determined in most protein spectra due to overlapping of the Trp doublet with bands caused by CH bending vibrations of aliphatic side chains. In the difference spectrum obtained by subtraction of the Arc-F10H spectrum from that of the Arc-wt spectrum, the intensity difference of the Fermi doublets could be detected as a trough/peak feature at 1361/1351 cm^{-1} because of the elimination of all other signals. The trough/peak feature is probably caused by an upshift of the 1360 cm^{-1} component or alternatively, by a higher intensity of the 1360 cm^{-1} component and lower intensity of the 1340 cm^{-1} component, consistent with a more hydrophobic environment of the indole ring environment in Arc-F10H. However, the second alternative is in contradiction with fluorescence measurements.

The very strong Trp band near 761 cm^{-1} (W18 mode) is a sensitive marker to the amphipathicity of the environment of the indole ring (*85*). A tryptophan side chain in hydrophilic environment gives rise to a very strong band while in hydrophobic environment the band becomes weaker (*85*). In the Arc-wt spectrum a very strong and sharp band is located at 767 cm^{-1}. In the Arc-F10H spectrum the band looses 35 % of its relative intensity, whereas a weak shoulder at 757 cm^{-1} increases its intensity. These changes result in a peak/trough feature (768/757 cm^{-1}) of the protein difference spectrum.

The F10H mutation produces a downshift of the W16 mode from 1011.5 (Arc-wt) to 1010 cm^{-1} (Arc-F10H) that is clearly visible in the difference spectrum as a peak/trough feature at 1013/1008 cm^{-1}. Effects of the environment on the position of the W16 mode were studied for several tryptophan derivatives in the crystalline state (*109*). However, to

our knowledge up to now the dependence of intensity or position of this band on the environment has not been elucidated for solution conditions.

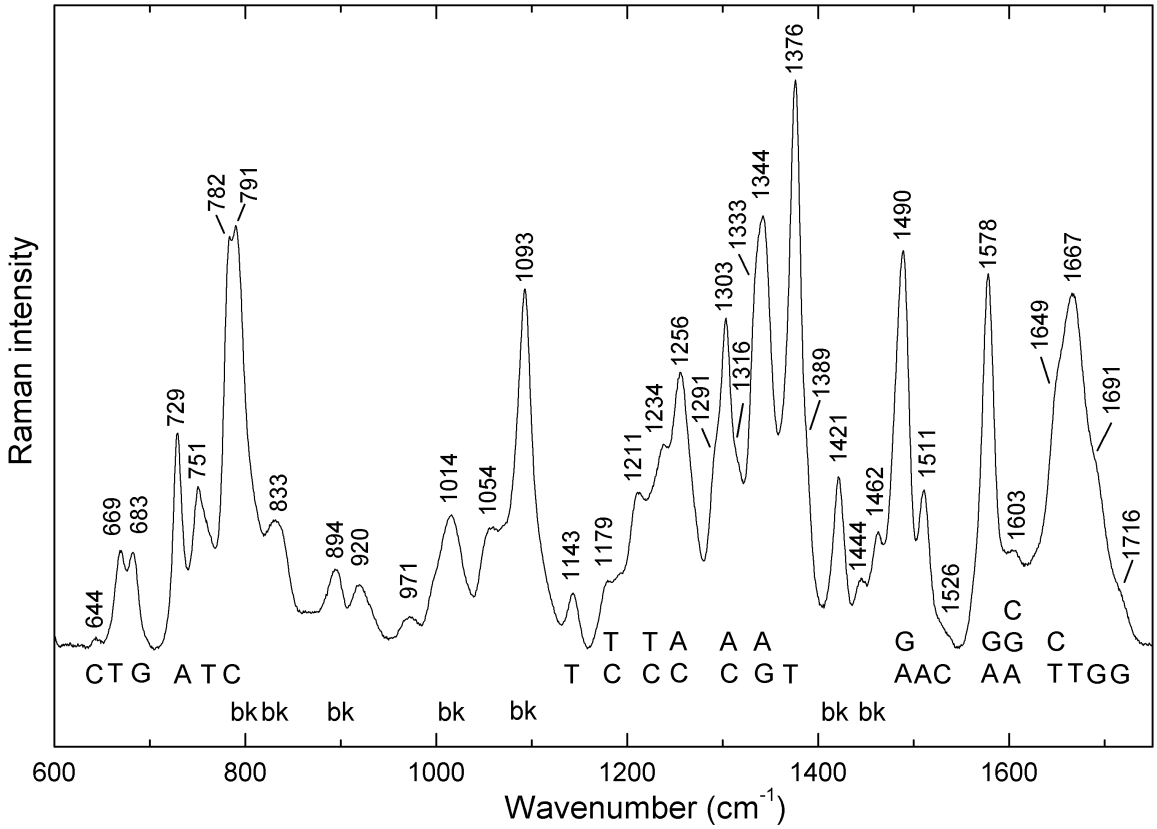

Figure 5.16: Raman spectrum of the 22-mer Arc repressor operator DNA at 24 mg/mL concentration. Experimental conditions are as given in the legend of Figure 5.15. Peak positions of prominent Raman bands are labelled. Abbreviations are as follows: G, guanine; T, thymine; C, cytosine; A, adenine; bk, deoxyribose backbone.

5.3.3. Raman Signature of the Arc Repressor Operator DNA

Figure 5.16 shows the Raman spectrum and the sequence of the 22-mer operator site DNA (21-bp and one base 5' overhang) in the 600-1750 cm^{-1} wavenumber region. The sequence of the oligonucleotide is exactly that used in the crystallographic analysis of the Arc-operator DNA complex (*29*). Wavenumber positions and assignment of the major peaks are in accordance with those given previously in the literature (*88-89, 93-94* and references therein). The backbone conformation markers at 833 and 1093 cm^{-1} are diagnostic of B-DNA (*89*), and the nucleoside conformation markers at 669 cm^{-1} (dT), 683 cm^{-1} (dG), 729 cm^{-1} (dA), 751 cm^{-1} (dT), and 1256 cm^{-1} (dC) identify C2'-*endo*/*anti* conformers. The spectrum serves as basis for the interpretation of the difference spectra shown in Figure 5.17.

5.3.4. Raman Analysis of the Arc Repressor–Operator DNA complex

Figure 5.17 shows the Raman spectra of the complexes of Arc-wt (panel A, top trace) and Arc-F10H (panel B, top trace) with operator DNA. In panel A and B, the middle trace is the computed difference spectrum that was obtained by subtraction of the component spectra (Figures 5.15 and 5.16) from the spectrum of the complex, and the bottom trace shows four times enlarged difference spectra. More than 30 Raman peaks and troughs in the difference spectra demonstrate structural perturbations as a result of the complex formation.

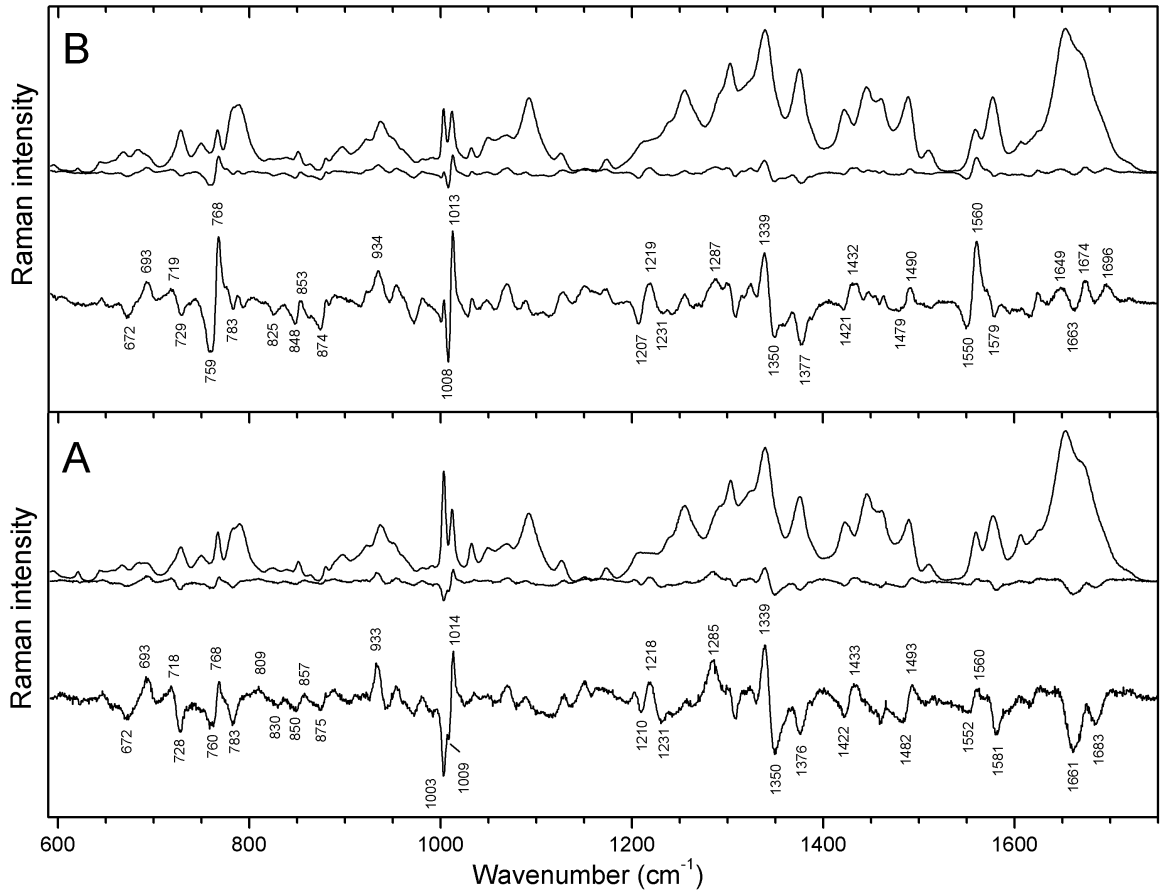

Figure 5.17: Panel A: Raman spectrum of the Arc-wt-operator DNA complex in 2:1 molar ratio (top trace). Raman difference spectrum obtained by subtraction of the isolated component spectra from the experimental spectrum of the complex (middle trace); four times enlarged difference spectrum (bottom trace). Panel B: Raman spectrum of Arc-F10H-operator DNA complex in 2:1 molar ratio (top trace). Raman difference spectrum obtained by subtraction of the isolated component spectra from the experimental spectrum of the complex (middle trace); four times enlarged difference spectrum (bottom trace). Experimental conditions are as given in the legend of Figure 5.15.

(1) Backbone and Deoxynucleoside Conformation of the Operator DNA. In the 600-900 cm^{-1} region Raman markers of deoxynucleoside conformation and DNA backbone geometry are located (*89*). The 782 cm^{-1} band in the Raman spectra of DNA is assigned to

cytosine. The 791 cm^{-1} band is assigned to a stretching vibration of backbone phosphodiester groups and diagnostic of B-form DNA backbone geometry, specifically of torsion angles α and ζ in *gauche*$^-$ range (*100, 104-105*). In DNA spectra, usually the cytosine and backbone bands overlap to one band near 784 cm^{-1}, whereas these bands are partially resolved in the spectrum of the Arc operator DNA. The difference trough near 783 cm^{-1} exhibits a decrease in the cytosine band intensity. A peak at 809 cm^{-1} and trough at 830 cm^{-1} in the difference spectrum of Arc-wt (Figure 5.17-A) and a trough near 825 cm^{-1} in the difference spectrum of Arc-F10H (Figure 5.17-B) result from changes in the broad B-DNA backbone band near 830 cm^{-1}.

The peaks at 669 (thymine) and 683 cm^{-1} (guanosine) in the spectrum of the operator DNA (Figure 5.16) are nucleoside conformation markers for B-form DNA and sensitive to altered deoxynucleoside conformation. In the difference spectrum, there is a trough at 672 and a peak at 693 cm^{-1} (Figure 5.17-A). A downward shift of the 729 cm^{-1} adenosine marker band is indicated by a difference feature with peak near 718 and trough near 728 cm^{-1}. Altogether, the difference features near 672, 693, 728, and 783 cm^{-1} are consistent with altered deoxynucleoside conformations of guanosine, thymidine, adenosine, and cytosine in the complex.

(2) Deoxyribose Ring and Protein CH_2/CH_3 Vibrations. Furanose vibrations were identified in Raman spectra of DNA near 930, 1420 and 1460 cm^{-1} and assigned to backbone vibrations (*95, 99-100*). In the spectrum of the Arc operator DNA the peak positions of those bands are at 920, 1421 and 1462 cm^{-1} (Figure 5.16). Protein bands overlap with DNA in these spectral regions. An intense band at 939 cm^{-1} is due to a C-C stretch of α-helices; COO^- symmetric stretch vibrations cause the 1402 cm^{-1} peak; a band at 1424 cm^{-1} reflects CH_2 and CH_3 deformations; at 1444 cm^{-1} CH_2 scissoring modes are found (Figure 5.15). In Figure 5.17 the peak/trough feature at 1433/1422 cm^{-1} and a peak at 933 cm^{-1} may be assigned to backbone vibrations of the DNA and/or changes in the protein. The crystal structures of Arc-wt–DNA and Arc-F10V–DNA indicate that Arc repressor binding slightly bends the operator DNA (*24, 29*). Alterations of DNA helix geometry may contribute to the spectral differences observed upon Arc binding (Figure 5.17). Changes in these spectral regions were described for a SRY HMG box–DNA complex because of induced bending and/or unwinding of the DNA (*100*).

(3) Purine Environment. The crystal structure of an Arc-wt–DNA complex (Figure 1.4) indicates several direct contacts between protein and purine moieties in the major groove (*29*). On the first half site of operator DNA, residues Arg13/13' form hydrogen

bonds with N7 and O6 of the two guanine bases. On the second half site, Arg13' binds to adenine N7 instead to guanine N7. Gln9/9' form specific hydrogen bonds to N6 and N7 of adenine (*29*).

In accordance with the crystal structure we expect prominent Raman features assignable to major groove interaction with guanine and adenine in the difference spectra of the Arc repressor–operator DNA complex (Figure 5.17). A trough at 1482 cm^{-1} and a peak at 1493 cm^{-1} of the guanine N7 band near 1490 cm^{-1} probably result from hydrogen bonding to guanine N7 that causes up-shifting of the 1490 cm^{-1} band. A similar feature near 1490 cm^{-1} was recently observed in a KorB-N–DNA complex (*91*). The crystal structure of the KorB-N–DNA complex revealed direct contacts of the protein with guanine and cytosine bases in the major groove of the DNA (*57*). Cytosine does not contribute to the 1490 cm^{-1} band, therefore the observed spectral feature can be correlated with guanine. The adenine band near 1344 cm^{-1} produces a prominent peak/trough feature at 1339/1350 cm^{-1} that indicates a direct contact of Arc with the $N6H_2$ and/or N7 positions of adenine; at present we cannot discriminate between these two possibilities.

The guanine and adenine band at 1578 cm^{-1} result from the superposition of several components, one due to $N6H_2$ scissor vibration and others due to an adenine or guanine ring mode (*105, 108*). The band exhibits a slight decrease in intensity at 1581 cm^{-1} after Arc repressor binding. In addition to guanine contributions, this intensity increase may result from adenine contributions.

(4) Pyrimidine Environment and Secondary Structure. Arc repressor contacts cytosines and thymines (*29*). Asn11 forms a hydrogen bond with cytosine $N4H_2$, and Asn11' binds to thymine O4. Thus two hydrogen bonds are formed to pyrimidines on each half-site of the operator whereas four contacts are formed to purine bases. Three thymine $C5H_3$ groups interact with protein side chains.

Thymine exhibits at 1376 cm^{-1} a prominent Raman band of its exocyclic $C5H_3$ group. The intensity of the band increases with increasing hydrophilicity in the surrounding of $C5H_3$ and *vice versa* (*85*). The observed intensity decrease of the 1376 cm^{-1} band in the spectra of Arc-wt–DNA and Arc-F10H–DNA indicates increased hydrophobicity of $C5H_3$ groups which are interacting with hydrophobic protein side chains. Thymine C4=O Raman bands are located at 1649 and 1667 cm^{-1} (*105-108*). In the spectrum of Arc-wt–DNA the thymine bands overlap with amide I bands of Arc. Figure 5.17-A shows a trough at 1661 cm^{-1}, Figure 5.17-B shows a complicated feature with two peaks at 1674, 1649 cm^{-1} and a trough at 1663 cm^{-1}. Amide I bands reflect secondary structure of protein. Since minor

differences in the conformation of free Arc-wt and Arc-F10H exist (Figures 5.14 and 5.15) it is possible that small conformational differences between Arc-wt and Arc-F10H persist in the complexes as suggested by minor deviations of the amide I features of the difference spectra (Figure 5.17). These deviations concern changes in thymine C4=O Raman bands that are overlapped by contributions of amide I protein bands.

Raman bands in the interval 1300-1750 cm^{-1} are sensitive to specific interactions of protein residues and DNA bases (*93-94, 106-107*). Cytosine has very weak bands in this region compared to adenine, guanine and thymine. Between 1200 and 1300 cm^{-1} cytosine bands overlap with bands of thymine. In the complex, amide III bands are located in this region. A peak/trough at 1285/1264 cm^{-1} and a trough/peak/trough feature at 1210/1218/1231 cm^{-1} are possible consequences of Arc interaction to cytosine. Both Arc-wt and Arc-F10H exhibit very similar features. Minor differences in the conformations of Arc-wt and Arc-F10H in the complex are indicated in the amide III region by a higher intensity at 1285 cm^{-1} and a lower intensity at 1231 cm^{-1} in the spectrum of the Arc-wt–DNA complex compared to the spectrum of the Arc-F10H–DNA complex.

(5) Phenylalanine. Arc-wt contains the phenylalanines Phe10/10' and Phe45/45'. In the dimer, all four Phe residues are buried in a hydrophobic core. It is a remarkable structural feature of the complex that the side chains of Phe10 and Phe10' flip out from the hydrophobic core and pack between phosphate oxygens of the operator DNA (*29*). This movement of Phe10 and Phe10' reduces the intensity of the ring breathing vibration in the complex in comparison to that of free Arc-wt which is reflected in the difference spectrum (Figure 5.17-A, bottom trace) by a trough at 1003 cm^{-1}.

(6) Tryptophan. Arc contains only the Trp residues Trp14/14', this facilitates the detection of key tryptophan markers in the Arc–operator DNA complex. Trp14/14' does not directly participate in the binding of the protein to the operator DNA (*29*). Nevertheless, Arc-wt and Arc-F10H binding to operator DNA result in spectral perturbations of tryptophan marker bands.

The perturbation of the W3 mode near 1559 cm^{-1} is connected with a perturbation of the $C_\alpha C_\beta$-C_3C_2 torsion angle $|\chi^{2,1}|$. The change of the angle is probably small, because the position of the band remains near 1559 cm^{-1}. Angle $\chi^{2,1}$ has in solution an average value of –9° (NMR structure of Arc-wt, PDB code 1BAZ); angles of –9° (1PAR) and –12° (1BDT) were identified in two crystal structures.

NMR data of Arc-wt indicate that Trp14/14' are buried in a very strong hydrophobic environment. Trp14/14' are surrounded by valines and side chains of Phe10/10' and

Tyr38/38' that point to the Trp14/14' rings. Upon complex formation Phe10 and Phe10' move in such way that the hydrophobicity of the environment of the Trp residues alters, resulting in Raman difference signals. The W17 mode decreases its intensity at 875 cm^{-1}, this reflects changes in the hydrogen bonding state of Trp 1NH. The W18 mode shifts to a lower wavenumber and produces a peak/trough feature at 768/760 cm^{-1}. Both bands reflect a change in the hydrophobicity of the Trp environment. The very sharp W16 mode downshifts upon complex formation as indicated by a peak/trough feature at 1013.5/1008.5 cm^{-1}. This effect is probably directly related to the movement of the Phe10/10' side chains.

In Arc-F10H, the hydrophobic core is disturbed by His10/10' in a manner that effects the surrounding of Trp14/14'. Subsequently, the Trp14/14' rings change their positions relative to the residues in the neighbourhood. This is reflected in the Raman spectrum by a shift of the W3 mode to 1555 cm^{-1} (Figure 5.15). Upon complex formation (Figure 5.17-B), the W3 mode shifts from 1555 to 1559 cm^{-1}, i.e. to the same wavenumber that was found in Arc-wt, pointing to similar $\chi^{2,1}$ values of Trp14/14' in free Arc-wt and in the DNA complexes of Arc-wt and Arc-F10H.

Another effect of the Arc-F10H-operator DNA complex formation is the elimination of the 757 cm^{-1} shoulder of the W18 mode that gains intensity at 768 cm^{-1}. The peak/trough feature is located near 768/759 cm^{-1}. The W17 mode looses 30 % of its relative intensity resulting in a trough at 874 cm^{-1}. The W16 mode upshifts from 1010 to near 1012 cm^{-1} close to its position in the Arc-wt–operator DNA complex.

(7) Tyrosine. Arc contains one unique tyrosine Tyr38 per monomer. The OH group of Tyr38/38' is located at the protein surface and probably forms very strong hydrogen bonds with solvent water molecules. Ring atoms of Tyr38/38' are directed towards Trp14/14'. Similar peak/trough features at 853/848 cm^{-1} are observed in the DNA complexes of Arc-wt and Arc-F10H (Figure 5.17) and in the difference spectrum between the free proteins (Figure 5.15).

5.3.5. The Arc-wt in Complex with Non-Operator DNA

Raman spectra of mixtures of Arc repressor and oligonucleotide REF2 were measured in control experiments. REF2 is an oligonucleotide with arbitrary sequence that was already used in ω_2-DNA studies (REF2, Figure 5.1) for the discrimination between specific and unspecific interactions of ω_2 with DNA. Arc repressor binds to REF2 and

forms an unspecific complex, despite of the arbitrary sequence of REF2, because of the high concentrations of DNA and protein used in these measurements.

Figure 5.18 compares the Raman difference spectra of the Arc-wt–operator DNA (green trace) and the unspecific complex of Arc-wt with REF2 (red trace). Both difference spectra reflect many similarities. The difference features of Trp14 at 1560/1552, 1014/1009, 875, and 768/760 cm^{-1} as well as the difference trough of Phe10 at 1003 cm^{-1} preserve the same position and intensity. These Raman difference features indicate that in both complexes Phe10 leaves the hydrophobic core and probably interacts similarly with the phosphates of operator DNA and REF2 (*29*).

However, differences are visible between the difference spectra of Arc-wt–operator DNA complex and unspecific Arc-wt–REF2 complex. These differences reflect specific interactions assigned to direct contacts of Arc-wt with its operator. The troughs at 1661 and 1376 cm^{-1} were assigned to interactions with thymine C4=O and exocyclic $C5H_3$ groups, respectively. The guanine N7 interaction marker at 1493/1482 cm^{-1} is clearly missing in the difference spectrum of the unspecific Arc-wt–REF2 complex; also missing is the peak trough feature near 1339/1350 of the Arc-wt–operator DNA complex, indicating that Arc-wt does not interact with adenine $N6H_2$ and/or N7 of REF2. The difference peak at 1285 cm^{-1} and the peak/trough feature near 1218/1231 cm^{-1}, which are probably caused by interaction of Arc-wt and operator DNA, decrease their intensity by approximately one half. Nucleoside conformation markers in the region between 600 and 900 cm^{-1} also reduce their intensities. The peak/trough feature at 1433/1422 cm^{-1} preserves the intensity profile. This feature is proposed to indicate DNA bending and possibly reflects a similar bending of operator DNA and REF2. Alternatively, the difference feature may exhibit perturbations of CH_2 vibrations caused by interactions of Arc-wt amino acid side chains with DNA and/or Arc dimer-dimer interactions.

The peak/trough features near 1068/1057, 932/944 and 1433/1422 cm^{-1} as well as difference peaks at 1201, 1165 and 1087 cm^{-1} can be attributed to reorientation and repacking of side chains of Arc-wt as a consequence of Arc-wt–REF2 complex formation and/or Arc-wt tetramerization. The troughs at 1580 and 1350 cm^{-1} indicate changed stacking of adenine residues. Difference features at 718, 693, and 677 cm^{-1} reflect changes in dA, dG, and dT conformations, respectively.

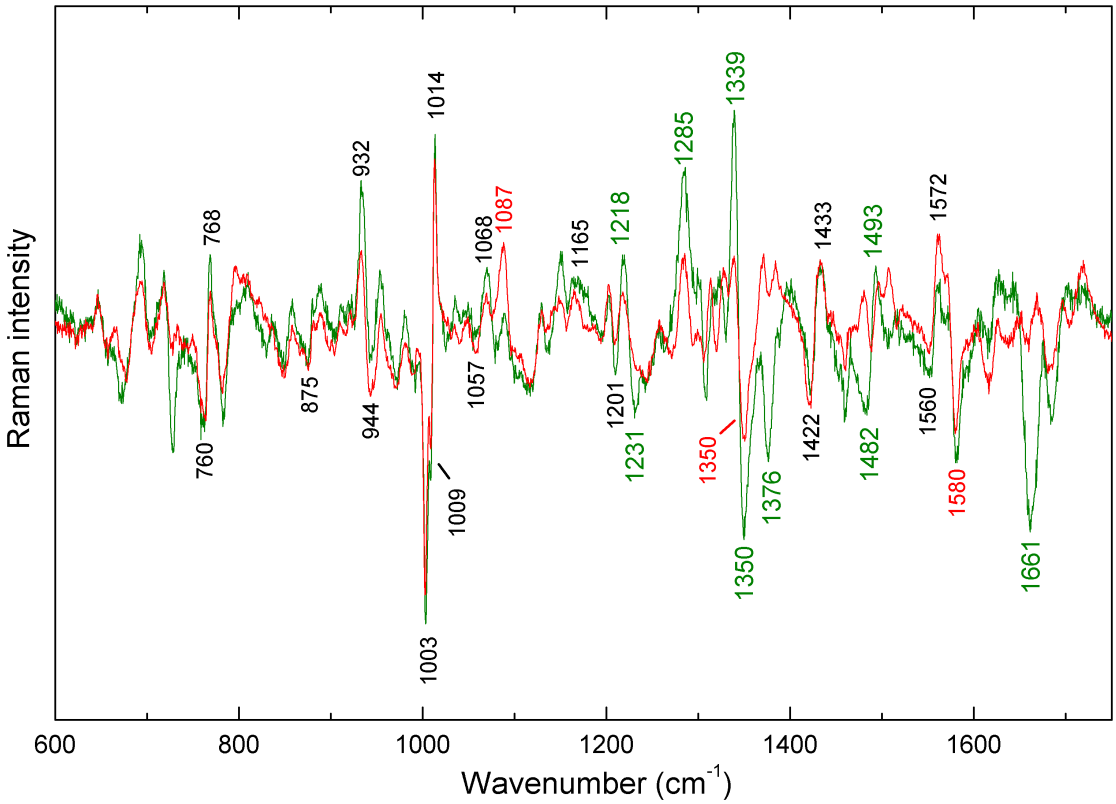

Figure 5.18: Enlarged Raman difference spectra. The green trace represents the Arc-wt–operator DNA complex and the red trace represents the unspecific Arc-wt–REF2 complex. The most prominent differences are labelled by respective wavenumbers. Black color indicates the differences in both Arc-wt–operator DNA and unspecific Arc-wt–REF2 complex. The green color corresponds to the interactions that are observed only in Arc-wt–operator DNA complex and the red color indicates interactions of the unspecific Arc-wt–REF2 complex. The concentrations of Arc-wt–operator DNA and Arc-wt–REF2 complex are 65 mg/mL and 70 mg/mL, respectively. Experimental conditions are as given in the legend of Figure 5.15.

5.3.6. The Interaction of Arc-F10H with Non-Operator DNA

Figure 5.19 shows the Raman difference signature of the Arc-F10H–operator DNA complex (black top trace), and two difference spectra of the unspecific Arc-F10H–REF2 complex measured 15 min (red trace) and 13 hours (black bottom trace) after mixing the components. The three difference spectra differ significantly. The difference spectra obtained after an incubation of Arc-F10H and REF2 DNA for 13 hours exhibits completely different features compared to the difference spectrum of the Arc-F10H–operator DNA complex. It is obvious that interactions between Arc-F10H and REF2 DNA completely differ from that in the unspecific Arc-wt–REF2 complex (compare Figures 5.18 and 5.19).

Arc-wt binding to operator DNA and REF2 has some similar characteristics. This is indicated by the fact that several features are identical in the Raman difference spectra of Arc-wt–REF2 and Arc-wt–operator DNA complex. Nevertheless, in the Raman difference

spectrum of Arc-wt–REF2 complex Raman markers are missing that have been assigned to direct interactions with bases of operator DNA (Figure 5.18).

Raman difference features that are identical in Arc wt-REF2 and Arc wt-operator DNA complexes are assigned to the Trp14/Trp14' near 1010, 764, and 1555 cm^{-1} and Phe10/Phe10' near 1003 cm^{-1} which indicate the interaction of β-ribbon of Arc with DNA. The Phe10/Phe10' interaction marker disappeared by the exchange of Phe10 to His10 in the Arc-F10H–operator DNA complex. However, several markers assigned to Trp14/Trp14' increase their intensities in the difference spectrum of the Arc-F10H–operator DNA complex because of modifications in the hydrophobic core caused by the substitution of Phe10 to His10. In the difference spectrum of the Arc-F10H–REF2 complex the difference features of Trp14/Trp14' disappear (Figure 5.19 black traces). This observation is consistent with a binding mode without recognition of the major groove of REF2 by the β-ribbon of Arc-F10H. The Trp14 vibrations near 1010, 764, and 1555 cm^{-1}, which are very sensitive against changes of the surrounding, remain unchanged upon the interaction of Arc-F10H and REF2. However, these Trp Raman markers exhibit very small peak/trough features in the difference spectrum that was obtained 15 min after mixing of the components (Figure 5.19 red trace). The difference features reflect only 10-20 % intensity change compared to those in the difference spectrum of the Arc-F10H–operator DNA complex (Figure 5.19 black top trace). The magnitude of the features suggests that after 15 min incubation of REF2 and Arc-F10H only 10-20 % of the molecules form a complex by using the β-ribbon. After 13 hour incubation, the situation is completely different. None or only very few molecules of the Arc-F10H interact with REF2 DNA by using the side chains of the β-ribbon. In contrast, all Arc-wt molecules recognize the REF2 DNA by using the β-ribbon (Figure 5.18).

The difference spectrum of the unspecific Arc-F10H–REF2 complex (black bottom trace of Figure 5.19) exhibits significant features. The most prominent features are those in the amide I and III regions. Amide I exhibits two peaks at 1690 and 1662 cm^{-1} and Amide III indicates a peak at 1240 cm^{-1} and a trough at 1260 cm^{-1}. Amide I and III bands are strongly overlapped by DNA vibrations in the mixture. The difference features reflect either small secondary structure modifications of Arc-F10H or conformational changes of REF2 DNA upon binding. Raman difference features at 981, 1144, 1344, 1410 and 1447 cm^{-1} are possibly caused by reorientation of Arc-F10H side chains upon binding to REF2

DNA. CD spectroscopy was employed to prove whether the protein secondary structure is preserved or perturbed (see below).

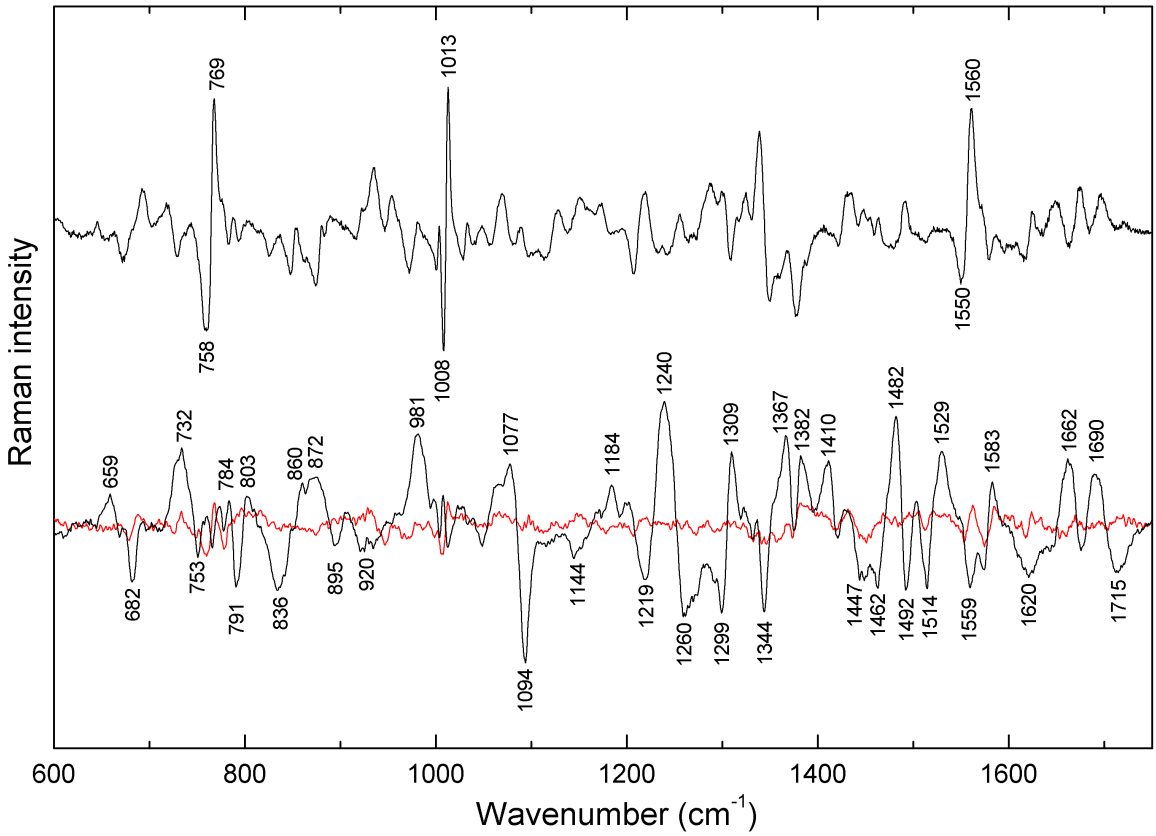

Figure 5.19: Enlarged Raman difference spectra of complexes of Arc-F10H with REF2 and operator DNA. The black top trace corresponds to the specific Arc-F10H–operator DNA complex from Figure 5.17, the black bottom trace indicates the unspecific Arc-F10H–REF2 complex after 13 hour incubation of both components, and the red trace is a difference spectrum measured 15 minutes after preparing the Arc-F10H–REF2 mixture. The concentration of the Arc-F10H–REF2 mixture is 60 mg/mL, and experimental conditions are as given in the legend of Figure 5.15. Spectra were smoothed using the 11-point Savitsky-Golay algorithm.

Significant perturbations of the DNA backbone are exhibited by several peaks and troughs. The 791 component of the 782/791 cm^{-1} doublet is due to a vibration localized in phosphodiester groups of B-DNA and is diagnostic of B-form backbone geometry. The peak/trough/peak feature at 803/791/784 cm^{-1} indicates that the presence of the Arc repressor induces a conformational change in DNA phosphodiester moieties. An intensity loss at 836 cm^{-1} and a concomitant gain at 860 and 872 cm^{-1} also points to a structural transformation. The intensity reduction observed at 836 of ~50-70 % is extremely high. The Raman band near 836 cm^{-1} is correlated with AT domains of DNA (*88-89*), therefore its intensity loss implicates AT sites as direct targets of Arc-F10H interaction. The phosphate band near 1092 cm^{-1} changes significantly after 13 hours of incubation. The

intensity decrease at 1094 cm^{-1} amounts to 30 % of the parent band in free REF2 DNA. In complexes with minor groove binding proteins, slight broadening of the phosphate band was observed that was interpreted to indicate changes in the local electrostatic environment (*96*).

The difference band at 925 cm^{-1} originates from an intensity loss of about 70% of its 920 cm^{-1} parent band. This band is assigned to furanose ring vibrations (*99*), and exhibits the largest intensity loss of a DNA backbone band so far observed in our experiments. The DNA backbone band at 895 cm^{-1} looses 50 % of its intensity when the equilibrium of REF2 DNA and Arc-F10H was reached. In addition to these changes in DNA phosphodiester and deoxyribose geometry, the deoxynucleoside conformations are also altered in the mixture. A trough at 753 cm^{-1} and a peak at 659 cm^{-1} are consistent with a change in the dT conformation. Similarly, a very prominent peak near 732 cm^{-1} and a small trough near 682 cm^{-1} indicate changes in dA and dG conformations. Altogether, these differences support the proposal that Arc-F10H binding perturbs mostly AT-paired regions of REF2.

The difference peaks at 1240, 1482, and 1583 cm^{-1} are attributed to the recovery of Raman hypochromism (*105, 110-111*), due to base unstacking with Arc-F10H interaction. A very weak band at 1529 cm^{-1} is assigned to cytosine ring vibration. This band exhibits an intensity increase of about 100 %, the largest perturbation in the difference spectrum. Other stronger cytosine bands are overlapped by very intense features of amide III bands and are difficult to discriminate. The peak/trough feature of the adenine band at 1309/1299 cm^{-1} probably indicates a direct contact of adenine residues.

5.3.7. Time Dependence of Arc-F10H Binding to Non-Operator DNA

Spectral changes in both DNA and protein regions were observed in the CD spectra of an Arc-F10H–REF2 sample (Figure 5.20) when the measurements were performed in 30 min steps after mixing. Two isosbestic points appear at 253 nm and at 236 nm. The positions of the isosbestic points indicate that the CD spectra are mainly determined by three components. Two of the components are free DNA and free protein, and the third component most probably represents the protein-DNA complex. The CD spectra indicate conformational changes in DNA structure upon binding of Arc-F10H. The Raman data also show large perturbations of the DNA backbone (Figure 5.19). The CD spectrum measured after 15 min indicates that DNA and protein probably have not completed the formation of a complex, whereas after 13 hours an equilibrium is reached and the

measured spectrum probably corresponds to the finally formed complex. When a complex was formed after ~13 hours, control CD measurements were performed to check whether the Arc-F10H-REF2 DNA complex is stable at lower concentrations. Two dilution steps were chosen, 100x and 5000x, corresponding to final concentrations of 14 µM and 280 nM, respectively. These data are shown in the insert of Figure 5.20. The spectra in the insert of Figure 5.20 indicate identical changes in the DNA backbone at the concentration of ~1.4 mM and at the very low concentration of ~280 nM. Thus, a complex preformed at the high concentration of ~1.4 mM remains stable after dilution to the low concentration of ~280 nM .

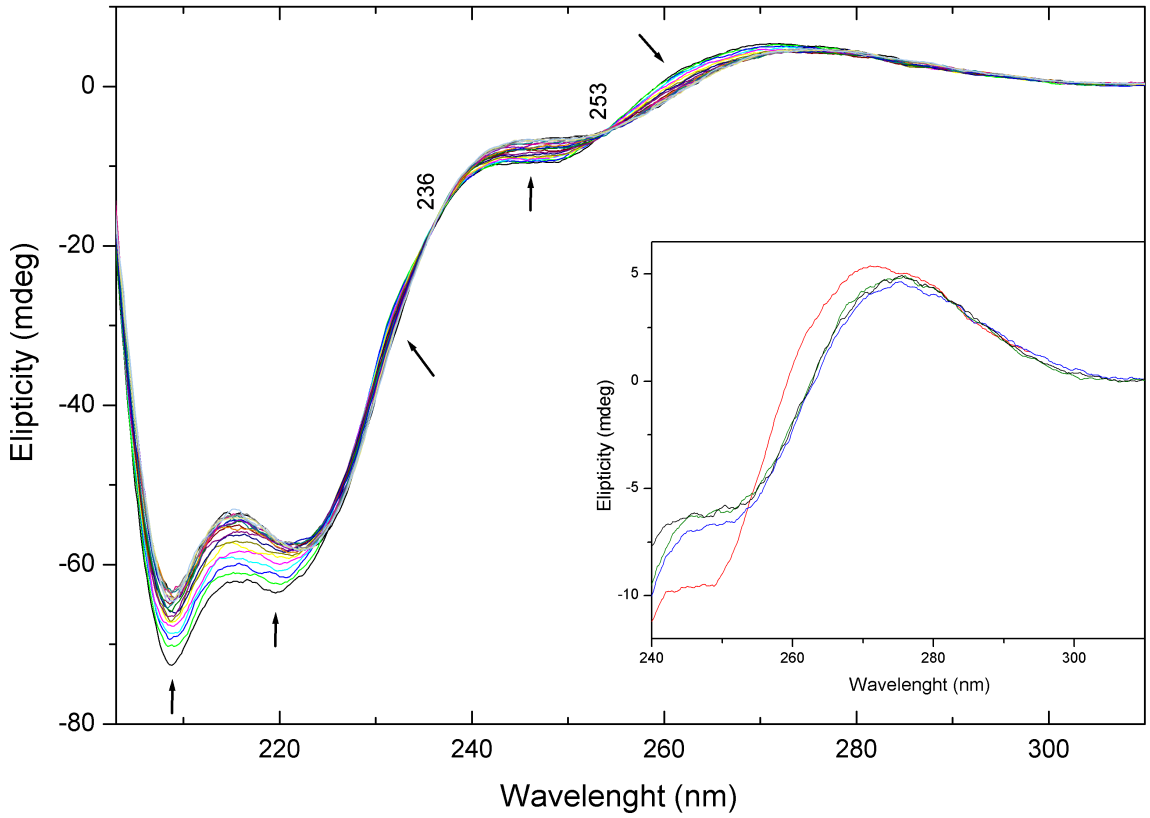

Figure 5.20: Kinetics of complex formation between Arc-F10H and REF2 DNA. Time dependent changes and their directions in the CD spectrum (in black) are indicated by arrows. Concentration of the Arc-F10H–REF2 mixture is 60 mg/mL (1.4 mM). The data were collected in ~30 min steps. Insert: The red spectrum represents the Arc-F10H–REF2 mixture after 15 minutes incubation. The blue trace corresponds to the Arc-F10H–REF2 complex measured after 13 hours incubation. The green trace was measured with a 100 times diluted sample of the Arc-F10H–REF2 complex and the black trace was obtained after 5000 fold dilution. Buffer is as given in the legend of Figure 5.15.

Figure 5.21 shows the time-dependence of the ellipticity of the Arc-F10H–REF2 mixture at the given wavelengths. The reduction of the ellipticity at 220 nm (Figure 5.21-E) reflects the modification of ordered α-helical structures. The development of ellipticity

at 224 nm, first increasing and then decreasing (Figure 5.21-D), probably demonstrates some kind of transformation of secondary structures of Arc-F10H during the complex formation. The changes in DNA backbone conformation are revealed by ellipticity perturbations at 264 nm (Figure 5.21-A) and ~247 nm (Figure 5.21-B). Interestingly, Figure 5.21-A indicates a two step transformation of the DNA backbone. The CD spectra below 240 nm have very strong protein contributions to the negative ellipticity. Thus, the decrease at 231 nm (Figure 5.21-C) might be caused by changes in DNA backbone and/or protein secondary structure.

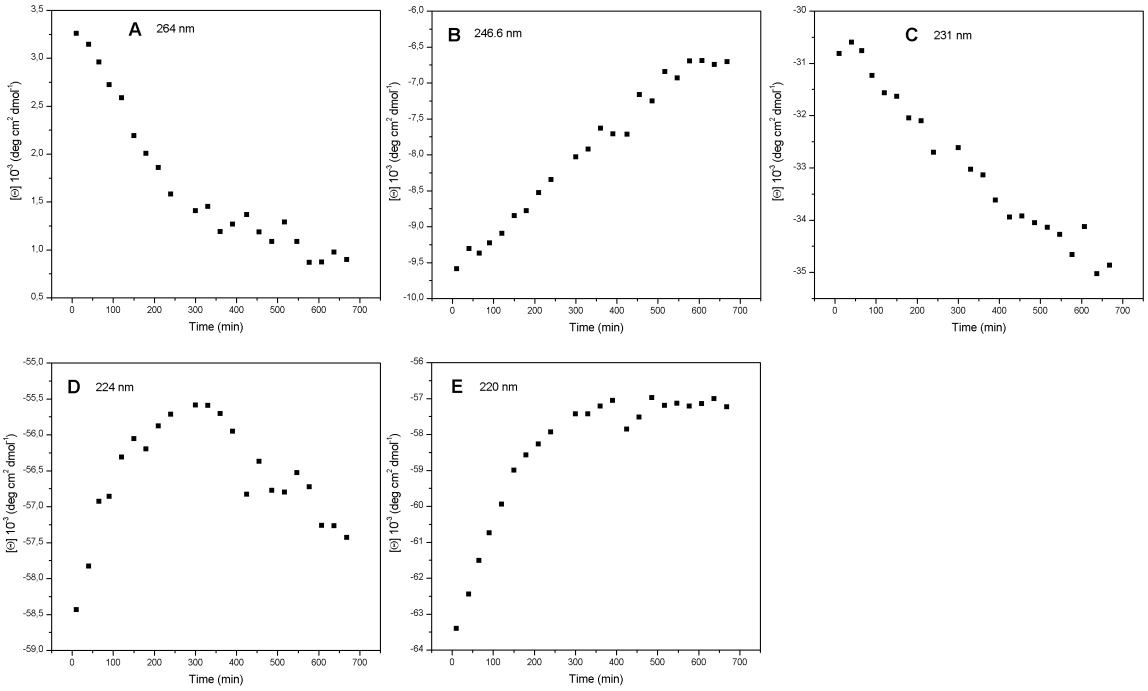

Figure 5.21: Time-dependent development of ellipticity of the Arc-F10H–REF2 mixture. In (A), (B), (C), (D), and (E) are plotted the ellipticity changes at 264, 246.6, 231, 224, and 220 nm, respectively. Data are extracted from the spectra of Figure 5.20.

Raman spectra were collected simultaneously with the CD spectra. Raman difference spectra of the Arc-F10H–REF2 sample shown in Figure 5.22 were obtained by subtraction of spectra measured in 30 min intervals from the spectrum that was collected after 15 min of incubation. The difference spectra were multiplied by factor -1 to show the decrease of intensity of a parent band as a trough and an increase of intensity of a parent band as a peak. The last calculated difference spectrum of Arc-F10H–REF2 complex (with the highest intensity of peaks and troughs) represents the difference spectrum between the 15 min-spectrum and the 13 hours spectrum. It is nearly identical to the difference spectrum computed by subtraction of the spectra of free Arc-F10H and REF2 DNA from the

spectrum of the complex that was measured after 13 hour incubation of the mixture of both components (Figure 5.19). The time-dependence of the difference spectra indicates that the interaction between Arc-F10H and REF2 DNA and the accompanying conformational changes occurs slowly. The difference spectra show large conformational perturbations in both DNA and protein developing during the observation period. Interpretation of the difference spectra is similar to that given above for the Arc-F10H interaction with non-operator DNA REF2. This experiment is a simple repetition of the previous measurement of the spectrum of the Arc-F10H–non-operator complex (Figure 5.19) and extends the information for the kinetics of the reaction showing time-dependent conformational changes of both components accompanying the complex formation.

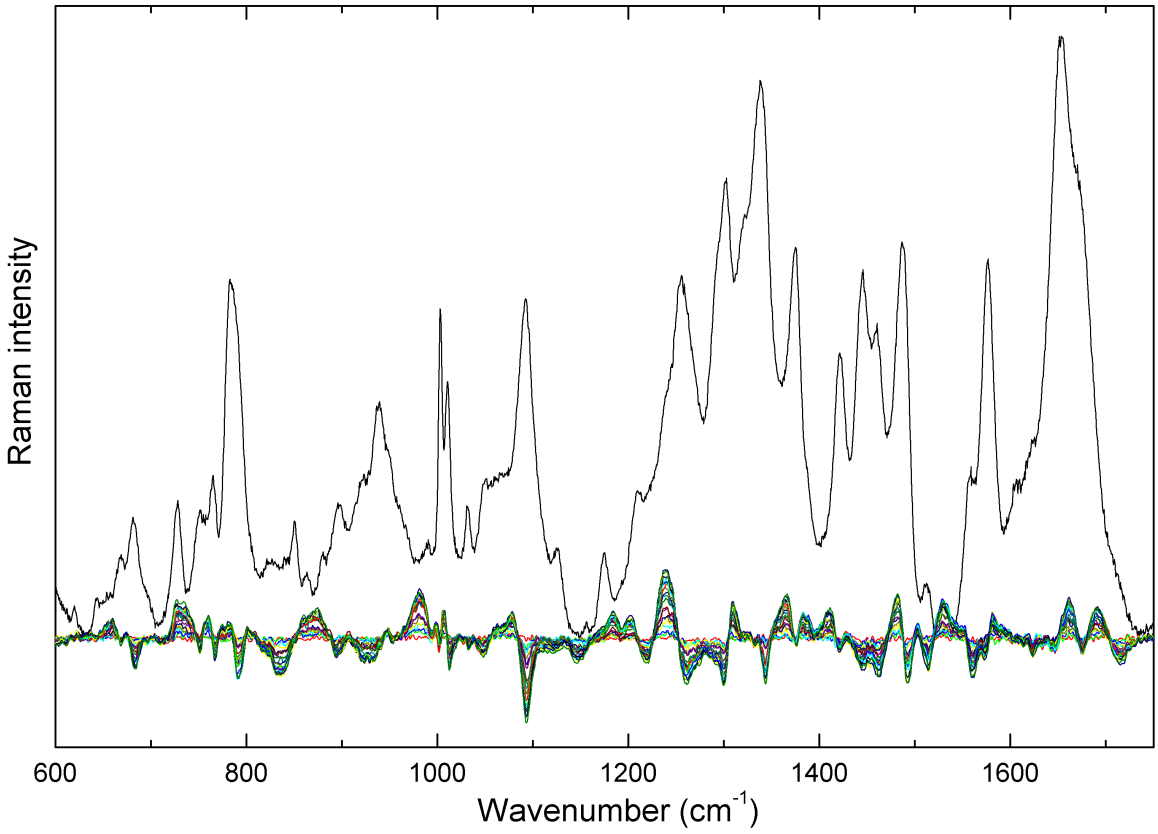

Figure 5.22: Time-dependent changes of Raman spectra of the Arc-F10H–REF2 mixture. The black Raman spectrum at the top was obtained 15 min after mixing of the components. The colored difference spectra (bottom traces) were obtained from Raman spectra that were measured in 30 min steps. The intensities of difference bands and troughs of the difference spectra increase with time indicating the time-dependent progress of the reaction. The experimental conditions are as given in the legend of Figure 5.19. The difference spectra were smoothed using the 11-point Savitsky-Golay algorithm.

5.4. Discussion: Arc Repressor

5.4.1. Arc-Operator DNA Complex

An essential aspect of the complex formation of Arc-wt with operator DNA is the movement of the Phe10/10' side chains out of the hydrophobic core of the protein and their packing between oxygens of the operator DNA backbone (*29*). Trp14/14' is located close to Phe10/10' but does not participate in a direct interaction with the DNA (*29*). Nevertheless, a peak/trough feature can be assigned to the W16 mode of Trp14/14' in the Arc-wt–DNA complex (Figure 5) that demonstrates a pronounced effect of complex formation on the spectral properties of Trp14/14'. The Cζ-H atoms of Phe10/10' are in 4 Å distance to the Trp14/14' phenyl rings (PDB 1BAZ); therefore hydrogen bonds to the π–electrons of the Trp14/14' rings would be possible (*112*). However, the mutation of Phe10/10' to Val10/10' did not significantly decrease the free energy of the variant protein, which might occur if this hydrogen bond exists in Arc-wt but not in the mutant. Similar peak/trough features assignable to the W16 mode of Trp14/14' were observed in the Arc-F10H–DNA complex (Figure 5.17-B) and in the Arc-wt–Arc-F10H difference spectrum (Figure 5.15). These spectroscopic observations may be explained in the following manner: In free Arc-F10H, Trp14/14' leaves the proximity of Tyr38/38' and looses van der Waals contacts which leads to a wavenumber downshift of the W16 mode. In the complex, Trp14/14' of Arc-F10H approaches again a close neighbourhood to Tyr38/38' and restores van der Waals contacts. The wavenumber upshift found in the spectrum of the Arc-wt–DNA complex suggests a tight interaction of Trp14/14' to Tyr38/38'. The Cβ atom of Tyr38/38' is 3.49 Å apart from $C\varepsilon^2$ of Trp14/14' whereas in the free protein the distance is 4.07 Å. We conclude that changes in the position of the W16 band reflect the strength of van der Waals interactions with the phenyl ring of Trp14/14'.

In the complex, Trp14/14' of Arc-wt prefers to stay in proximity to Tyr38/38' rather than to move to any space that could become accessible after the movement of Phe10/10' out of the hydrophobic core, and the hydrophobicity of the Trp14/14' surrounding does not change significantly upon complex formation (Figure 5.14). In the free Arc-F10H, Trp14/14' is probably located between Tyr38/38' and His10/10'. Upon complex formation, Trp14/14' of the Arc-F10H variant moves (Figure 5.15) to a more favourable position that seems to be similar to that occupied by Trp14/14' of the Arc-wt–DNA complex. In the free dimeric form, residues Phe10/10' of Arc-wt protein are buried in the hydrophobic core and point at Trp14/14' (*25*). Val, Tyr, or His mutations of Phe10/10' reduce the stability of the

free variant of Arc protein by only 0.2, 0.6, 1.0 kcal/mol, respectively (*24*). Raman and fluorescence spectra (Figure 5.14, 5.15), however, show a significant effect of the F10H mutation on the hydrophobic core. The Raman spectra indicate different conformations of the Trp14/14' residues in Arc-wt and in Arc-F10H, significant differences were observed in the $\chi^{2,1}$ rotation angles. Possibly, His10/10' try to occupy the same space in the protein core as Phe10/10'. Concomitantly, Trp14/14' take up modified positions in a now more hydrophilic environment. Consistent with those considerations is the observation that the free energy of Arc-F10H is more decreased as that of Arc-F10V compared to Arc-wt because Val10/10' reduces the hydrophobicity of the Trp14/14' environment (*24*) much less than the more hydrophilic His10/10' (Figure 5.14, 5.15).

The Trp14/14' residues assume very similar positions in free Arc-wt and in DNA-bound Arc-wt. Contrarily, Trp14/14' assumes a different position in free Arc-F10H, whereas the Raman features of the Arc-F10H–DNA complex suggest a position similar to that in Arc-wt. A reasonable explanation might be that upon complex formation the His10/10' side chains similar to that of Phe10/10' move out of the core, and restore in the Arc-F10H–DNA complex a wild type like neighbourhood of Trp14/14'.

According to the fluorescence spectra, the hydrophobicity of the Trp14/14' environment differs in the Arc-F10H– and Arc-wt–DNA complexes (Figure 5.14). However, as might be expected the Trp14/14' surrounding is more hydrophobic in both complexes compared to the free proteins.

Arc-wt has the highest affinity to operator DNA followed by F10H, F10Y, and F10V. Phe10/10' is an essential determinant to operator DNA binding affinity and specificity (*24*). Free energy measurements (*24*) revealed that the point mutations F10H, F10Y, and F10V reduce the free energies of their complexes with DNA by 2.3, 4.9, and 5.6 kcal/mol, respectively, in comparison to that of Arc-wt (*24*). A quantitative explanation of the stability differences remains elusive. From the crystal structures of Arc-F10V and Arc-wt it is known that the side chains of Val10/10' and Phe10/10' point similarly towards Trp14/14'. In the complex, $C\gamma^1$ of Val10/10' rotates out from the hydrophobic core (*24*). Similar considerations are reasonable for the positioning of His10/10' and Tyr10/10' in the Arc-F10H–DNA and Arc-F10Y–DNA complexes. The rings of His10/10' and Tyr10/10' might make contacts with phosphate oxygens in the complexes. However, the repulsion of the Tyr10 OH group and phosphates is probably responsible for the lower binding energy of Arc-F10Y–DNA.

Why do the amino acids side chains of Arc repressor at position 10 loop out in complexes with operator DNA? Apparently, looping out of the Phe10 side chain enhances the specific interaction with the DNA and results in energetically favourable complexes. Amino acids in position 10 are in the neighbourhood of amino acids Gln9, Asn11, and Arg13 that make direct contacts with DNA by the formation of hydrogen bonds. A moderate rearrangement of the short DNA-binding β-sheets of the proteins is indicated in the crystal structures of Arc-wt–DNA and Arc-F10V–DNA (*24, 29*). These rearrangements are confirmed by the spectral differences in the amide I region of the Raman spectra of free and DNA bound Arc-wt and Arc-F10H (Figure 5.17). Also, Trp14/14' move closer to Tyr38/38' and amino acids 10/10' leave the hydrophobic core. With Phe or His in position 10 energetically favourable structures are formed. Val at position 10 cannot come into energetically favourable close distance to DNA phosphates, therefore the binding affinity of Arc-F10V to operator DNA is much lower than that of Arc-wt and Arc-F10H.

5.4.2. Arc–Non-Operator DNA complex

It has been shown that Phe10 contributes not only to binding specificity, but also to binding affinity (*24*). However, the question "How does the Phe10 contribute to binding specificity?" is still open. Several models have been presented to explain why Phe10 makes better energetic contacts with the DNA backbone of an operator site than with the DNA backbone of a non-operator site. All the models predicted that Phe10 would have different geometrical relationship to the backbone of operator and non-operator sites and thus the free energies of these interactions would differ significantly (*24*).

The Raman difference spectrum of the Arc-wt–non-operator DNA complex indicates (Figure 5.18) that Phe10/10' change their conformation and perhaps contact the phosphates. In addition, the vibrations of Trp14/14' are perturbed significantly; the observed spectral features are nearly identical to that of the specific Arc-wt–operator DNA complex. The contribution of Phe10 and phosphate backbone interaction to the binding specificity of Arc-wt and operator DNA reaction has been shown to be significant (*24*). The free energy of the Arc-F10V–operator complex for one binding subsite is 4.2 kcal/mol lower than that of the Arc-wt–operator complex for one binding subsite. In comparison, the reduction of free energy for a single non-specific subsite of Arc-F10V–non-operator complex in comparison with Arc-wt–non-operator complex amounts only 0.8 kcal/mol (*24*).

It has been shown that the conformation of the DNA is strongly dependent on the base-pair sequence and only one base pair exchange might influence the conformation significantly (Figure 5.2). The conformation of DNA is determined by its sequence. Therefore, the base sequence of arc operator has an unique conformation of DNA which is contacted by several amino acids and Phe10/10'. Provided the interaction of Phe10/Phe10' and DNA backbone in the Arc-wt–operator DNA complex is indicated by reduction of intensity of the phenylalanine Raman band, then the contacts of Phe10/Phe10' with the non-operator DNA are probably very similar to those in Arc-wt–operator complex because the Raman spectrum of Arc-wt–non-operator DNA complex shows the same reduction of intensity of the Phe10/Phe10' band (Figure 5.18). However, it is impossible to determine whether these contacts contribute to the same extent to the stability as in the Arc-wt–operator complex. The different DNA conformation and a lack of other specific and weak interactions including water contributions might change the stabilities of Arc-wt–non-operator complex as well.

Figure 5.19 demonstrates striking dissimilarities between the Arc-F10H–non-operator DNA mixture and the Arc-F10H–non-operator DNA complex. The difference spectrum reflects very weak interaction of Arc-F10H and non-operator DNA in the mixture 15 min after preparation. However, complex is formed and equilibrium reached within approximately 13 hours after mixing of both components. The time dependent measurements show a slow reaction that results in large spectral effects after sufficiently long reaction times. Secondary structures of Arc-F10H and DNA backbone are perturbed significantly as indicated by both Raman and CD spectroscopy (Figures 5.20 and 5.22). Both components probably need surprisingly long time to adjust their conformations to fit together and reach equilibrium. After dilution of the complex to the final concentration of 280 nM no complex dissociation was detected indicating the formation of a rather stable complex. CD spectra of the Arc-F10H–non-operator DNA complex in the DNA region are very similar at the concentrations of 1.4 mM, 140 μM, and 280 nM.

Why is the reaction mechanism between Arc-F10H and non-operator DNA slow? The answer for this question still remains to be determined.

5.5. Results and Discussion: Regulatory Protein KorB

5.5.1 Raman Spectrum of the Unbound 17-bp O_B DNA

The Raman spectrum of the 17-bp O_B DNA in the 600-1760 cm^{-1} wavenumber region is shown in Figure 5.23. Wavenumber positions of the major peaks as given in the figure are in accordance with those given previously in the literature (*88-89, 93-94* and references therein).

The backbone conformation markers at 830 and 1092 cm^{-1} are diagnostic of B-DNA (*89*), and the nucleoside conformation markers at 670 cm^{-1} (dT), 682 cm^{-1} (dG), 729 cm^{-1} (dA), 752 cm^{-1} (dT), and 1256 cm^{-1} (dC) identify C2'-*endo*/*anti* conformers (*88-89*). The spectrum is the signature of the O_B DNA model and provides the basis for the interpretation of the difference spectrum.

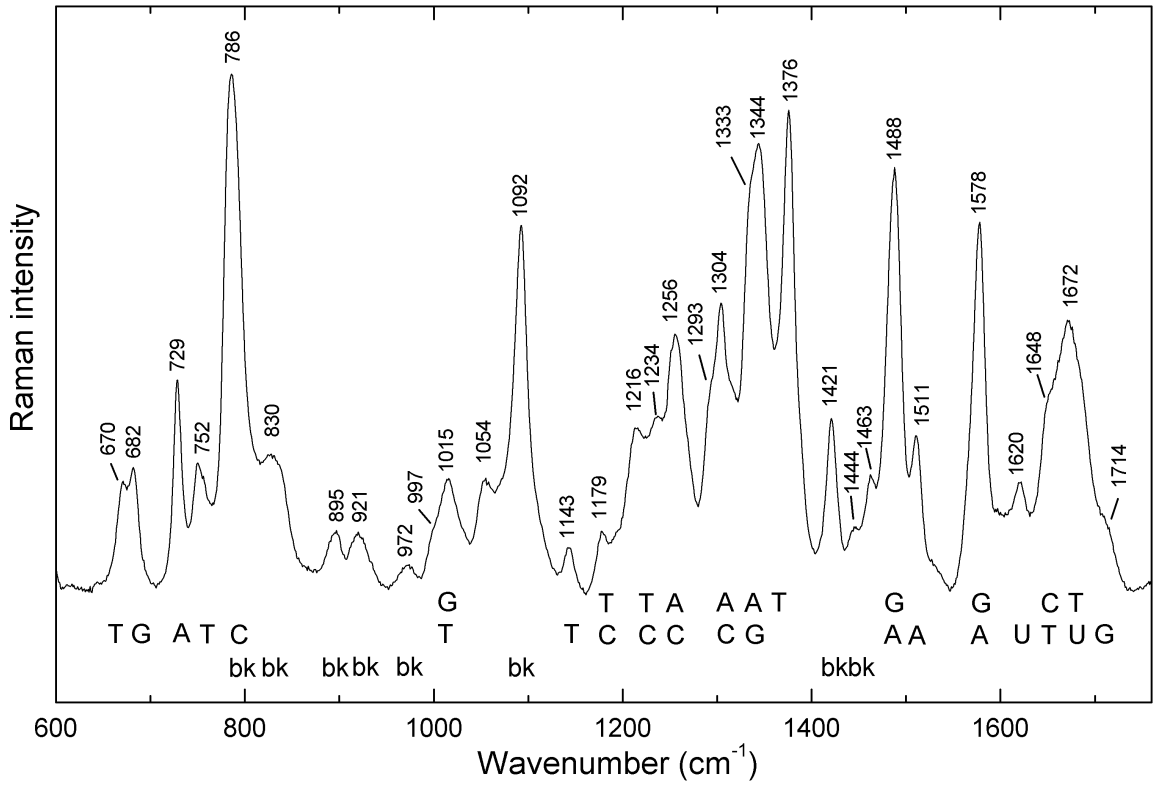

Figure 5.23: Raman spectrum of 17-bp oligonucleotide designed as operator DNA model (5'-A^{Br}UTTTAGCGGCTAAAAG–3' / 5'–C^{Br}UTTTAGCCGCTAAAA^{Br}U–3') in the region 600-1750 cm^{-1}. Sample buffer is 20 mM Tris pH 7.6 and 50 mM NaCl; data were collected at 22 °C. Peak positions of prominent Raman bands are labeled. Wavenumbers are accurate to within ± 0.5 cm^{-1}. Abbreviations are as follows: G, guanine; T, thymine; C, cytosine; A, adenine; U, uracil; bk, deoxyribose backbone.

5.5.2. Raman Spectrum of KorB-O

Figure 5.24 shows the Raman spectrum of KorB-O. Wavenumber positions of the major peaks are labelled by respective wavenumbers. Peak assignments of amide I (1640-1680 cm^{-1}) and amide III bands (1230-1300 cm^{-1}), bands of aromatic and non-aromatic amino acids, and the α-helical skeletal mode (~935 cm^{-1}) were done according to the literature (*102, 113* and references therein).

Secondary Structure of KorB-O. In accord with the crystal structure (*57*), α-helices are the principal type of secondary structure elements of KorB-O as indicated by the positions of main-chain vibrations of the amide I and amide III bands. The prominent amide I peak centred at 1653 cm^{-1}, the intensity at 1273 to 1302 cm^{-1} in the amide III region, and the high intensity in the C–C stretch region around 940 cm^{-1} indicate a high content of α-helices. The 1237 cm^{-1} shoulder of the amide III peak at 1249 cm^{-1} exhibits a minor contribution from β-structures to the spectrum. The intense amide III band at 1249 cm^{-1} and the shoulder of the amide I band near 1678 cm^{-1} indicate a significant content of irregular and turn structures.

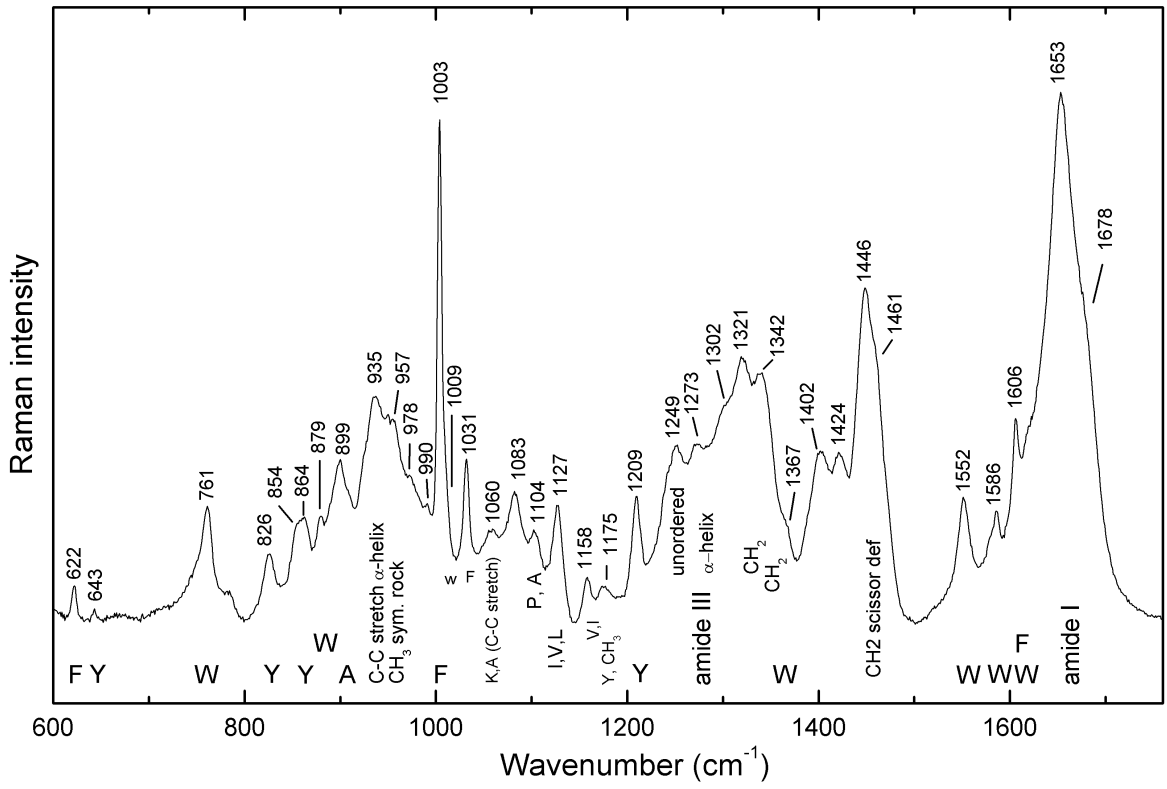

Figure 5.24: Raman spectrum of KorB-O in the region 600-1750 cm^{-1}. Sample buffer is 20 mM Tris pH 7.6 and 50 mM NaCl; data were collected at 22 °C. Peak positions of prominent Raman bands are labelled by the respective wavenumbers. Wavenumbers are accurate to within ± 0.5 cm^{-1}. One-letter code is used for amino acids. Abbreviations: CH_2, methylene; CH_3, methyl; C–C, carbon–carbon bond.

Environment of Tyrosine Side Chains. A tyrosine doublet at ~850 and ~830 cm^{-1} is caused by Fermi resonance of the normal mode ν_1 (ring breathing fundamental) and the second harmonic $2\nu_{16a}$ (ring deformation overtone) of the para-substituted phenolic side chain (*82*). The intensity ratio I_{850}/I_{830} is sensitive to hydrogen bonding of phenolic OH groups and, therefore, an indicator of the tyrosine environment. In the spectrum of KorB-O, a sharp peak appears at 826 cm^{-1} and a rather broad peak is seen around 858 cm^{-1} at the position of the tyrosine doublet. The intensity ratio I_{858}/I_{826} = 1.5 is in the range expected for tyrosines acting as both donor and acceptor of moderately strong hydrogen bonds as is the case when they are exposed to solvent H_2O molecules (*82*). The sharp 826 cm^{-1} peak obviously belongs to the Fermi doublet of Y2 and Y21, the two tyrosines present in the chain of KorB-O. The broad 858 cm^{-1} peak can be decomposed into two bands at 854 and 864 cm^{-1}. The 864 cm^{-1} band possibly arises from an aromatic side chain that is yet to be assigned.

Tryptophan. Two Trp residues, W7 and W114, contribute to the spectrum of KorB-O (Figure 5.24). Indole ring vibrations of W7 and W114 cause the peak at 879 cm^{-1} (called W17 mode) and a 1367 cm^{-1} shoulder of the 1342 cm^{-1} peak. The 879 cm^{-1} band position in the KorB-O spectrum can be attributed to exposed Trp residues with medium strong hydrogen bonds of the exocyclic Trp 1NH donors to water molecules. The Trp vibrations are sensitive to the indole ring environment; buried residues form sharp intense peaks, whereas the intensity is low for exposed residues. For the W17 mode, a frequency range between 883 and 871 cm^{-1} was observed; without H-bonding at the N1 site this band is located at 883 cm^{-1}, and at 871 cm^{-1} with strong H-bonding (*84*).

The frequency of the Trp band near 1550 cm^{-1} (called W3 mode) assumes values between 1542 and 1557 cm^{-1} depending on the absolute value of the $C_\alpha C_\beta$-C_3C_2 torsion angle $|\chi^{2,1}|$ which varies between 60° and 120° (*109*). The 1552 cm^{-1} position of the Trp band indicates an average $|\chi^{2,1}|$ value of ~90° for the two Trp residues of KorB-O.

KorB. Full length protein KorB was used to control whether its binding to operator DNA is similar to that of KorB-O. The KorB spectrum (Figure 5.25) is characterized by a very strong band of amide I near 1657 cm^{-1} and a very broad amide III band at 1250 cm^{-1}. Positions of these bands indicate large contribution of irregular and turn structures and a contribution of α-helices. The shoulders of the two bands at 1236 and 1672 cm^{-1} reflect the presence of β-sheet structures. The crystal structures of KorB-C (*43*) and KorB-O (*57*)

were recently determined. However, the structures of KorB-N (N-terminal part of KorB) and wild type KorB are still not known.

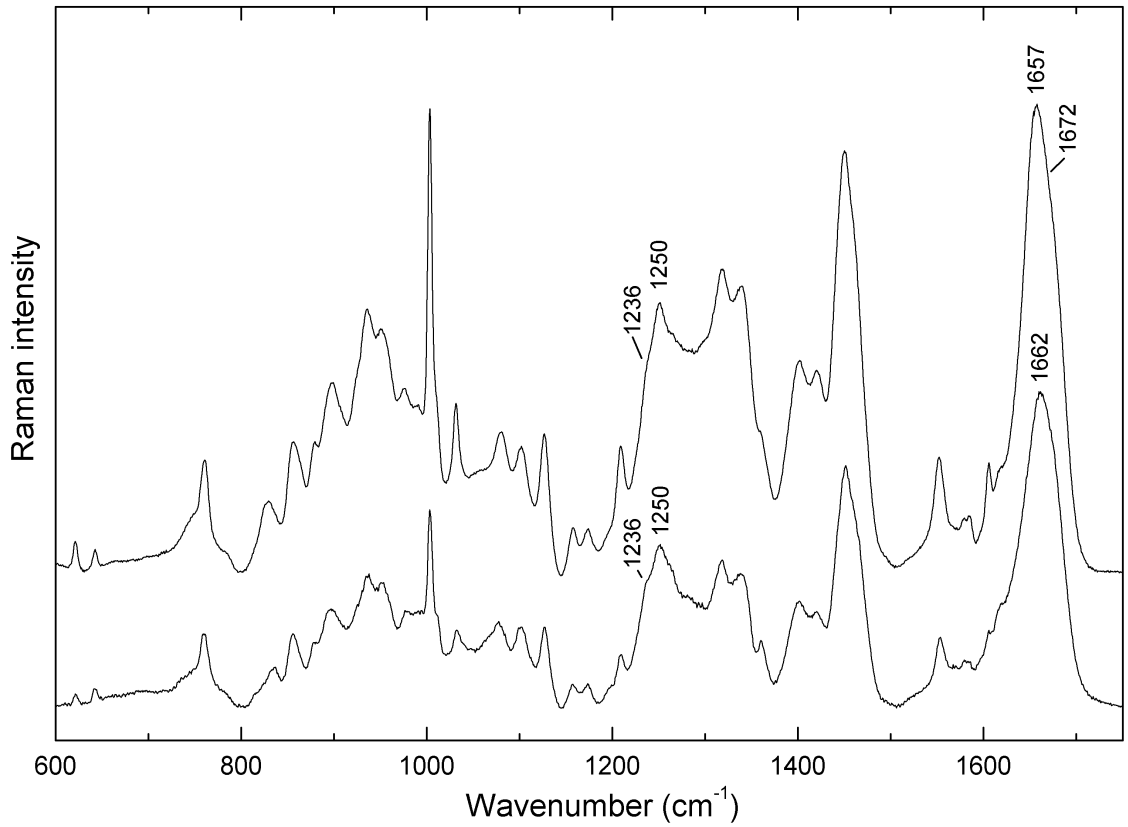

Figure 5.25: Raman spectrum of wild type KorB (top trace) and Raman spectrum of the sum of both KorB-C and KorB-N (bottom trace). The sum of KorB-C and KorB-N was calculated by subtraction of KorB-O–operator DNA complex from KorB–operator DNA complex. The complexes were normalized according to the phosphate band at 1092 cm^{-1}. The amide I and amide III bands are labelled by respective wavenumbers. The experimental conditions are as given in the legend of Figure 5.24.

To identify the secondary structure of KorB-N, the spectrum of KorB-O–operator DNA complex was subtracted from the spectrum of KorB–operator DNA complex. The perturbations caused by complex formation (see below) are very similar for the two protein complexes and therefore the difference spectrum might be a reliable representation of the Raman spectrum of the KorB-C and KorB-N domains. Figure 5.25 shows the resulting Raman spectrum of the KorB-C and KorB-N domains of KorB. The position of the amide I band at 1662 cm^{-1} indicates that the secondary structure of KorB-C and KorB-N is composed mostly of unordered and β-sheet structures and minor contributions of α-helical structures. The amide III bands at 1250 and 1236 cm^{-1} reflect the same. The KorB-C contains β-sheet, unordered structures and small amounts of α-helical structures (*43*). Possibly KorB-N is mostly unordered which would explain experimental difficulties to crystallize the KorB-operator DNA complex (D. Khare, personal communication).

5.5.3. Raman Analysis of the KorB– and KorB-O–DNA complexes

The Raman spectrum of the KorB-O–DNA complex is shown in the top of Figure 5.26 (red trace). The green trace represents the DNA spectrum from Figure 5.23, and the blue trace is the KorB-O spectrum from Figure 5.24. The black trace is the difference spectrum obtained by subtraction of the component spectra from the spectrum of the complex. A positive difference peak indicates an increased Raman intensity at the respective wavenumber region in the spectrum of the complex compared to the sum of component spectra, and a negative trough is caused by a lower intensity in the spectrum of the complex.

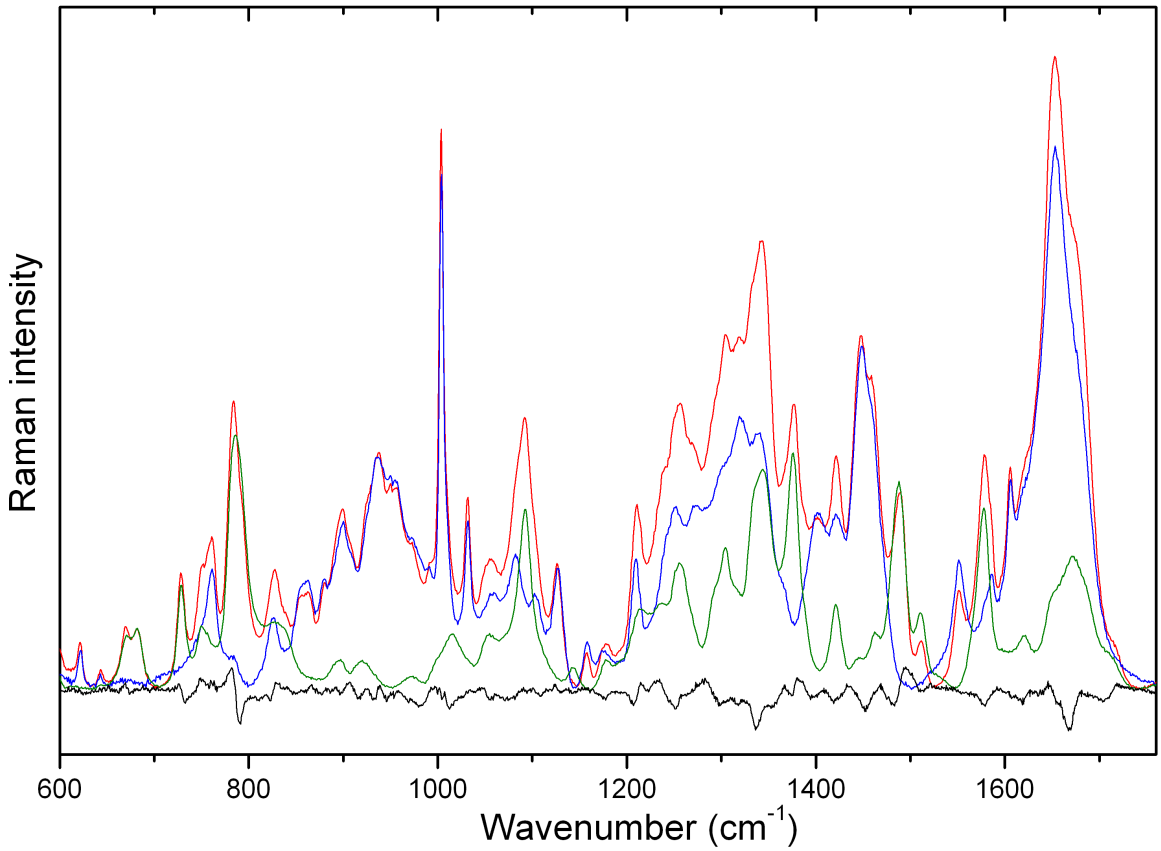

Figure 5.26: Raman spectrum of KorB-O in complex with 17-bp operator DNA (KorB-O–DNA) in the region 600-1750 cm^{-1} (red trace). The blue trace shows the Raman spectrum of the isolated protein from Figure 5.24. The green trace shows the Raman spectrum of DNA from Figure 5.23. The black bottom trace shows the computed difference spectrum obtained by subtraction of the isolated component spectra from the experimental spectrum of the complex. The spectra are normalized to represent the same amounts of protein and DNA in the complex and in free form.

The amplified and, for clarity, smoothed difference spectrum from Figure 5.26 (black bottom trace) and the smoothed Raman difference spectrum of KorB-DNA operator complex (top trace) are shown in Figure 5.27. These spectra have been used for the further

analysis. The features of the difference spectrum provide information about conformational changes, structural rearrangements and interactions between DNA and protein. A reliable and detailed interpretation of the difference bands is easier in spectral regions with separate vibrations of DNA and protein and difficult where bands of both components overlap.

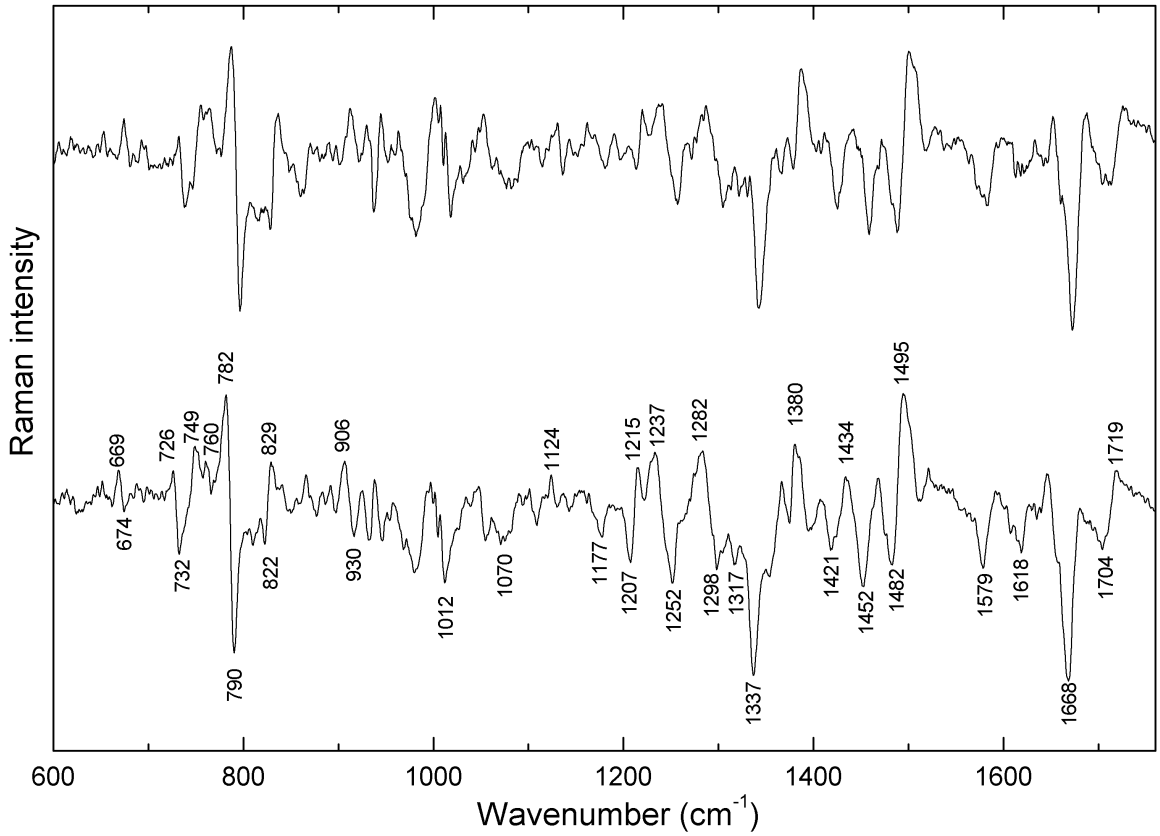

Figure 5.27: Enlarged Raman difference spectra. The top trace shows the difference spectrum of KorB–operator DNA complex and the bottom trace is the difference spectrum of KorB-O–operator DNA complex from Figure 5.26. Spectra were smoothed using the 11-point Savitsky-Golay algorithm.

Backbone and Deoxynucleoside Conformation of the DNA. The 600-900 cm^{-1} region contains Raman markers of deoxynucleoside conformation and DNA backbone geometry (*89*). The peaks at 670 and 682 cm^{-1} in the spectrum of the O_B DNA (Figure 5.23) are thymine and guanosine nucleoside conformation markers, respectively, for B-form DNA and sensitive to altered deoxynucleoside conformation. In the difference spectrum, there is a peak at 669 and a trough at 674 cm^{-1}. This feature possibly reflects a minor downward shift of the 670 thymine band. A difference feature with peak at 726 and trough at 732 is observed indicating a downshift of the 729 cm^{-1} adenosine marker band. The peak at 749 cm^{-1} is probably caused by a downshift or intensity change of the 752 cm^{-1} band of

thymidine. Altogether, these difference features signalize altered deoxynucleoside conformation of thymidine and adenosine in the complex.

A 782 cm^{-1} peak in the Raman spectra of DNA is assigned to cytosine, and a 794 cm^{-1} peak is assigned to a stretching vibration of backbone phosphodiester groups and diagnostic of B-form DNA backbone geometry, specifically of torsion angles α and ζ in *gauche*$^-$ range (*100*). The 782 cytosine and 794 backbone bands overlap in the O_B DNA spectrum to a large 786 cm^{-1} peak. In the difference spectrum a prominent derivative feature (~ 20% relative intensity change) with 782 and 790 cm^{-1} peak and trough, respectively, is located in this region. The difference feature may be caused by changes in one or both bands and signalize cytosine interactions and/or changes in the backbone conformation.

In the difference spectrum a clear derivative feature is present with trough at 822 and peak at 829 cm^{-1}. In this region the 830 cm^{-1} B-DNA backbone band and the 826 cm^{-1} peak of tyrosine overlap, therefore, this difference feature could be caused by DNA and/or protein contributions. The derivative feature suggests an intensity shift centred near 826 cm^{-1} and therefore points a minor frequency change of the Tyr band. Another and more probable explanation is a shift of the GC conformation marker band located at 828 ± 2 cm^{-1} (*89*) to higher wavenumbers.

The B-DNA backbone conformation marker band of AT base pairs is located at 839 ± 2 cm^{-1}. Difference features in the 840-860 cm^{-1} region were observed indicating distortion of the B-DNA backbone upon protein binding to AT base pairs (*100, 104*). In the KorB-O–DNA difference spectrum, the features in the region around 840 and 860 cm^{-1} do not fulfil the criteria of significance indicating that the distortion of the backbone of AT base pairs is less pronounced than that of GC base pairs.

Deoxyribose Ring and Protein CH_2/CH_3 Vibrations. Furanose vibrations were identified in Raman spectra of DNA at 1419 and 1455 cm^{-1} and assigned to backbone vibrations (*100*). In the spectrum of the 17-bp O_B DNA the peak positions of these bands are at 1421 and 1463 cm^{-1}, and a further minor peak is located at 1444 cm^{-1}. Protein bands are also located in this spectral region. A COO^- symmetric stretch vibration causes the 1402 cm^{-1} peak, a band at 1424 cm^{-1} reflects CH_2 and CH_3 deformations and at 1446 cm^{-1} CH_2 scissoring modes are found. Therefore, the difference features observed between 1418 and 1452 cm^{-1} may be assigned to backbone vibrations of the DNA and/or changes in the protein. These backbone vibrations are mainly caused by 2'-CH_2 scissoring vibrations of

the furanose residues which, coming in contact with protein side chains, are influenced and give rise to the observed difference feature. Also, CH_2 and CH_3 scissoring modes of the protein side chains may contribute to the difference spectrum. The contributions of the DNA may potentially be caused by alterations of the DNA helix geometry as induced by bending and/or unwinding as described for a SRY HMG box–DNA complex (*100*). However, the bending was not observed in the crystal structure (*57*) and therefore, the perturbations in these regions are coming mostly from alterations of protein side chain vibrations upon binding and altered furanose residue environments caused by hydrophobic contacts with protein (*57, 100*).

Major-Groove Binding of KorB-O. Protein-DNA complexes studied by Raman spectroscopy provide examples for major-groove binding, minor-groove binding, and interaction with single-stranded DNA (*89, 93-94, 100, 106-107*). Recently, Raman markers of different protein/DNA recognition motifs were proposed (*93*). Comparison of features of the KorB-O–DNA difference spectrum with proposed Raman markers will be discussed below.

Raman bands in the interval 1300-1750 cm^{-1} are sensitive to specific interactions of major groove-binding proteins to DNA bases (*93-94, 106-107*). Several features of the KorB-O–DNA difference spectrum indicate major groove binding.

The prototype Raman marker of protein-DNA interaction in the major groove is considered the guanine band near 1490 cm^{-1}. At this spectral position, Raman intensity of G and A overlaps, with a significantly larger contribution from G. Therefore, in the spectra of DNA the intensity of this band strongly depends on the base composition of the DNA. For DNA composed of only A and T base pairs the band is weak and located at 1482 cm^{-1} (*30*). This band shifts to near 1470 cm^{-1} upon hydrogen-bond donation to the N7 guanine ring acceptor (*90, 94, 106*), resulting in a characteristic derivative band profile with difference peak at ~1470 cm^{-1} and trough at ~1490 cm^{-1}. Such a derivative band profile is clearly missing in the difference spectrum of the KorB-O–DNA complex. Instead, in this spectral region a large trough at 1482 cm^{-1} and a large peak at 1495 cm^{-1} are observed. The crystal structure indicates two direct contacts of Arg240 with guanine at position N7 and O6 at both half-sites of the operator DNA. Accordingly, the observed peak/trough feature at 1495/1482 cm^{-1} is caused by hydrogen bond formation of guanine N7 and arginine.

Major-groove binding of proteins may cause a reduction of Raman intensity at 1717 cm^{-1} attributed to guanine O6 interactions (*90, 106*) and lead to a trough in the difference spectrum. For the free DNA a corresponding band is identified at 1714 cm^{-1}, and in the

difference spectrum a derivative feature with trough at 1704 and peak at 1719 cm^{-1} is observed. The difference feature indicates a surprisingly large change in the relative intensity and position of the G O6 band and provides a strong evidence for major groove binding of KorB-O.

The adenine and guanine Raman marker bands at 1344 and 1578 cm^{-1} exhibit large effects upon protein binding (*100, 36*) and probably cause the large difference troughs at 1337 and 1579 cm^{-1}. In the case of significant purine unstacking, an intensity increase of the 1344 and 1578 cm^{-1} bands and corresponding difference peaks in these spectral regions would be visible. However, difference peaks at ~1340 and ~1585 cm^{-1} are missing and therefore no significant purine unstacking is induced by KorB-O binding.

From experiments analyzing temperature effects on the Raman spectrum of poly(dA–dT)·(dA–dT), Raman markers were identified for pre-melting and melting transitions of AT-rich DNA sequences. Hydrogen bonding interactions between the bases and the geometry of phosphodiester backbone are perturbed throughout the premelting (*105*). The most significant perturbation during premelting was observed near 1340 cm^{-1} in the band of adenine, which shifts from 1345 to 1330 cm^{-1} (1345→1330). Other significant temperature-dependent changes of adenine bands emerged near 1578 (1579→1571) and 1511 (1516→1502), and near 1485 an intensity increase was observed. During complex formation, an opposite effect could be expected, provided that binding of the protein is connected with increased stability of terminal A–^{Br}U base pairs which are fraying to some extent in the free DNA. Increased stability of the base pairs should cause a frequency shift of the 1330 and 1571 cm^{-1} bands of breathing adenine to 1344 and 1578 cm^{-1} and a significant hypochromic effect. This explains the observed troughs near 1337 and 1578 cm^{-1}.

This interpretation is encouraged by the appearance of the trough at 1618 cm^{-1} assigned to bromodeoxyuridine. Bromodeoxyuridine is located at the ends of both strands of the oligonucleotide and base-paired with adenine. Reduced fraying of those A-^{Br}U base pairs should have a hypochromic effect on the 1620 cm^{-1} uridine band and the reduced Raman intensity should cause a trough at this position, as in fact can be observed in the difference spectrum.

In DNA spectra a peak at 1378 cm^{-1} is assigned to the thymine exocyclic $C5H_3$ group. Increased hydrophobicity in the surrounding of thymine $C5H_3$ groups increases the intensity of the 1378 band, as observed in wild type λ repressor–operator DNA complex (*90*) where the thymine $C5H_3$ groups are shielded by hydrophobic side chains of the

repressor. Similarly, the difference spectrum of KorB-O–DNA complex shows a large difference peak at 1380 cm^{-1} indicating shielding of thymine $C5H_3$ groups from water environment. A small wavenumber shift from 1376 to 1380 might be caused by an additional, still unidentified effect, as e.g. interaction with protein groups. Thus, the 1380 difference peak is consistent with KorB-O binding in the major groove. The crystal structure of KorB-O–operator DNA complex exhibits several van der Waals interactions with thymine $C5H_3$ (*57*) reflected by a difference peak at 1380 cm^{-1}. The interaction with thymine would be further supported by a very large and sharp trough at 1668 cm^{-1} at the position of the thymine band at 1672 cm^{-1} assigned to thymine C=O4, but the crystal structure does not indicate such a contact. Alternatively, the trough might reflect thymine hypochromism (*105, 108*) which is consistent with the previous assumption about reduced fraying of both ends of operator DNA.

Secondary Structure Changes of KorB-O and Interaction with Cytosine. The difference spectrum of KorB-O–DNA reveals significant but not very large spectral changes in the region between 1200 and 1340 cm^{-1} where the intensive bands of KorB-O (amide III, CH_2 twist/wag) overlap with the wide, intense 1256 cm^{-1} band of cytosine and thymine of the 17-bp O_B DNA. Thus, vibrations of protein, DNA or both components of the complex can cause the observed features of the difference spectrum. The situation is similar in the 1640-1690 cm^{-1} region, where the intensive amide I protein bands overlap with guanine and thymine bands. However, in interpreting any changes in the secondary structure of KorB-O, possible contributions from DNA to the amide I and amide III regions must be taken into account.

The crystal structure of KorB–operator DNA complex indicates two hydrogen bonds of Thr211 to cytosine $N4H_2$. The cytosine exhibits most prominent bands between 1200 and 1300 cm^{-1} which overlap with contributions of thymine and amide III bands. Interactions with cytosine may be indicated in this region.

In the 1200-1340 cm^{-1} region, troughs around 1207, 1252, 1298, 1317 and 1337 cm^{-1} are present; difference peaks are at 1215, 1237 and 1282 cm^{-1}. The 1252 cm^{-1} trough is possibly caused by diminished intensity of the amide III band at 1249 cm^{-1} pointing to a reduction of unordered structures. Alternatively, changes in the 1256 and 1234 cm^{-1} cytosine/thymine bands have to be considered as cause of the 1237/1252 cm^{-1} peak/trough feature. The large difference trough at 1668 cm^{-1} provides a further hint to conformational changes reducing turns and irregular structures in the secondary structure of KorB-O.

Another difference feature in the amide III region is composed of a 1298 cm^{-1} trough and 1282 cm^{-1} peak. Amide III bands at 1273 and 1302 cm^{-1} are assigned to α-helices. The observed difference feature may be caused by intensity and/or frequency shifts of the helix vibrations, reflecting conformational changes in the protein including helical structures. More probably, the peak/trough feature at 1282/1298 reflects the downshift of the cytosine marker band at 1293 cm^{-1}.

Changes in Side Chains of Nonaromatic Amino Acids of KorB. The difference spectrum of KorB-O–DNA (Figure 5.27) reveals perturbations in Raman bands of nonaromatic amino acids (C-C or/and C-N stretch, CH_2 and CH_3 vibrations) (*102*). Relevant features are a difference peak at 760 cm^{-1} (possible contributions of Trp and CH_2 rock of several amino-acid side chains), difference features around 930 cm^{-1} (CH_3 symmetric rock), a broad difference trough at 1070 cm^{-1} (C-O stretch of serine, threonine, glutamic acid and aspartic acid, C–C stretch of alanine and lysine, C-N stretch of proline, possibly complicated by buffer subtraction problems and potential overlapping of the PO_2^- vibration), a peak at 1124 cm^{-1} (C–C stretch of valine, leucine and isoleucine), trough at 1177 cm^{-1} (CH_3 symmetric rock, contribution of Tyr) and the troughs at 1337 cm^{-1} (lysine CH_2 twist/rock, alanine CH_2 bend and a large contribution from DNA as discussed above) and 1452 cm^{-1} (C–C stretch and contribution from 2'-CH_2 scissoring vibration of DNA backbone). The large trough at 1452 cm^{-1} surrounded by small peaks on both sides shows widening and slight shift of the 1446 cm^{-1} parent band assigned to CH_2 and CH_3 deformation vibrations. These perturbations show changes in the conformation of non-aromatic amino-acid side chains. This may indicate structural rearrangements of KorB upon complex formation as well as interaction with O_B DNA.

5.6. Results and Interpretation: Sac7d Protein

5.6.1. Raman Spectrum of d(GAGGCGCCTC)$_2$

The self-complementary DNA sequence of the decameric oligonucleotide d(GAGGCGCCTC)$_2$ used in this study is closely related to that of the octamers studied previously in crystal structure analyses of Sac7d–DNA complexes (*68-70*). Figure 5.28 shows the Raman spectra of d(GAGGCGCCTC)$_2$ in H_2O and D_2O buffer.

Wavenumber positions of the major peaks are given in Figure 5.28. The peak positions are in general accordance with those of DNA given previously in the literature (*88-89, 93-94* and references therein).

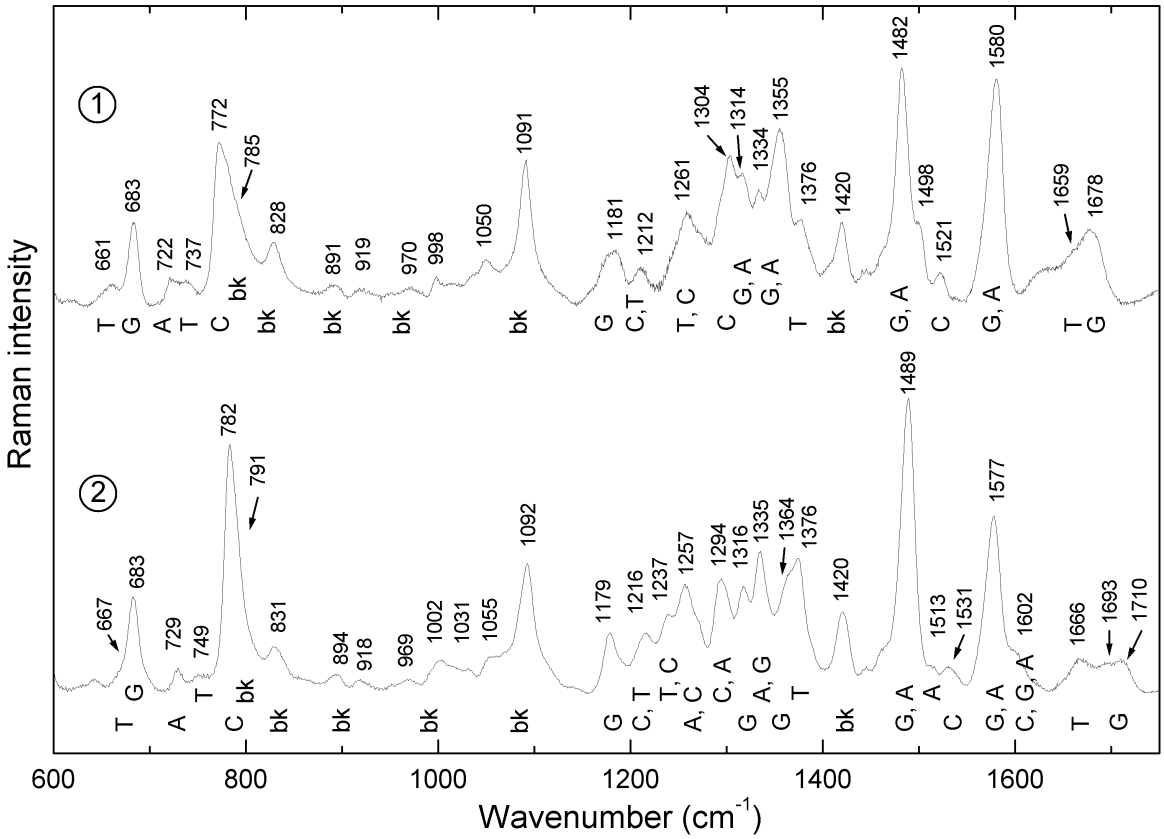

Figure 5.28: Raman spectra of 10-bp oligonucleotide d(GAGGCGCCTC)$_2$ (decamer I) in H_2O (2) and D_2O (1) solution. Sample buffer is 50 mM Tris-HCl pH 7.3 for spectrum (2) or pD 7.5 for spectrum (1) and 50 mM NaCl; data were collected at 22 °C in the region 590-1750 cm^{-1}. Concentrations are 12 mg/mL (H_2O) and 13 mg/mL (D_2O). Spectra were normalized with respect to the integrated intensity of the phosphate band near 1092 cm^{-1} and the adenine-guanine band near 1580 cm^{-1} (*94-95*). Peak positions of prominent Raman bands are labeled, the given wavenumbers are accurate to within ± 1 cm^{-1}. Abbreviations are as follows: G, guanine; T, thymine; C, cytosine; A, adenine; bk, deoxyribose backbone.

The backbone conformation markers at 831 and 1092 cm^{-1} in H_2O and at 828 and 1091 cm^{-1} in D_2O are diagnostic of B-DNA (*89*). The positions of the nucleoside conformation markers shift upon deuteration [from 667 cm^{-1} to 661 cm^{-1} (dT); 729 cm^{-1} to

722 cm^{-1} (dA); 749 cm^{-1} to 747 cm^{-1} (dT); 782 cm^{-1} to 772 cm^{-1} (dC); 1257 cm^{-1} to 1261 cm^{-1} (dC)]. The 683 cm^{-1} dG marker band does not shift.

The nucleoside conformation markers identify C2'-*endo*/*anti* conformers. The spectra shown in Figure 5.28 are the signature of $d(GAGGCGCCTC)_2$, and provide the basis for the interpretation of the difference spectra shown in Figure 5.31.

5.6.2. Raman Signature of Sac7d

The Raman spectrum of Sac7d in H_2O (Figure 5.29, trace 2) is characterized by a strong amide I band (1640-1680 cm^{-1}) centered at 1670 cm^{-1} and a broad, complex amide III band (1230-1310 cm^{-1}) with a major contribution at 1242 cm^{-1} and weak shoulders at 1250 (irregular structures), 1268, 1285, and 1306 cm^{-1} (α-helix). The features of the amide I and amide III band indicate β-strands as the main secondary structure elements of Sac7d. Calculation of the Sac7d secondary structure based on the amide I band intensity profile (*114*) gives 50 ± 4% β-strand, 15 ± 4% α-helix, and 35 ± 3% irregular structures. The data are in agreement with the crystal structure of Sac7d (*68*). Figure 5.29 shows the Raman spectrum of Sac7d in fully protonated (non-exchanged) form measured in H_2O buffer (trace 2), and the Raman spectrum of the partially deuterated Sac7d obtained in D_2O (trace 1). Trace 3 shows the computed Raman difference spectrum (trace 1 minus trace 2) and represents the native exchange, i.e. the exchange of hydrogen atoms that are exchangeable in the folded state of Sac7d. Information about the secondary structure of natively exchanged and protected sites of Sac7d can be deduced from the large difference features at the positions of the amide I and amide III bands (in H_2O) and the positions of the amide I' and amide III' bands (in D_2O). The Raman intensity at the positions of the amide III and amide I bands is reduced and causes troughs in the difference spectrum.

Concomitantly, the Raman intensity at the positions of the amide III' and amide I' bands is increased and gives rise to difference peaks. Several trough/peak features are caused by the native state-deuteration induced frequency shift of amide III to amide III´. The trough/peak feature near 1239 and 986 cm^{-1} is caused by β-strands, and that near 1251 and 926 cm^{-1} is caused by irregular structures. Deuteration of the few α-helical secondary structures present in Sac7d results in complicated features at 1305, 1282, 1265 and 948 cm^{-1}. In the amide III region of Sac7d remain weak bands because of incomplete deuteration under the applied conditions of native exchange. The features of the amide I and amide I´ bands with trough and peak, respectively, near 1674 and 1658 or 1640 cm^{-1}

provide additional Raman signatures for native (incomplete) deuterium exchange of secondary structure elements.

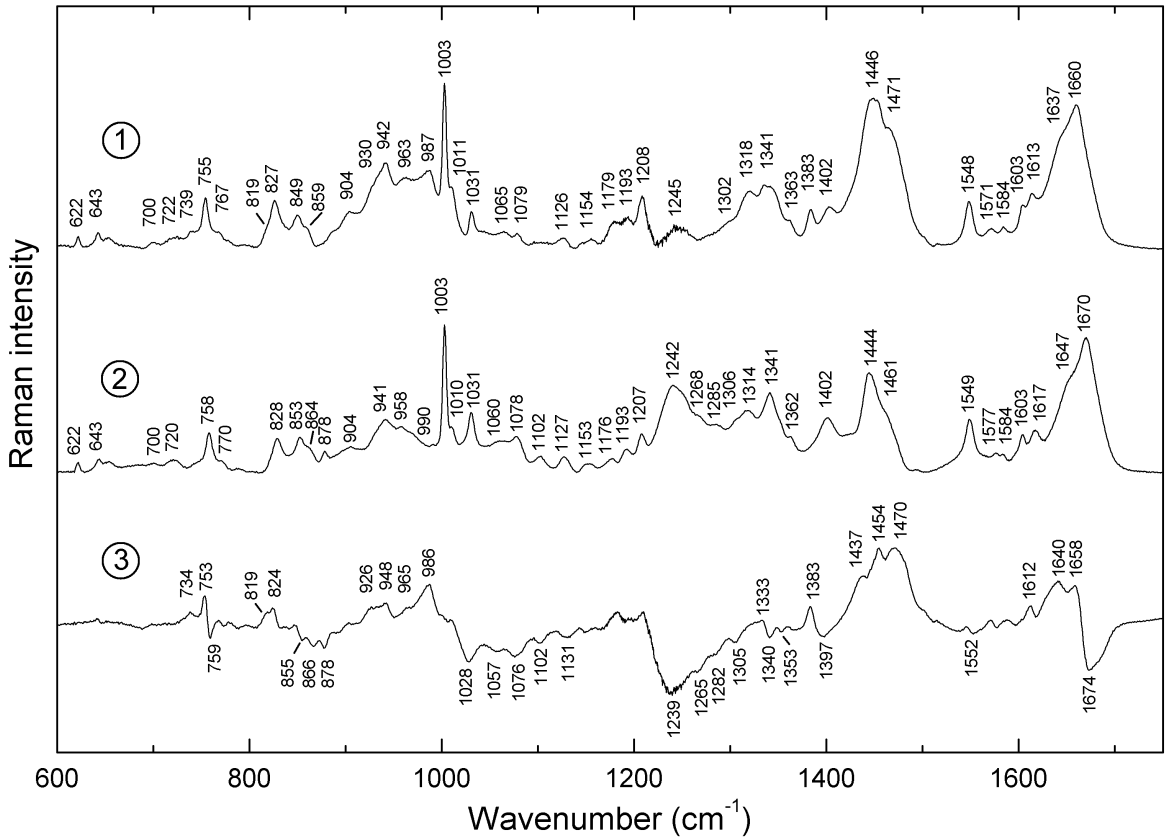

Figure 5.29: Raman spectra of Sac7d. (1) Natively H→D exchanged Sac7d. (2) Native Sac7d. (3) Difference spectrum (spectrum 2 minus spectrum 1). Excitation at 488 nm, spectral region 600-1750 cm^{-1}, protein concentrations are 22 mg/ml (H_2O) and 17 mg/mL (D_2O), buffers are 50 mM Tris-HCl, pH 7.5 in H_2O and pD 7.5 in D_2O, and 50 mM NaCl; data collection at 22 °C. Spectra 1 and 2 were normalized to the integrated intensity of the phenylalanine band at 1003 cm^{-1}, which is not effected by deuteration (*20*). For the calculation of the difference spectrum 3 the normalized spectra 1 and 2 were subtracted such that the intensity at the 1003 cm^{-1} phenylalanine band becomes zero. Peaks in the difference spectrum 3 appear when natively unprotected protons are exchanged against deuterons and the Raman bands are shifted. Peak positions of prominent Raman bands are labelled by the respective wavenumbers that are accurate to within ± 0.5 cm^{-1}.

A very weak amide II band at 1550 to 1560 cm^{-1} (Figure 5.29-2) represents N-H in-plane bending and C-N stretching of the trans peptide group. Deuteration of those groups causes an intense amide II' band at 1471 cm^{-1} (Figure 5.29-1), and results in the most prominent feature of the difference spectrum with peak at 1470 cm^{-1} (Figure 5.29-3). This band can be assigned to non-α-helical (unprotected) sites of Sac7d (*101*).

Amino Acid Side Chains. The Raman spectra of Sac7d (Figure 5.29, traces 1 and 2) show typical contributions of aromatic side chains of tryptophan (1), phenylalanine (2), tyrosine (2), and bands of non-aromatic amino acids (Table 5.3). Assignments were performed according to literature (*101-103* and references therein).

Table 5.3: Vibrational Assignments for Raman Markers of Sac7d in H_2O and D_2O solutions[a]					
H_2O	D_2O	Assignment[b]	H_2O	D_2O	Assignment[b]
622	622	F	1153	1154	V, I
643	643	Y	1176	1179	Y, [CH_3]
654	653	?	1193	1193	?
700	700	M	1207	1208	F,Y
720	722	Y	1242	1245	AmIII (strand)
758	755	W	1268	-	AmIII (helix)
770	767	W	1285	-	AmIII (helix)
828	827	Y	1306	1302	[CH_2], AmIII (helix)
853	849	Y	1314	1318	[CH_2]
878	859	W	1341	1341	[CH_2]
904	904	Q, S, T	1362	1363	W
-	930	AmIII (coil, turns)	-	1383	W
941	942	K, V, L, AmIII (helix)	1402	1402	[COO^-]
958	963	K, L	1444	1446	K, I, L, [CH_2]
-	987	AmIII (strand)	1461	-	A, I, V, L, W, Y [CH_2]
990	-	I	-	1471	AmII
1003	1003	F	1549	1548	W
1010	1011	W	1577	1571	W
1031	1031	F	1584	1584	F
1060	1065	K, A (C-C stretch), F	1603	1603	F,Y
1078	1079	C-C, C-N stretch	1617	1613	W
1102	-	P, A	1647	1637	AmI (helix)
1127	1126	I, V, L	1670	1660	AmI (strand, coil)

[a] Raman data are from Sac7d spectra shown in Figure 5.29.
[b] Assignments to specific amino acid side chains (one letter abbreviations) are based upon literature data (*101-103*). Square brackets indicate chemical group frequencies common to more than one type of side chain. Amide (Am) modes are diagnostic of the indicated secondary structure.

Environment of Tyrosine Side Chains. Two tyrosines, Y8 and Y34, are present in Sac7d. A tyrosine doublet at ~850 and ~830 cm^{-1} (about the same position in H_2O and D_2O) is caused by Fermi resonance of the normal mode ν_1 (ring breathing fundamental) and the second harmonic $2\nu_{16a}$ (ring deformation overtone) of the para-substituted phenolic side chain (*82*).

The intensity ratio I_{850}/I_{830} is sensitive to hydrogen bonding of phenolic OH groups, and therefore an indicator of the tyrosine environment. In the H_2O spectrum (Figure 5.29-2) of Sac7d, two relatively sharp peaks of approximately equal intensity appear at 828 and 853 cm^{-1}. The intensity ratio $I_{853}/I_{828} = 1$ is in the range expected for tyrosines acting as

both donor and acceptor of moderately strong or weak hydrogen bonds, as is the case when they are exposed to solvent H_2O molecules (*82*). After H→D exchange (Figure 5.29-1) these bands marginally shift to 827 and 849 cm^{-1}, respectively, and change the intensity profiles, with the band at 827 cm^{-1} becoming sharper and more intense than the band at 849 cm^{-1}.

Tryptophan. The Trp vibrations are sensitive to the indole ring environment. Buried residues form sharp intense peaks, whereas the intensity is low for exposed residues. The position of the indole ring vibration at 878 cm^{-1} (called W17 mode) of the unique Trp24 residue is indicative for exposed Trp residues with medium strong hydrogen bonds of the exocyclic Trp 1NH donors to water molecules. For the W17 mode, the frequency varies between 883 and 871 cm^{-1}; without H-bonding at the N1 site of Trp, this band is located at 883 cm^{-1}, and with strong H-bonding the band shifts to 871 cm^{-1} (*84*). In D_2O buffer the 878 cm^{-1} band of Sac7d vanishes and a new 859 cm^{-1} band appears. A similar downshift on deuteration was observed for free tryptophan (*103*).

The frequency of the Trp band near 1549 cm^{-1} (called W3 mode) assumes values between 1542 and 1557 cm^{-1} depending on the absolute value of the $C_\alpha C_\beta$-C_3C_2 torsion angle $|\chi^{2,1}|$ which varies between 60° and 120° (*105*). The position of the W3 mode does not vary in the spectra of deuterated and non-deuterated samples, and its position of 1548 ± 0.5 cm^{-1} indicates an average $|\chi^{2,1}|$ value of ~88°.

The Fermi doublet of tryptophan with components at about 1360 and 1340 cm^{-1} (with similar positions in the H_2O and D_2O spectra) serves as a hydrophobicity marker. The upper 1360 cm^{-1} component of the doublet is strong in hydrophobic solvents whereas in hydrophilic environment the lower 1340 cm^{-1} component is stronger. The intensity ratio, $R=I_{1360}/I_{1340}$, is below 0.9 for hydrophilic and higher than 1.1 for hydrophobic solvents (*84*). The intensity ratio is usually not detectable in proteins due to overlapping with bands caused by CH bending vibrations of aliphatic side chains. The Fermi doublet might be detected in difference spectra obtained by subtraction of the spectrum of the deuterated protein from that of the non-deuterated protein. Both bands of the doublet downshift for approximately 8 cm^{-1} upon deuteration (*84, 105*) that might result in detectable features of the difference spectrum. In fact, a very weak difference band near 1353 cm^{-1} and a relatively strong trough/peak feature at 1340/1333 cm^{-1} is visible in Figure 5.29-3 resulting from the downshift of both Fermi doublet components. The ratio, $R \approx 0.5$, of the two bands

of the Trp Fermi doublet is consistent with the presence of a surface localized tryptophan indole ring being exposed to the water molecules of the buffer.

Several other tyrosine and aliphatic amino acid side-chains contribute to the Sac7d Raman spectra shown in Figure 5.29-1 and 5.29-2. The assignment of Raman bands and corresponding H→D exchange wavenumbers are listed in Table 5.3.

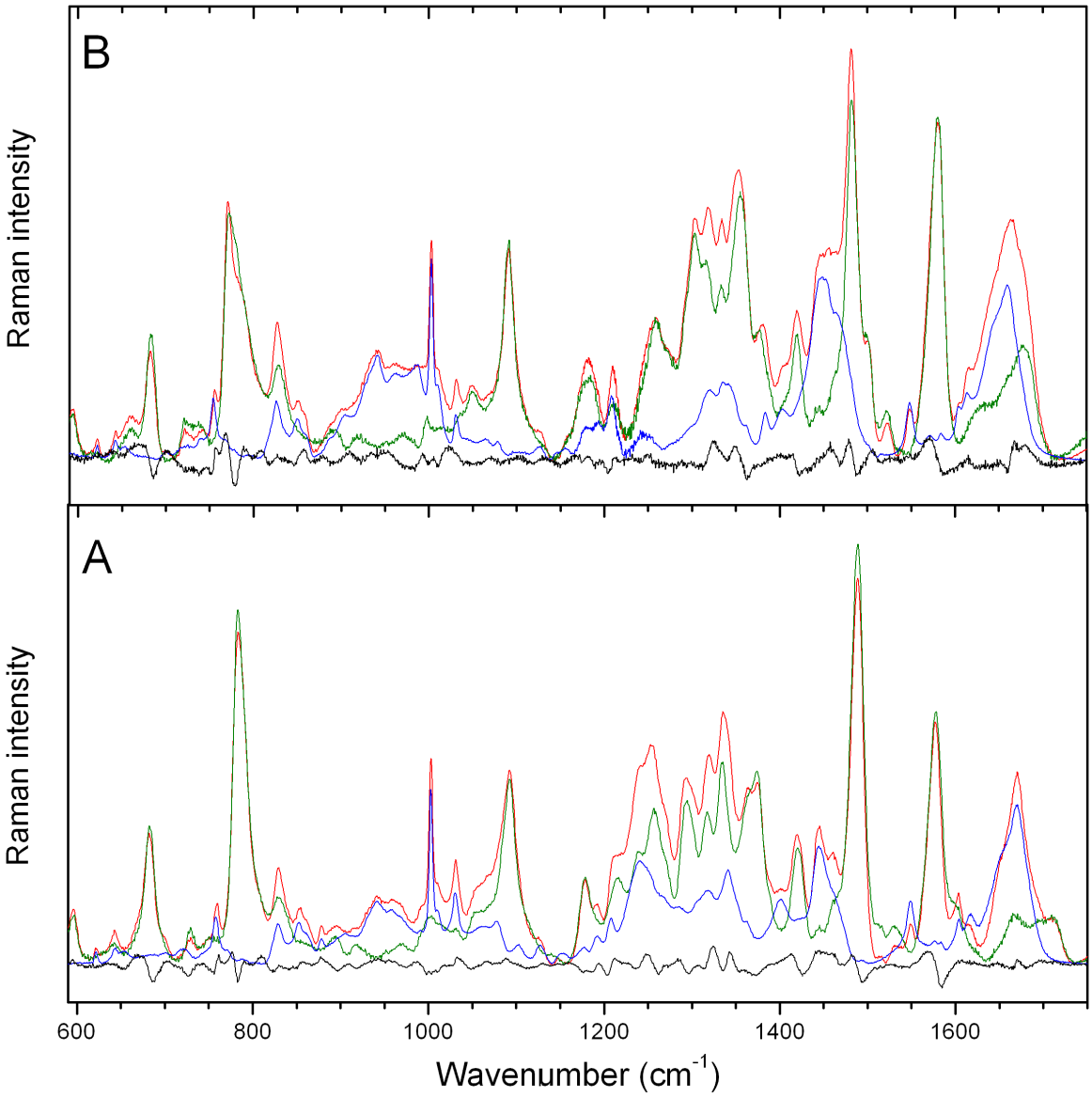

Figure 5.30: Raman spectra of Sac7d, d(GAGGCGCCTC)$_2$ and Sac7d–d(GAGGCGCCTC)$_2$ complex (Sac7d–decamer I). (A) Protein in H_2O buffer; (B) protein in D_2O buffer (50 mM Tris-D_2O, pH or pD 7.5 and 50 mM NaCl). Protein concentrations are 50 mg/ml (H_2O) and 36 mg/mL (D_2O); spectra were excited at 488 nm, and data were collected at 22 °C in the region 600-1750 cm^{-1}. The blue traces show the Raman spectra of the isolated native and natively exchanged Sac7d from Figure 5.29. The green traces show the Raman spectra of decamer I from Figure 5.28. The red traces show the spectra of the Sac7d–d(GAGGCGCCTC)$_2$ complex. The black bottom traces show the computed difference spectra obtained by subtraction of the isolated component spectra from the experimental spectrum of the complex. The spectra are normalized to represent the same amounts of protein and DNA in the complex and in free form.

5.6.3. Raman Analysis of the Sac7d–d(GAGGCGCCTC)$_2$ Complex

The Raman spectra of the Sac7d–d(GAGGCGCCTC)$_2$ complex and its components are given in panels A and B of Figure 5.30. Panel A shows the Raman spectrum of fully protonated Sac7d, and panel B shows the spectrum of partially deuterated Sac7d. The blue, green, and red traces represent the spectra of Sac7d, d(GAGGCGCCTC)$_2$, and complex , respectively, as given before in Figures 5.28 and 5.29. The black trace is the computed difference spectrum that was obtained by subtraction of the component spectra (green and blue traces) from the spectrum of the complex (red trace). Numerous peaks and troughs demonstrate spectral changes caused by complex formation of Sac7d with DNA. A positive difference peak indicates increased Raman intensity in the spectrum of the complex compared to the sum of component spectra, and a negative difference trough is caused by a lower intensity in the spectrum of the complex. When necessary, peak positions of deuterated samples will be given in parentheses.

Figure 5.31 shows the two amplified and, for clarity, smoothed difference spectra from Figure 5.30 (black traces) that are used for the further analysis. The features of the difference spectra provide information about conformational changes, structural rearrangements and interactions between the components of the complex.

Backbone Conformation of d(GAGGCGCCTC)$_2$. The 700-900 cm^{-1} region is characteristic for Raman markers of DNA backbone geometry (*89*). The 782 (772) cm^{-1} peak in the Raman spectra of DNA is assigned to cytosine. The 791 (785) cm^{-1} peak is assigned to a stretching vibration of backbone phosphodiester groups and diagnostic of B-form DNA backbone geometry, specifically of torsion angles α and ζ in *gauche*$^-$ range (*26-28*). The 782 cm^{-1} cytosine and 791 cm^{-1} backbone bands overlap in the H_2O spectrum of DNA spectrum to form a large 784 cm^{-1} peak. In D_2O, the frequency of the cytosine peak changes to 772 cm^{-1}, and a broad band is formed with the backbone vibration that is indicated by a shoulder at 785 cm^{-1}. The difference spectra show a prominent peak/trough/peak feature that is probably composed by contributions from the DNA backbone band and the cytosine band. Changes in the DNA backbone band result in the peak at 790 (788) cm^{-1} and trough near 782 (779) cm^{-1}, and cytosine causes the peak at 776 (768) cm^{-1} with trough near 782 (779) cm^{-1}. The corresponding features in the D_2O difference spectrum (with band positions as given above in parentheses) support this assignment. The H_2O and D_2O difference features indicate small conformational perturbations to the C5′-O5′-P-O3′-C3′ backbone network of DNA upon Sac7d binding. This is in agreement with previous observations (*96, 100*).

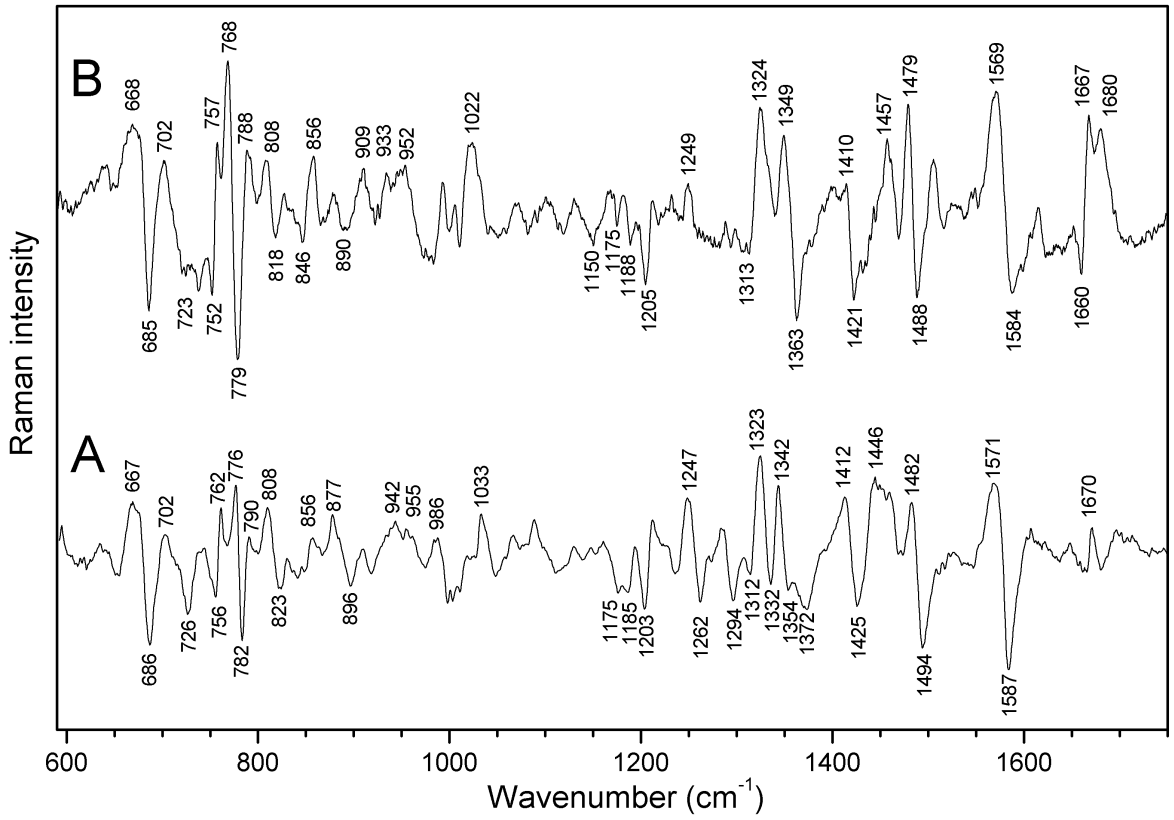

Figure 5.31: Enlarged Raman difference spectra (black bottom traces from Figure 5.30) of Sac7d–decamer I complex in H_2O buffer (A) and in D_2O buffer (B). Spectra were smoothed using the 11-point Savitsky-Golay algorithm.

Deoxynucleoside Conformation of d(GAGGCGCCTC)₂. Sac7d binding alters the furanose ring geometry. The double stranded oligonucleotide $d(GAGGCGCCTC)_2$ used in this study is composed of 80% GC and 20% AT. The difference spectra (Figure 5.31) indicate perturbations of the deoxynucleoside conformation of GC and AT base pairs. A very small adenosine band at 729 (722) cm^{-1} is distorted under the influence of Sac7d binding. The intensity decrease of this band at 726 (723) cm^{-1} and a peak/trough feature at 1342/1332 (Figure 5.31-A) indicate perturbations at dA. Difference features with trough/peak near 685/668 cm^{-1} and 1313/1324 cm^{-1} (Figure 5.31-B) are consistent with small changes at dG. Perturbations in cytosine nucleoside conformation markers are indicated in the difference spectra A (H_2O) and B (D_2O) by the respective peak/trough features at 776/782 (768/779) cm^{-1} and 1247/1262 (1249/-) cm^{-1}. Altogether, the observed spectral changes are consistent with partial transitions from C2′-endo/anti to C3′-endo/anti deoxynucleoside conformation at dG, dC and dA. Similar shifts of those Raman markers accompany the canonical B- to A-form transition of DNA (*95, 115-116*).

In DNA, for AT-rich sequences the phosphodiester B-form marker is located near 838-840 cm^{-1}, for GC-rich sequences the corresponding marker occurs near 828-830 cm^{-1}, and in the A-form DNA a phosphodiester marker appears near 807 cm^{-1} (*88*). In the difference spectrum of the Sac7d–d(GAGGCGCCTC)$_2$ complex a prominent difference peak/trough feature at 808/823 cm^{-1} and a small peak at 856 cm^{-1} are indicative of a distortion of the DNA backbone and provide additional evidence for the backbone changes described above.

Deoxyribose Ring and Protein CH_2/CH_3 Vibrations. Furanose vibrations were identified in Raman spectra of DNA near 1420 and 1460 cm^{-1} and assigned to backbone vibrations (*95, 99-100*). In the spectrum of d(GAGGCGCCTC)$_2$ (Figure 5.28) the peak positions of those bands are at 1420 and 1461 cm^{-1}. Protein bands are also located in this spectral region. A COO^- symmetric stretch vibration causes the 1402 cm^{-1} peak, a very weak band at 1424 cm^{-1} reflects CH_2 and CH_3 deformations; at 1444 cm^{-1} CH_2 scissoring modes are found (Figure 5.29-1 and 5.29-2). Difference features visible in Figure 5.31 between 1410 and 1460 cm^{-1} may be assigned to backbone vibrations of the DNA and/or changes in the protein. X-ray structure analyses indicate that DNA binding does not cause any significant distortion to the protein secondary structure relative to the free protein in solution, but only causes rearrangement of some protein side chains (*68, 73*). Since the protein contributions to the 1424 cm^{-1} band are very small we conclude that vibrations of furanose residues are the main cause for the difference feature near 1420 cm^{-1}, whereas the peak near 1450 cm^{-1} is mostly due to rearrangement of some protein side chains. The spectral effects might reflect either direct contacts of the furanose residues with protein side chains or conformational perturbations of the furanose rings. The difference feature near 1420 cm^{-1} shows about 20% intensity change, which implies that approximately two bases of each DNA strand undergo conformational perturbations (*93, 96, 100*).

Purine Environment. The crystal structure of Sac7d with the oligonucleotide octamer d(GCGATCGC)$_2$ (Figure 1.6) indicates two direct contacts between protein residue Ser31 and guanine G3 in the minor groove (*68*). Ser31 forms a hydrogen bond with the N2 amino group of the guanine base at position 3 (G3) that acts as the proton donor; and the indole N1H group of Trp24 forms a specific hydrogen bond to G3-N3 (*68*). A basically similar 3D structure is expected but still not available for the Sac7d–d(GAGGCGCCTC)$_2$ complex. In accordance with this expectation prominent features in the difference spectra of the Sac7d–d(GAGGCGCCTC)$_2$ complex (Figure 5.31) are assignable to minor groove interaction of Sac7d with guanine N3.

Sac7d binding to guanine N2 and N3 causes changes of purine marker bands that result in the peak/trough features at 1342 (1349) / 1354 (1363) cm^{-1} (overlapping with tryptophan Fermi doublet and adenosine conformation marker) and 1571(1569) / 1587 (1584) cm^{-1} of the difference spectra (Figure 5.31-A, B). The band near 1355 cm^{-1} (in D_2O) was assigned to guanine ND_2 deformation vibration (*117*). The D_2O difference spectrum (Figure 5.31-B) clearly exhibits a peak/trough difference feature 1349/1363 cm^{-1}; this feature is probably the spectral evidence for the contact of Ser31 with the N2 amino group of one or both guanines at positions 3 and/or 6 (see Chapter 5.7) in the minor groove. A similar feature but at higher wavenumber is expected to appear in the H_2O spectrum, instead that peak/trough feature arises at lower wavenumber at about 1342/1354 cm^{-1} (Figure 5.31-A). The possible explanation is that the intense vibration of the N2 amino group of guanine (observed in D_2O near 1355 cm^{-1}) has in H_2O two weak components (Figure 5.29-2), the first one near 1364 cm^{-1} (shoulder of the thymine 1376 cm^{-1} band) and the second near 1348 cm^{-1} (shoulder of adenine band near 1341 cm^{-1}). A tryptophan contribution of the Fermi doublet is not excluded by this consideration, but in any case not completely responsible for the observed difference feature because of downshift upon deuteration. Components of the Fermi doublet are expected to form difference bands in H_2O solution near 1357 and 1340 cm^{-1} and in D_2O near 1350 and 1333 cm^{-1} (*103*).

Unexpected is the appearance of a difference feature with peak at 1482 (D_2O: 1479) and trough at 1494 (D_2O: 1488) cm^{-1} (Figure 5.31-A, B). This difference feature is a purine ring vibration of guanine N7 which was several times observed as a result of major groove DNA binding of proteins (*93-94, 106-107*). In the Sac7d–d$(GCGATCGC)_2$ system major groove binding is excluded by the X-ray structure analysis (*68-70*), and by extrapolation it is rather unlikely for the Sac7d–d$(GAGGCGCCTC)_2$ complex. There are some possible explanations for the observed guanine N7 difference feature. First, Sac7d binding mediates an increase of the strength of the hydrogen bond of guanine N7 that is formed with a water molecule from the surroundings. Second, the guanine N7 ring vibration might be affected by the interactions of Sac7d with guanine ring N3 and/or N2 that are observed in the X-ray structure of the complex. Third, the B- to A-form transition of the DNA might cause a change in the guanine N7 vibration (*116*). The band near 1577 cm^{-1} (in D_2O 1580 cm^{-1}) is probably altered because of hydrogen bond formation between guanine N3 and the indole N1H group of tryptophan that acts as proton donor.

Tryptophan. The Sac7d protein carries only one Trp residue (W24) that actively participates in binding of Sac7d to an 8-bp oligonucleotide (*68*) and thus facilitates the

detection of key tryptophan markers in Sac7d-DNA complexes. Binding of Sac7d to $d(GAGGCGCCTC)_2$ results in spectral perturbations in tryptophan marker bands. In protein spectra, a Trp vibration called W17 mode results in a band that is located between 883 and 871 cm^{-1}, and a Trp band called W18 mode is located around 761 cm^{-1}. A tryptophan side chain in hydrophilic environment gives rise to a very strong W18 band while in hydrophobic environment the band becomes weaker (*85*).

In the spectrum of the Sac7d–$d(GAGGCGCCTC)_2$ complex, the W17 and W18 modes exhibit large spectral changes in comparison to the component spectra. However, the effects observed for the W17 and W18 modes show opposite tendencies in comparison to the expected ones. The interaction should increase the strength of the hydrogen bond and result in a downshift of the W17 band. The position of the W17 mode does not show this expected frequency shift, it is located at the same frequency (878 cm^{-1}) as in the spectrum of free Sac7d (Figure 5.31-A), but the intensity of the band increases by about 30%. This result is confirmed by the large intensity increase of the W17 mode in the D_2O spectrum; the band is observed at 859 cm^{-1} in agreement with the 20 cm^{-1} shift described upon N1 deuteration (*85*). For the W18 mode an intensity increase is expected (*85*). To the contrary, the W18 mode does not increase its intensity but causes a very strong and sharp peak/trough feature at 762/756 (in D_2O at 757/752) cm^{-1} that indicates a downshift of the frequency. The changes observed here for the Sac7d–$d(GAGGCGCCTC)_2$ system clearly indicate the participation of Trp24 in DNA binding despite of the differences in the behaviour of the W17 and W18 modes in the lysozyme binding to inhibitors (*85*).

Sac7d Secondary Structure. In the difference spectra are no features that could be assigned to conformational changes of Sac7d upon complex formation. In the complex, amide III and amide I overlap with strong bands of DNA. Therefore in some spectral regions it is difficult to discriminate between spectroscopic signals from protein or DNA. H→D exchange helps to assign at least the amide III band because it shifts from 1230-1310 cm^{-1} in H_2O to the lower wavenumbers (900-1000 cm^{-1}) of the amide III' band where DNA bands do not overlap. However, comparison of the H_2O and D_2O difference spectra does not exhibit clear spectral changes in regions of the amide III band. We conclude that Sac7d has the same conformation in the complex and free in solution. This is in agreement with NMR data (*73*) and the results of the X-ray crystal structure analyses (*68*).

5.7. Discussion: Sac7d Protein

Raman spectroscopy of the Sac7d–d(GAGGCGCCTC)$_2$ complex indicates significant perturbations to the B-form DNA backbone as a consequence of Sac7d binding to the DNA decamer d(GAGGCGCCTC)$_2$. Several nucleotides (G, C, A) change their conformation from C2´-endo/anti to C3´-endo/anti. Evidence for partial transition from B- to A-form is found in several regions of the difference spectra. Relevant spectral perturbations are summarized in Table 5.4. The phosphate band near 1092 cm^{-1} does not change significantly upon complex formation. The 1092 cm^{-1} band is commonly used as intensity standard because of its invariance to effects of protein binding (*90*). By contrast, in complexes with minor groove binding proteins slight broadening of the phosphate band was observed that was interpreted to indicate changes in the local electrostatic environment (*96*). Since Sac7d binds in the minor groove of DNA octamers also for the Sac7d–d(GAGGCGCCTC)$_2$ system minor changes of the 1092 cm^{-1} band are not excluded. The identification of intensity differences is not possible in our experiments since the 1092 cm^{-1} band was used as an intensity standard for spectra normalisation. However, broadening might occur and would yield a peak/trough like feature. This was not observed and suggests a conservation of the local electrostatic environment of the phosphates upon minor groove binding of Sac7d.

High resolution structures exist for several Sac7d–DNA octamer complexes. This provides the possibility to analyze the available Raman spectra in the context of the wealth of known structural details. Crystal structures were resolved of Sac7d and Sso7d complexes with seven different octameric oligonucleotides. Several observations are in common. The DNA was found sharply kinked at the C2pG3 step in the Sac7d–(5'-GCGATCGC)$_2$ complex, at the A3pA4 step in the Sac7d–(5'-GTAATTAC)$_2$ complex (*6*), for a T-G mismatched base pair at the T6pG7 step in the Sac7d–(5'-GCGATTGC)$_2$ complex (*69*), and the base at the 3'-end of the intercalating site is always purine, with Trp 24 N1 forming a hydrogen bond to its N3 atom. Kinks were not observed at the GpC or the GpT steps, likely because of their more favorable base-base stacking energies (*69*). The sequence of d(GAGGCGCCTC)$_2$ used for the present study does not contain TpG or ApA (TpT) steps.

Table 5.4: A- and B-form DNA conformation markers in H_2O[a]						
Changes expected for B to A DNA transition[b]				Changes observed upon complex formation[c]		
A-form (cm^{-1})		B-form (cm^{-1})	assignment	(cm^{-1})		(cm^{-1})
665	inc		G	667	inc	
	dec	680	G		dec	686
781	shift	787	C, bk	776	shift	782
808	inc		C3'-endo	808	inc	
	dec	829	C2'-endo		dec	823
1252	shift	1260	C	1247	shift	1262
1314	inc/shift	1318	G	1312	shift	1323
1334	inc/shift	1341	A	1332	shift	1342
1417	shift	1420	bk	1412	shift	1425
1482	shift	1489	G	1482	shift	1494
1574	shift	1578	G	1566	shift	1584

[a] dec, decrease in intensity; inc, increase in intensity; shift, change in peak position; G, guanine; C, cytosine; A, adenine; bk, backbone.
[b] Raman data from reference (*116*).
[c] Raman difference features from Figure 5.31-A.

The Raman results presented here show that in the Sac7d–$d(GAGGCGCCTC)_2$ complex one of the guanines serves as a binding site, and it is reasonable that the XpG steps of the $d(GAGGCGCCTC)_2$ sequence serve as intercalation sites. Potential candidates are the A2pG3, G3pG4 and C5pG6 steps. It has been suggested previously that a preferred site for protein side chain binding might be connected with the base-base stacking energies (*69*). Up to now, to our knowledge base-base stacking energy calculations are not available that could be considered for a qualified discussion of the potential protein binding site in our system. In view of the size of $d(GAGGCGCCTC)_2$ the suggestion that the A2pG3 step could serve as a binding site implies the possibility that two Sac7d molecules bind to the oligonucleotide. However, gel electrophoresis of a complex formed in 1:1 molar stoichiometry did not provide any evidence in support of this assumption (data not shown).

The third base at the 3' end of the intercalation site is a thymine that forms a hydrogen bond with its O2 thymine oxygen to Arg43 (*69*). In the $d(GAGGCGCCTC)_2$ sequence studied here the third base at the 3' ends of the two suggested intercalation sites is a cytosine. It is possible that Arg43 forms a hydrogen bond to cytosine-O2, but the difference spectra do not provide feasible evidence for such a contact. It is not excluded from the data that Sac7d forms only two hydrogen bonds to guanine. The crystal structure of Sso7d–$(5'\text{-}GTGATCGC)_2$ shows that Arg43 NH1 is close to the third base (distance to

T5-O2: 2.99 Å) and the fourth base (distances to C6-02 and C6-O4: 2.88 Å and 3.09 Å, respectively) at the 3'-ends of the intercalation sites (*69*). In the case that Sac7d kinks d(GAGGCGCCTC)$_2$ at the C5pG6 step, thymine is the fourth base at the 3' end of the intercalation sites. The Sac7d's Arg43 could be in a similar position as Arg43 of the Sso7d–(5'-GTGATCGC)$_2$ complex and form a hydrogen bond with T9O2. This could increase the probability of forming a complex with the kink at the C5pG6 step.

The structural adjustment of DNA to Sac7d binding occurs with little or no apparent consequences to the secondary structure of Sac7d, suggesting an induced fit mechanism with more flexible DNA conformation. This is consistent with the highly stable secondary structure of Sac7d that was confirmed by both NMR (*73*) and crystallographic (*68*) studies.

DNA minor groove binding by Sac7d generates large conformational perturbations in the DNA, including a kink of approximately 60° and slight roll of roughly 10°, altogether making a bend of ~ 70° in the helical axis of d(GCGATCGC)$_2$. Many nucleotides that surround the wedge site adopt the less common C3′-endo (N-type) sugar puckers (*68*). The DNA Raman spectrum responds with extraordinarily large perturbations, which are consistent with the crystal structures of Sac7d/Sso7d–DNA complexes (*68-70*). These complexes exhibit unusual conformational features resembling A-DNA (as in an RNA duplex). The extent of the Raman changes is unusually high and varies from band to band. About 30 % intensity change relative to the parent bands were observed for Raman bands directly connected with nucleoside vibrations. The bands carrying information about base environments show ~ 10-15 % relative intensity change. A direct quantitative analysis of B- to A-DNA partial transitions is difficult because of the complexity of the Raman signals, where the relevant bands overlap with contributions from base-base interaction and changes in the surrounding of bases. Nevertheless, from the extent of intensity changes we estimate that 2-6 bases resemble an A-DNA like conformation. The Raman spectroscopic data provide evidence for the involvement of guanine, adenine and cytosine in Sac7d–d(GAGGCGCCTC)$_2$ complex formation, directly by serving as hydrogen bond donor or acceptor or indirectly by changing their conformation. There is strong spectroscopic evidence for intercalation; however, it is not possible to determine the intercalation site. Potential sites are the A2pG3, G3pG4 and C5pG6 steps. It should be mentioned that neither Sac7d nor Sso7d crystallize so far as complexes with d(GAGGCGCCTC)$_2$. Sac7d binding to more than one of the A2pG3, G3pG4 or C5pG6 sites and formation of heterogeneous mixtures of complexes would render crystallization difficult and explain this failure.